ARO 24150.4-MS-A

(2)

AD-A222 951

CORROSION PROTECTION OF METAL MATRIX COMPOSITES

FINAL REPORT

F. MANSFELD, S. LIN AND H. SHIH

APRIL 1990

U. S. ARMY RESEARCH OFFICE

CONTRACT/GRANT NUMBER
DAAL03-86-K-0156

UNIVERSITY OF SOUTHERN CALIFORNIA

UNCLASSIFIED
SECURITY CLASSIFICATION OF THIS PAGE

MASTER COPY - FOR REPRODUCTION PURPOSES

REPORT DOCUMENTATION PAGE

1a. REPORT SECURITY CLASSIFICATION: Unclassified	1b. RESTRICTIVE MARKINGS
2a. SECURITY CLASSIFICATION AUTHORITY	3. DISTRIBUTION/AVAILABILITY OF REPORT: Approved for public release; distribution unlimited.
2b. DECLASSIFICATION/DOWNGRADING SCHEDULE	
4. PERFORMING ORGANIZATION REPORT NUMBER(S)	5. MONITORING ORGANIZATION REPORT NUMBER(S): ARO 24150.4-MS-A
6a. NAME OF PERFORMING ORGANIZATION: UNIVERSITY OF SOUTHERN CALIF. / 6b. OFFICE SYMBOL (If applicable)	7a. NAME OF MONITORING ORGANIZATION: U. S. Army Research Office
6c. ADDRESS (City, State, and ZIP Code): Contracts and Grants, Los Angeles, CA 90089-1147	7b. ADDRESS (City, State, and ZIP Code): P. O. Box 12211, Research Triangle Park, NC 27709-2211
8a. NAME OF FUNDING/SPONSORING ORGANIZATION: U. S. Army Research Office / 8b. OFFICE SYMBOL (If applicable)	9. PROCUREMENT INSTRUMENT IDENTIFICATION NUMBER: DAAL03-86-K-0156
8c. ADDRESS (City, State, and ZIP Code): P. O. Box 12211, Research Triangle Park, NC 27709-2211	10. SOURCE OF FUNDING NUMBERS: PROGRAM ELEMENT NO. / PROJECT NO. / TASK NO. / WORK UNIT ACCESSION NO.

11. TITLE (Include Security Classification)

CORROSION PROTECTION OF METAL MATRIX COMPOSITES

12. PERSONAL AUTHOR(S) F. MANSFELD, S. LIN and H. SHIH

13a. TYPE OF REPORT	13b. TIME COVERED	14. DATE OF REPORT (Year, Month, Day)	15. PAGE COUNT
FINAL REPORT	FROM 10/86 TO 4/90	1990/5/1	109

16. SUPPLEMENTARY NOTATION The view, opinions and/or findings contained in this report are those of the author(s) and should not be construed as an official Department of the Army position, policy, or decision, unless so designated by other documentation.

17. COSATI CODES		
FIELD	GROUP	SUB-GROUP

18. SUBJECT TERMS (Continue on reverse if necessary and identify by block number)
Corrosion protection, polymer coatings, conversion coatings, anodizing Al alloys, Magnesium, localized corrosion, passivation, electrochemical techniques

19. ABSTRACT (Continue on reverse if necessary and identify by block number)

ABSTRACT: Corrosion protection of Al alloys, Al-based metal matrix composites (MMCs), and Al-Li alloy by conversion coatings, anodized layers, polymer coatings, and chemical passivation in $CeCl_3$ has been evaluated in a simulated marine environment (0.5 N NaCl) by electrochemical impedance spectroscopy (EIS). Conversion coatings, anodizing, polymer coatings have been evaluated for MgAZ31B.

Chromate conversion coatings (Alodine 600) provided corrosion protection for Al/SiC and Al/Gr MMCs, but were not as effective as for Al 6061. For Al/SiC it was observed that sulfuric acid anodizing did not produce the corrosion resistance obtained for the Al 6061. The corrosion resistance for hard anodized Al/SiC was less than that for conventional anodized Al/SiC. This unusual result is considered to be due to the presence of the SiC particulates and has been explained by a new mechanism and a new model for the formation of anodized

20. DISTRIBUTION/AVAILABILITY OF ABSTRACT ☐ UNCLASSIFIED/UNLIMITED ☐ SAME AS RPT. ☐ DTIC USERS	21. ABSTRACT SECURITY CLASSIFICATION: Unclassified
22a. NAME OF RESPONSIBLE INDIVIDUAL	22b. TELEPHONE (Include Area Code) / 22c. OFFICE SYMBOL

DD FORM 1473, 84 MAR 83 APR edition may be used until exhausted. All other editions are obsolete.

SECURITY CLASSIFICATION OF THIS PAGE
UNCLASSIFIED

layers on Al/SiC. For Al/Gr difficulties were encountered with the sulfuric anodizing process since as long as graphite was exposed in defects of the Al 6061 face sheet the proper anodizing conditions could not be reached. An increase of the thickness of the Al 6061 face sheet of Al/Gr has been suggested to enhance the corrosion resistance by anodizing.

A significant improvement of the corrosion resistance by chemical passivation in $CeCl_3$ has been observed for Al/SiC and Al/Gr. Chemical passivation in $CeCl_3$ provided better corrosion resistance than chromate conversion coatings (Alodine 600) or sulfuric acid anodizing. A comparison with the improvement of the corrosion resistance by treatment with chromate conversion coatings shows that chemical passivation provides a valuable alternative to chromate conversion coatings. A new mechanism for the formation of the passive film in $CeCl_3$ has been developed.

Polymer coatings and a combination of chemical passivation and a polymer coating provided excellent corrosion resistance for Al/SiC and Al/Gr. An accelerated corrosion test for polymer coatings and models for the delamination of polymer coatings have been developed to evaluate the lifetime and the quality of coatings in a short time.

For MgAZ31B, conversion coatings (Dow #1, Dow #7, Dow #23, chrome-manganese) and anodizing (Dow #17) did not provide significant protection, but an epoxy coating and a Cr-Mn conversion coating combined with the epoxy coating provided excellent corrosion resistance in 0.5 N NaCl.

EIS is a powerful tool to monitor the passivation process in $CeCl_3$ and the corrosion behavior during exposure to NaCl. Pitting and crevice corrosion of Al Alloys and Al-based MMCs can be detected by characteristic changes of the impedance spectra in the low frequency range, which can be described by the pitting model.

TABLE OF CONTENTS

1. INTRODUCTION

Metal matrix composites (MMCs) fabricated with lightweight Al and Mg alloy matrices and high modulus graphite or SiC reinforcements offer excellent structural properties. However, serious corrosion problems can occur, especially for Al/Gr and Mg/Gr MMCs, which contain some of the most powerful couples in the galvanic series. For Al/Gr or Mg/Gr, accelerated corrosion is likely to occur when the metal foils which cover the surface of the MMCs are penetrated by pitting attack, which leads to the establishment of a graphite/metal couple [1-4]. For Al/SiC MMCs into which SiC particulates are incorporated, this galvanic problem might be less bothersome due to the insulating nature of SiC.

Al alloys are usually protected by chromate conversion coatings, anodizing, or polymer coatings during exposure to corrosive atmospheres such as marine environments [5]. These protection schemes can also be applied to Al MMCs. The application of protective coatings such as chromate conversion coatings which are commonly used in aircraft structures is relatively simple. Chromate conversion coatings of Al alloys are generally applied in a solution containing hexavalent chromium ions and fluoride ions [5]. A thick film containing chromium oxide and hydroxide is formed to replace the original air-formed Al oxide film and to improve the corrosion resistance. However, chromate is toxic. The environmental and health risks associated with the use of chromate ions make it likely that the use of such coatings will be restricted in the future. It is therefore necessary to investigate other non-toxic coating processes with equal or even better corrosion protection.

As reported by Hinton and Arnott [6-8], new types of conversion coatings can be formed by immersion of Al alloys in a solution of cerium chloride or other rare earth metal chlorides such as lanthanum. This chemical passivation process has provided coatings which were more resistant to pitting than the naturally formed oxide film. This conclusion was based on the measurement of polarization curves in NaCl + $CeCl_3$ [7]. Cerium compounds are non-toxic [9]. It is very encouraging that simple immersion in a solution of rare earth metal chlorides can produce coatings which provide equal or even better corrosion resistance than the chromate conversion coating for Al 7075-T651 [7]. However, at present very little is known about the mechanisms by which these coatings are formed and obtain their superior corrosion resistance. Hinton et al. [6-8] have concluded from cathodic polarization curves that the "corrosion protection was achieved with these coatings through their suppression of the oxygen reduction reaction at cathodic sites on the metal surface". Results which have been obtained with XPS and Auger electron spectroscopy have suggested that the coatings contain a mixture of crystalline ceric oxide and hydrated cerium oxides in oxidation states 3 and 4 [6-8]. The mechanism of the formation of the protective film as suggested by Hinton et al.[7] proposes that the natural aluminum oxide dissolves in the alkaline surface condition due to oxygen reduction and is replaced by the precipitation of insoluble cerium oxides and hydroxides. However, they did not explain how the Ce^{+4} was formed in this chemical passivation system. In the present project, chemical passivation in $CeCl_3$ and the mechanism for the formation of the passive film during the passivation process have been studied for Al alloys and Al-based MMCs.

Anodizing of Al alloys is an electrochemical method of converting aluminum into aluminum oxide at the surface by applying an external current in an acid

electrolyte. The most widely used electrolyte is sulfuric acid. There are two types of sulfuric anodizing: conventional anodizing, which is performed at room temperature and provides about 8 μm of oxide thickness and a fairly hard surface, and hardcoat anodizing which is performed at around 0°C and provides about 50 μm of oxide thickness and extreme hardness. The oxide film consists of a thin nonporous barrier layer and a thick porous layer. The structure of the porous layer was characterized by Keller et al. [10] as a closed-packed array of columnar hexagonal cells which contain a central pore normal to the substrate surface. The porous layer can be sealed in hot water to close these pores. Anodizing provides excellent corrosion resistance for Al alloys. These anodizing techniques have been applied to Al/SiC MMCs and Al/Gr MMCs in this project.

Polymer coatings provide corrosion protection by acting as a barrier layer between the substrate material and the environment. However, all polymer coatings are to some degree permeable to water, gas (O_2), and ions (Cl^- and Na^+), depending on the characteristics of the polymer coating and the techniques of the coating application. When water, O_2 and/or Cl^- penetrate through the coating film and reach the substrate, corrosion reactions may occur and cause damage to the coating. Filiform corrosion and delamination have been observed on Al and Mg surfaces covered by polymer coatings [11-13]. The presence of a defect in the coating permits electrolyte to reach the substrate and accelerate the corrosion reactions which causes damage to the coating from the edge of the defect. In this project, a polymer with excellent resistance to marine environments has been applied to Al alloys and Al-based MMCs and has produced excellent corrosion resistance to 0.5 N NaCl. An accelerated corrosion test for polymer coatings has been developed.

The benefits of magnesium alloys such as high strength-to-weight ratio, excellent machinability and good casting qualities present possibilities to replace aluminum parts with magnesium alloys in the aerospace and automotive industries. However, the corrosion resistance of Mg alloys is much less than that of Al alloys, which limits their use without protective coatings. In this work, chromate conversion coatings (Dow # 7), a chrome-manganese coating, anodizing (Dow # 17), a polymer coating, and a combination of the chrome-manganese coating and the polymer coating have been applied to MgAZ31B. Since it was not possible to obtain Mg-based MMCs in a shape suitable for the passivation and corrosion tests or at a reasonable price, data are repeated only for MgAZ31B.

In this project, the corrosion behavior of bare and coated Al/Gr MMCs, Al/SiC MMCs, Al alloys, and MgAZ31B has been evaluated as a function of exposure time to 0.5 N NaCl or ASTM corrosive water using electrochemical impedance spectroscopy (EIS) and visual and/or microscopic observation of the samples after the test.

2. EXPERIMENTAL APPROACH

The materials studied in this work, the methods of surface preparation for the different materials, and the experimental approach for the EIS measurements will be described in the following.

2.1 Materials

The materials studied were Al 6061, Al 6061/Graphite (Gr), Al 6061/SiC, Al 7075-T6, Al 7075-T73, Al-Li 2091-T6 and MgAZ31B. The Al/Gr MMC (DWA Composites Specialties) contained 55 v% of P100 graphite fiber with eight alternating layers of graphite and Al 6061. It was cladded on each side with an Al 6061 face sheet of 50 μm thickness. The Al/SiC MMC (DWA) contained 25 v% of 10 μm SiC particulates, which were mixed with Al 6061 powder and processed with an extrusion method. The chemical composition of these materials is shown in Table I [13-15].

2.2 Surface Preparation

Conversion coatings, anodized coatings, chemical passivation in $CeCl_3$, a polymer coating, chemical passivation combined with a polymer coating, and a Cr-Mn conversion coatings followed by a polymer coating were applied to Al alloys, Al-based MMCs, Al-Li alloy and MgAZ31B. The details of each surface preparation procedure will be given in the following.

2.2.1 Conversion Coatings

Conversion coatings are produced by forming an adherent and protective surface layer in a chromate coating solution which contains hexavalent chromium, acid radicals, and film-forming chemicals.

2.2.1.1 Al 6061, Al/Gr MMCs, and Al/SiC MMCs

Chromate conversion coatings (Amchem, Alodine 600) were applied to Al 6061, Al/Gr, and Al/SiC for corrosion protection. The coating procedures were as follows [16]:

(a) The sample was wiped with hexanes using tissues.

(b) Degreasing: The sample was immersed in hexanes at 50°C for 15 min and then immersed in an alkaline solution (Ridoline 53, Amchem) at 66°C for 8 min.

(c) Deoxidizing: The sample was immersed in Deoxidizer 17 (Amchem) at R.T. for 10 min.

(d) Coating: Alodine 600 (Amchem) consists of 30-40 wt% of chromic acid, 40-50 wt% of sodium fluoborate, and 10-15 wt% of potassium fluozirconate. The coating bath contained 15 g/l Alodine 600 and 4 vol% toner 22 (Amchem). The pH of the solution was adjusted to 1.7-1.8 by concentrated HNO_3. The sample was immersed in the Alodine 600 solution at R.T. for 15 min.

(e) Rinsing in deionized water and drying in the hood.

(f) Aging in air for one week.

Table I. Nominal composition of Al alloys, Al-Li alloy, and Mg alloy (weight percent) [13-15]

	Li	Mg	Zr	Mn	Cu	Fe	Si	Cr	Zn	Ti	Al	Ni
Al 6061		1.0		0.15	0.25	0.7	0.6	0.25	0.25	0.15	*	
Al 7075		2.5		0.3	1.6	0.7	0.5	0.3	5.6	0.2	*	
Al-Li 2091	2.0	1.5	0.1	0.1	1.8	0.3	0.2	0.1	0.25	0.1	*	
MgAZ31B		*		0.2	low	low			1.0		3.0	low

Al/SiC : 25 vol% of 10 μm particulates and 75 vol% of Al 6061.

Al/Gr : 55 vol% of P 100 graphite fibers and 45 vol% of Al 6061 with eight layers each of graphite and Al 6061; cladded with an Al 6061 face sheet of 50 μm thickness.

* balance

2.2.1.2 MgAZ31B

Chrome pickle (Dow #1), dichromate (Dow #7), chrome-manganese (British specification DTD 911C), and stannate immersion (Dow #23) were applied to MgAZ31B for corrosion protection. The procedures were as follows:

2.2.1.2.1 Chrome Pickle (Dow #1) [15,17,18]

(a) The sample was wiped with hexanes using tissues.

(b) Degreasing: The sample was immersed in hexanes at 50°C for 15 min and then immersed in an alkaline solution (90 g/l NaOH) at 90°C for 10 min.

(c) Deoxidizing: The sample was immersed in an acid fluoride solution (25 g/l NH_4HF_2) at R.T. for 5 min.

(d) Coating: The sample was immersed in a solution which contained 180 g/l $Na_2Cr_2O_7 \cdot 2H_2O$ and 190 ml/l HNO_3 at R.T. for 2 min.

(e) Parts were held 5 sec above the tank and then rinsed in deionized water.

2.2.1.2.2 Dichromate (Dow #7) [15,17,18]

(a) Degreasing and deoxidizing: the same procedure as for Dow #1.

(b) Coating: The sample was immersed in a solution which contained 120 g/l $Na_2Cr_2O_7 \cdot 2H_2O$ and 2.5 g/l CaF_2 at boiling temperature for 20 min.

2.2.1.2.3 Chrome-Manganese [19]

(a) Degreasing and deoxidizing: the same procedure as for Dow #1.

(b) Coating: The solution contained 100 g/l $Na_2Cr_2O_7 \cdot 2H_2O$, 5 g/l $MnSO_4 \cdot 5 H_2O$ and 5 g/l $Mg_2SO_4 \cdot 7 H_2O$. The pH of the solution was adjusted to 4-6 by H_2SO_4. The sample was immersed in the solution at R.T. for 2 hr.

2.2.1.2.4 Stannate Immersion (Dow #23) [15,17,18]

(a) Degreasing and deoxidizing: the same procedure as for Dow #1.

(b) Coating: The sample was immersed in the solution which contained 10 g/l NaOH, 50 g/l $K_2SnO_3 \cdot 3H_2O$, 10 g/l $NaC_2H_3O_2 \cdot {}^3H_2O$, and 50 g/l $Na_4P_2O_7$ at 82°C for 20 min.

2.2.2 Anodic Coatings

Anodic coatings are produced by anodic oxidation in an acid bath to form an oxide layer.

2.2.2.1 Al 6061, Al/SiC MMCs, and Al/Gr MMCs

Conventional anodized coatings which are formed at around 20°C and hard anodizing coatings which are formed at around 0°C were applied to Al 6061, Al/SiC, and Al/Gr. The procedures were as follows:

2.2.2.1.1 Conventional Anodized Coatings [20]

(a) Degreasing and deoxidizing: the same procedure as for conversion coatings. For Al/Gr, an epoxy coating was applied prior to anodizing to the composite panel edges, where graphite was exposed.

(b) Coating: The sample was immersed in 10 vol% H_2SO_4 at R.T. and a constant current density (1 A/dm^2) was applied. The coating process was stopped when the voltage reached 15 volts. The coating time was about 30 min.

(c) Sealing: The anodized sample was immersed in hot water at 90-100°C for 20 min.

2.2.2.1.2 Hard Anodizing Coatings [20]

(a) Degreasing and deoxidizing: the same procedure as for conventional anodizing coatings.

(b) Coating: The sample was immersed in 15 vol% H_2SO_4 at 0°C and a constant current density (1 A/dm^2) was applied and stopped when the voltage reached at 60 volts. The coating time was about one hour.

(c) Sealing: The anodized sample was immersed in hot water at 90-100°C for 30 min.

2.2.2.2 MgAZ31B

Dow # 17 which is an anodized process was applied to MgAZ31B by the following procedure [15,17,18]:

(a) Degreasing and deoxidizing: the same procedure as for Dow #1.

(b) Coating: The sample was immersed in a solution which contained 225 g/l NH_4HF_2, 50 g/l $Na_2Cr_2O_7 \cdot 2H_2O$, and 50 ml/l H_3PO_4 at 70-80°C. A constant current density (0.5-5 A/dm^2) was applied for 25 min and the voltage finally reached 90-100 volts.

(c) Sealing: The anodized sample was immersed in a water glass solution which contains 164 g/l $Na_2O\ SiO_2 \cdot 9H_2O$ at boiling temp. for 15 min.

2.2.3 Chemical Passivation in $CeCl_3$

Chemical passivation in $CeCl_3$ is a new, nontoxic, and simple approach to the formation of chemical conversion coatings [7,8]. The procedures for Al 6061, Al/Gr, Al/SiC, Al 7075-T6, and Al 7075-T73 are as follows:

(a) Two kinds of pretreatments were used: degreasing, and degreasing followed by deoxidizing. For the degreasing treatment, the sample was wiped with

hexanes using tissues, immersed in hot hexanes for 15 min, and then rinsed in deionized water. For the deoxidizing treatment, the sample was first degreased, alkaline cleaned (Ridoline 53), rinsed in deionized water, deoxidized in Deoxidizer 17, and then rinsed in deionized water.

(b) The sample was immersed in 1000 ppm $CeCl_3$ solution at open-circuit for one week.

2.2.4 Polymer Coatings

Epoxy resin (G7-4102, Dexter Corp.) [21] was applied to Al 6061, Al/Gr, Al/SiC, Al-Li 2091-T6 and MgAZ31B by the following procedure:

(a) Degreasing and deoxidizing: the same procedure as for the conversion coating.

(b) Coating: The coating solution contained 30-40 vol% Hysol G7-4102 (Dexter Corp.) and 60-70 vol% aceton. The sample was immersed in the coating solution for a few seconds and dried in the hood for one day.

(c) Curing: The sample was cured in the oven at 200°C for 25 min.

(d) The thickness of the coating film was controlled by the concentration of the epoxy (Hysol G7-4102) in the coating solution. In order to obtain a uniform coating film, the concentration of epoxy (Hysol) should not be more than 50 vol%. For a coating film of about 25 μm thickness, two coating layers were applied. The samples were immersed in the coating solution (30 vol% Epoxy (Hysol)), cured in the oven, immersed a second time, and cured again.

2.2.5 Chemical Passivation Combined with Polymer Coatings

For the purpose of testing the adhesion between the passive film produced in $CeCl_3$ and the polymer coating, chemical passivation in $CeCl_3$ was followed by the application of the polymer coating using the following procedure:

(a) The sample was degreased and passivated in $CeCl_3$.

(b) The sample was immersed in the epoxy resin solution, dried in the hood, and cured in the oven.

2.2.6 Cr-Mn Conversion Coatings with Polymer Coatings

In order to enhance the adhesion between the polymer coating and MgAZ31B, a Cr-Mn conversion coating was applied followed by the polymer coating.

2.3 Electrochemical Impedance Spectroscopy (EIS) Techniques

The term EIS was first introduced by Mansfeld [23,24] in 1985 to replace the previously used term AC impedance. EIS is a relatively new and powerful method to characterize the electrical properties of materials and their interfaces during exposure to an electrolyte. EIS data are measured by applying a small AC signal at a constant applied potential such as the corrosion potential Ecorr to a linear, time-invarient system. Some of the advantages of the EIS

techniques are the use of only very small AC signals, which do not disturb the electrode properties to be measured, and the possibility to study the kinetics of corrosion reactions, the quality of the coatings in corrosive media [25,26], the rate of pit growth [27-30], the use in corrosion monitoring [31,32], and the measurement of corrosion rates in low conductivity media, where traditional DC methods fail.

2.3.1 Measurement of EIS-Data

EIS measurements have been used in this project to monitor the passivation processes in $CeCl_3$ and the corrosion processes in 0.5 N NaCl, ASTM corrosive water, deionized water, and 0.5 M Na_2SO_4 as a function of exposure time. The instruments used were a Solartron model 1250 Frequency Response Analyzer (FRA) and a Solartron model 1286 Electrochemical Interface (EI). The cell for the measurement of EIS data consists of the reference electrode (RE), the counter electrode (CE), and the working electrode (WE) (Fig.1). A saturated calomel electrode (SCE) was used as the reference electrode and was coupled to a Pt wire by a small capacitor to minimize the high-frequency phase shift in impedance measurement [22]. The material of the counter electrode was SS 316L. The exposed area of the working electrode was 20 cm^2. Fig.2 shows the experimental arrangement for the recording of the EIS data. The ac voltage sine wave generated by the Solartron 1250 FRA was applied to the cell at the corrosion potential which was measured by the Solartron 1286 EI. Software developed at CEEL/USC can set the parameters for the Solartron 1250 FRA, perform the measurement, display the spectra during the measurement, collect the EIS data, and provide data to the computer for disk storage. However, the parameters of Solartron 1286 EI have to be set manually. The spectra were obtained in at least two parts in order to achieve maximum sensitivity at all frequencies. Usually the current measuring resistor was changed at 1 Hz to a value that would match the impedance expected in the low-frequency range. The integration time is the time period used to measure impedance data at a certain frequency. An integration time of 10 seconds was used in the high-frequency range between 1 Hz and 65 kHz. 10 cycles was used in the low-frequency range between 0.01 Hz and 1 Hz. Auto integration with a long time can be used to obtain at least three readings of impedance data until the standard deviation falls below 1 % for each frequency. The maximum time of auto integration is determined by entering a value into integration time, such as 10 seconds for high-frequency range or 10 cycles for low-frequency range. The applied AC signal was 10 mV for bare metals, conversion coated, anodized coated, and $CeCl_3$ passivated samples. The maximum of the current measuring resistor in the Solartron 1286 EI is 10^5 ohm. For very protective polymer coatings, the impedance values at low frequencies were above 10^7 ohm and a 100 mV ac signal was applied to minimized the scatter.

2.3.2 Analysis of EIS Data

During each impedance measurement, the data were displayed as Bode-plots (log /Z/ versus log f and phase angle versus log f) to obtain an immediate assessment of the data quality. Bode-plots were employed because they provide more information in the entire frequency range than Nyquist-plots (-ImZ versus ReZ) [33]. EIS data can be fitted by the integration method [34] or other fitting procedures [35,36] to suitable models and equivalent circuits.

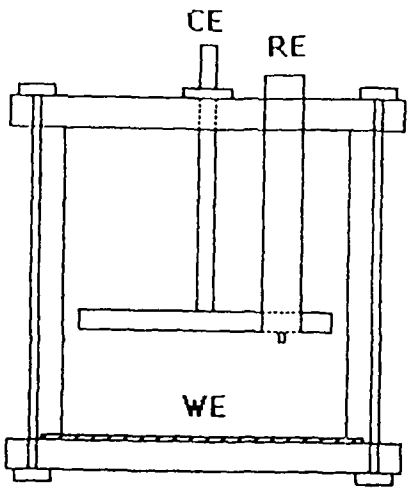

Fig.1 A test cell for the measurement of EIS data with a reference electrode (RE), a counter electrode (CE), and a working electrode (WE).

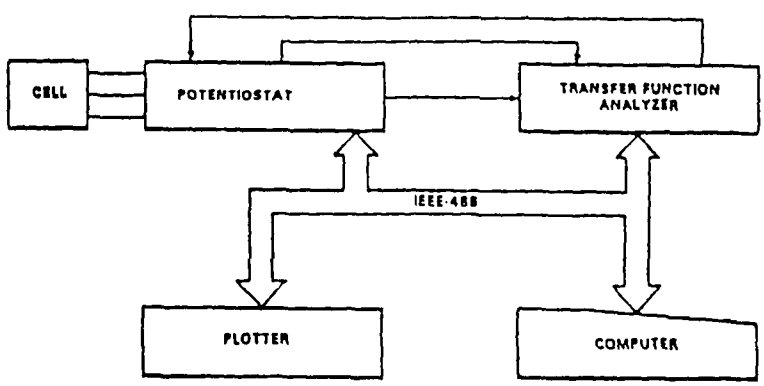

Fig.2 Experimental arrangement for recording of EIS data.

2.3.2.1 Integration Method

For simple impedance spectra which show only one time constant such as in Fig.3, the polarization resistance R_p can be determined by the integration method [34]. This method is suitable for low solution resistance, but even more so for high solution resistances, because the imaginary part of the impedance is independent of solution conductivity. An advantage of this technique lies in the fact that it is not necessary to determine the impedance at the dc limit, since only the maximum of the negative imaginary part -ImZ must be reached.

2.3.2.2 Fitting Procedures for the One-Time-Constant-Model

For samples which had very good corrosion resistance, no maximum of the imaginary part of impedance data could be obtained at the lowest measured frequency, which usually was 10 mHz. A new fitting procedure [35] was developed at CEEL/USC for these cases in which the experimental data were fitted to [36]:

$$/Z/ = R_s + R_p/(1+ (jwC_pR_p)^a) \qquad (2.1)$$

where a is the slope of the log /Z/ versus log f plot in the linear capacitive range, R_s is the solution resistance in ohm, R_p is the polarization resistance, and C_p is the electrode capacitance. This model has been used for bare and coated metals and MMCs for which the impedance spectra showed the one-time constant model, during exposure to 0.5 N NaCl before pitting or delamination occurred.

2.3.2.3 Fitting Procedures for the Pitting Model

For bare or $CeCl_3$ passivated Al alloys and Al-based MMCS, EIS-data showed characteristic changes in the low frequency range when pitting occurred. In this case the EIS-data can be explained by and can be fitted to the pitting model [27-30,32] shown in Fig.4.a. The parameters in this model are defined as follows: R_s is the solution resistance, C_p is the capacitance and R_p is the polarization resistance of the passive surface, C_{pit} is the capacitance and R_{pit} is the polarization resistance of the pitted area. W describes the transmission line behavior in the low-frequency range and is expressed as $W=(K/F)(jw)^n$, where n is the slope of the log/Z/ - logf curve in the transmission line range, K is an experimental parameter and F is the area fraction of the pitted surface ($0 \leq F \leq 1$). Impedance spectra which correspond to F = 0 and F = 0.005 are shown in Fig.4.b. The spectra show the resistive component R_s at the highest frequencies, linear capacitive behavior in the frequency range of 0.1 to 100 Hz for F = 0 (curve 1) and 1 to 50 Hz for F = 0.005 (curve 2), the resistive component R_p at the lowest frequencies for F = 0, and a second time constant below 0.1 Hz for F = 0.005 (Fig.4.b). The pronounced increase of the capacitance, the different frequency dependence of the impedance at the lowest frequencies and the occurrence of a second maximum of the phase angle at very low frequencies are characteristic of the pitting process. A fitting procedure (PITFIT) [38] has been applied to analyze impedance data which showed the characteristics of pitting behavior in the low-frequency range. The error of the fit in the whole range of frequencies is calculated from the differences between the experimental impedance data Z_{exp} and the fitted impedance data Z_{fit}. This error can be expressed as:

$$\text{error} = \frac{100}{N} \sum_{i=1}^{N} \frac{|Z_{exp}(f_i) - Z_{fit}(f_i)|}{Z_{exp}(f_i)} \qquad (2.2)$$

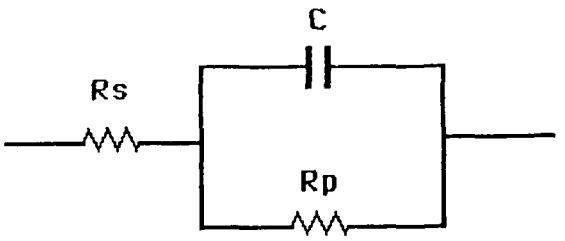

Fig.3.a Equivalent circuit (EC) for the one-time-constant-model (OTCM).

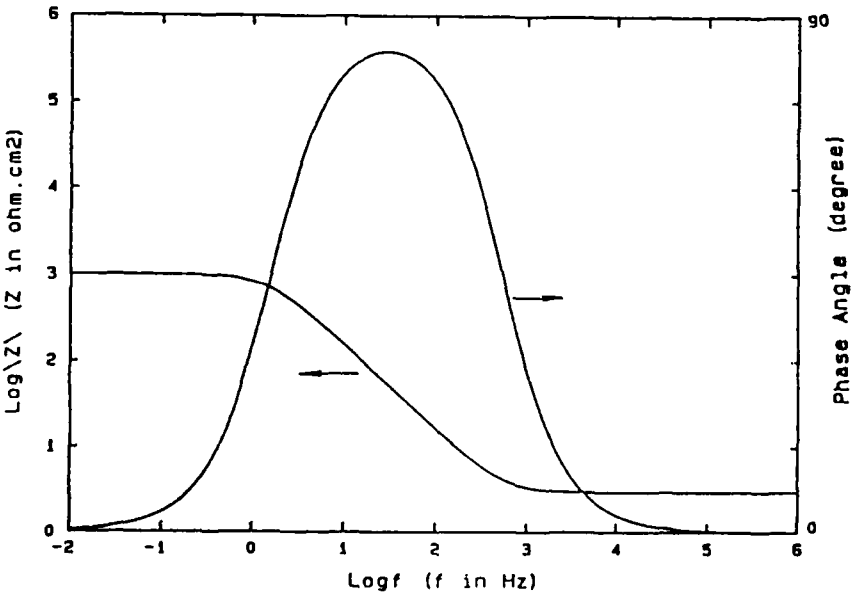

Fig.3.b Bode-plots for the OTCM.
R_S = 3 ohm, R_P = 10^3 ohm, C = 10^{-4} F, and A = 1 cm^2.

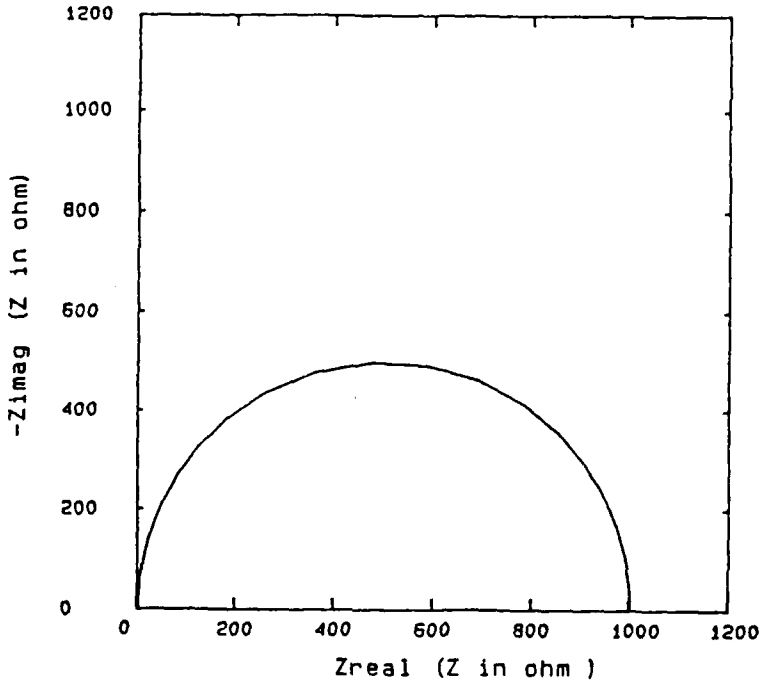

Fig.3.c Nyquist-plot for the OTCM.
R_S = 3 ohm, R_p = 10^3 ohm, C = 10^{-4} F, and A = 1 cm^2.

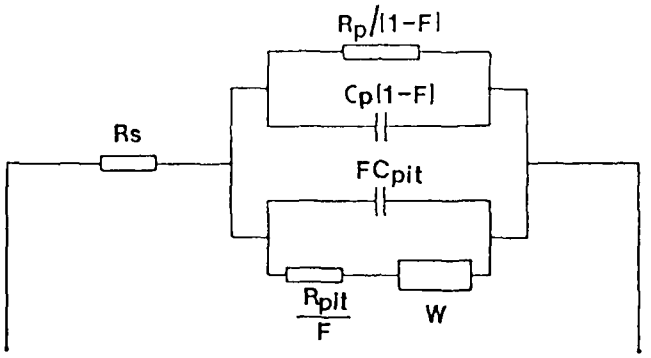

$$0 \leq F \leq 1 \qquad W = \frac{k}{F}(j\omega)^n$$

$$n < 0$$

Fig.4.a Equivalent circuit (EC) for the impedance of the pitting process on Al-based materials.

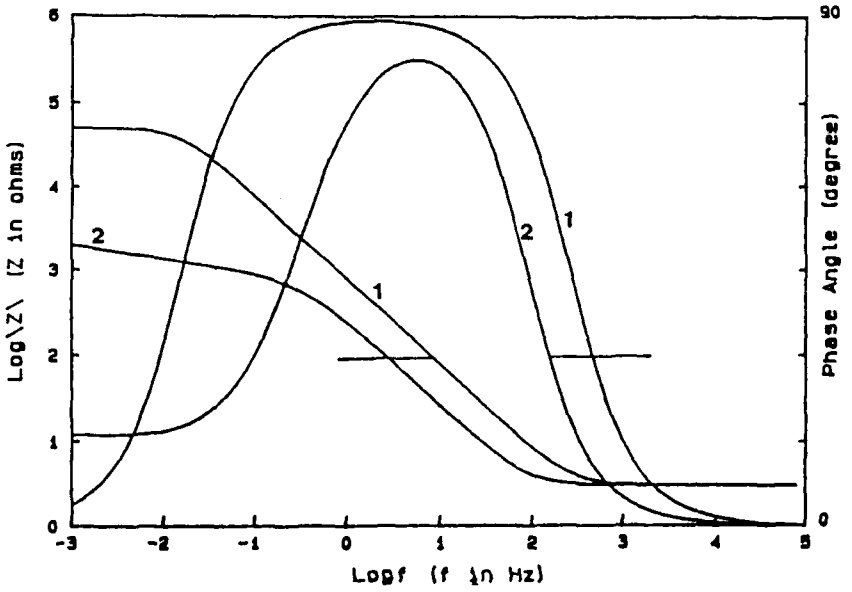

Fig.4.b Simulated spectra for $F = 0$ (curve 1) and $F = 5 \cdot 10^{-3}$ (curve 2), $R_p = 5 \cdot 10^4$ ohm, $R_s = 3$ ohm, $C_p = 2 \cdot 10^{-4}$ F, $R_{pit} = 25$ ohm, $C_{pit} = 0.08$ F, $K = 2.5$ ohm $(rad/s)^{-n}$, $n = -0.5$

where N is the number of the points for each EIS spectrum. Fig.5 shows the experimental results (curve 1) and fit results (curve 2) for as-received Al 6061 for which some pits had already initiated after 24 hr exposure to 0.5 N NaCl. The error in Fig.5 is 5 %. Very good agreement between experimental data and the fitted results was obtained. The fit results can also be used to extend the impedance spectra in the very low frequency range to the dc limit of the impedance. This limit occurs only at 10^{-6} Hz and is therefore beyond the range of the present instrumentation and realistic times for the measurement.

2.5.4 Fitting Procedure for Anodized Al Alloys

A model and equivalent circuits for anodized Al alloys have been proposed by Hoar and Wood [39] as early as 1962 based on their experimental results. A fitting procedure (ANODAL) developed at CEEL/USC has been used to analyze the impedance data for anodized Al alloys.

3. EXPERIMENTAL RESULTS

The application of conversion coatings, anodic coatings, polymer coatings, chemical passivation, chemical passivation combined with polymer coatings, and conversion coatings combined with polymer coatings was studied for the corrosion protection of Al alloys, Al-based MMCs, and a Mg alloy. The properties of the protective coatings and the corrosion reactions at the metal/coating interface were evaluated as a function of exposure time to 0.5 N NaCl (open to air) using electrochemical impedance spectroscopy (EIS). The exposure time depended on the corrosion resistance of the particular material. Visual observation of the sample surfaces was carried out after the exposure tests to correlate the coating damage with the observed changes in the impedance spectra. Software developed in this laboratory was used to collect and analyze the impedance data.

3.1 Conversion Coatings

Chemical conversion coatings were used as a pretreatment for polymer coatings to provide corrosion protection for Al or Mg alloys. Alodine 600 chromate conversion coatings were applied to Al 6061 and Al-bases MMCs. A dichromate conversion coating (Dow #7), a stannate immersion coating (Dow #23), and Cr-Mn conversion coating were applied to MgAZ31B.

3.1.1 Al 6061

For Al 6061 with the Alodine 600 chromate conversion coating, the Bode-plots in 0.5 N NaCl (Fig.6.a) show the ohmic component at the highest frequencies corresponding to the solution resistance R_s, linear capacitive behavior between 0.1 and 10 Hz, and an indication of a resistive component at the lowest frequencies corresponding to the polarization resistance R_p for curve 1. However, for curve 2 and 3 the spectra have become mainly capacitive, indicating that R_p had become very high. For simple spectra, the phase angle is symmetric with frequency and has a maximum at intermediate to low frequencies. Fig.6.b shows that the phase angle has a maximum at about 3 Hz for curve 1 and at about 1 Hz for curves 2 and 3. Fitting to a one-time-constant-model [35] was used for the analysis of the EIS data. The surface did not show pits after the 12-day corrosion test in 0.5 N NaCl, open to air. The surface of the coating became discolored due to the leaching of Cr^{+6} from the coating during exposure to NaCl.

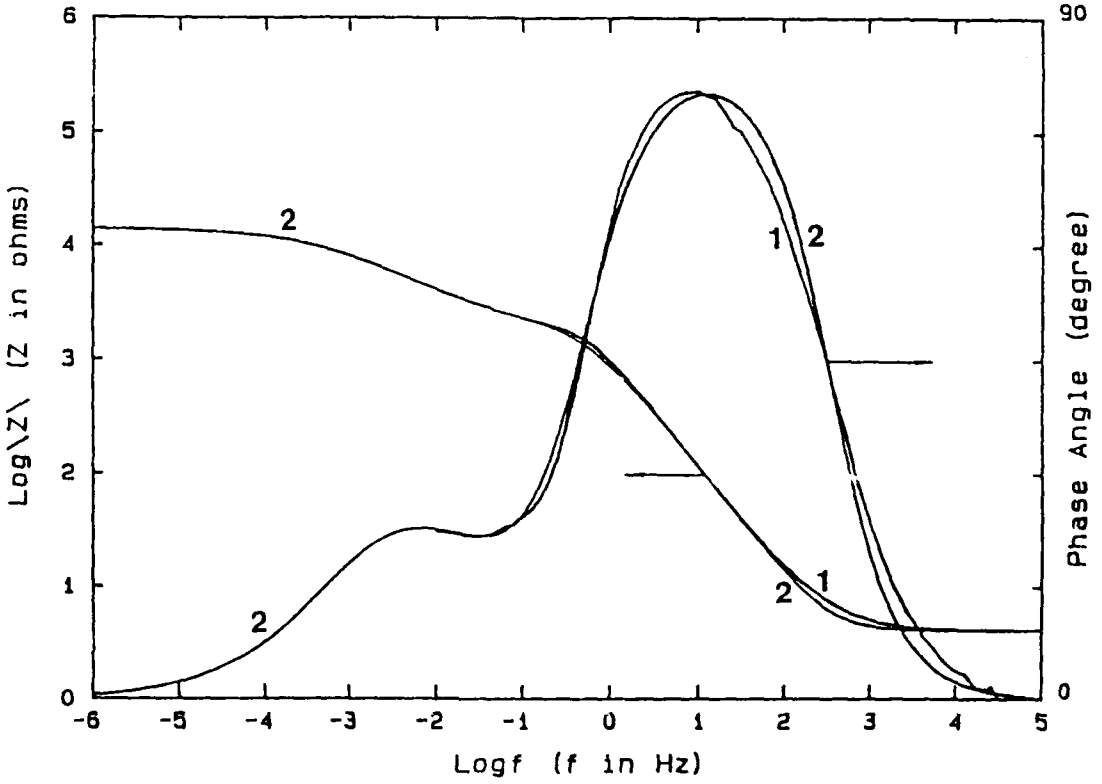

Fig.5 Bode-plots for deoxidized Al 6061 after exposure to 0.5 N NaCl for 24 hr.
Curve 1 - experimental spectra
Curve 2 - extrapolation of the fitted data to very low frequencies with R_s = 4.16 ohm, R_p = 14205 ohm C_t = 175 μF, R_{pit}/F= 2426 ohm, n = -0.59, and K/F= 541.3 ohm $(rad/s)^{-n}$.

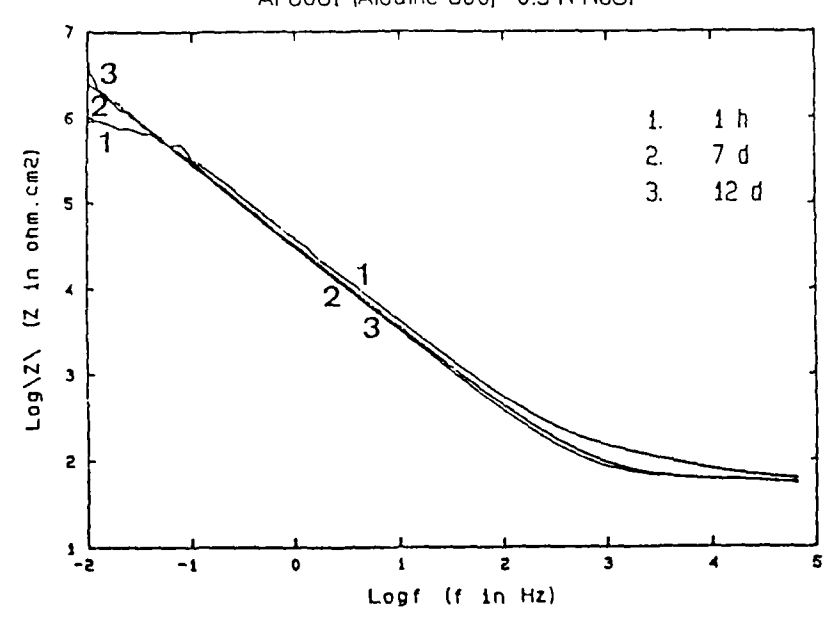

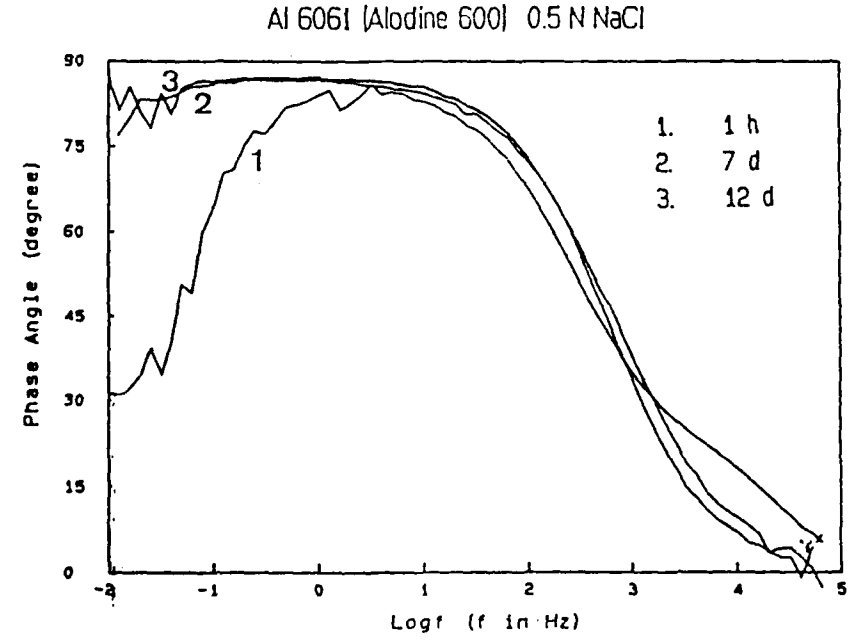

Fig.6.a and b Bode-plots for chromate conversion (Alodine 600) coated Al 6061 as a function of exposure time to 0.5 N NaCl..

The capacitance increased slightly with increasing exposure time and reached a constant value after 8 days (Fig.7.a). The polarization resistance R_p shown in Fig.7.b increased with increasing exposure time. The lower limit value of R_p was about $1 * 10^6$ ohm-cm^2 which corresponds to a corrosion rate of about 0.2 μm/year assuming that the Tafel constant is 20 mV. These results indicate that the Alodine 600 chromate conversion coating provided excellent corrosion resistance for Al 6061.

3.1.2 Al/SiC MMCs

For Al/SiC with the Alodine 600 conversion coating, the spectra in Fig.8.a show the ohmic component at the highest frequencies corresponding to the solution resistance R_s, the linear capacitive region between 0.5 and 5 Hz, and the dc limit at the lowest frequencies corresponding to the polarization resistance R_p. The capacitance decreased with increasing exposure time from curve 1 to curve 2. The spectra in Fig.8.b show that the phase angle was symmetric and had a maximum at about 10 Hz. The surface showed a few pits after 5 days and the coating became discolored due to the leaching of Cr^{+6} from the coating during exposure to NaCl. The capacitance remained constant for 5 days, then decreased slightly with increasing exposure time and reached a constant value after 7 days (Fig.7.a). This decrease may be due to the small capacitance of the pits which should be much less than that of the coating. Also, this small capacitance of the pits may be related to the presence of SiC particulates in the pits. The polarization resistance R_p decreased slightly with increasing exposure time (Fig.7.b). The lower limit value of R_p was about $1.3 * 10^5$ ohm-cm^2 which corresponds to a corrosion rate of about 2 μm/year. These results indicate that the Alodine 600 chromate conversion coating provided better corrosion resistance for Al 6061 than for Al/SiC.

3.1.3 Al/Gr MMCs

Fig.9.a and b show impedance spectra for Al/Gr with the Alodine 600 conversion coating during exposure to 0.5 N NaCl for 49 days. These spectra are very different from those shown in Fig.6 and 8 and show pronounced changes with exposure time. After about three weeks the spectra show a low-frequency dependence of the impedance with a slope $n \approx -0.2$ to -0.4 and a second maximum of the phase angle at the lower frequencies (curves 4-6). When pits penetrated the Al face sheet and reached the graphite fibers, blistering of the Al face sheet was observed and gas evolution occurred occasionally from some isolated spots on the blistered surface. The surface showed pits after 5 days, blisters after 5 days and the evolution of hydrogen gas after 21 days. The spectra show mainly capacitive behavior in the beginning of exposure. After blistering was observed, the spectra in the lower frequency range gradually changed to a transmission line type behavior (curves 4-6). The impedance data were fitted to the pitting model (Fig.4.a) after pitting had occurred. The capacitance shown in Fig.7.a increased with exposure time and increased again when blistering occurred. The polarization resistance R_p for the passive surface increased sharply after pitting initiated and then decreased with exposure time (Fig.9.c). This result suggests that leaching of chromate of valence state +6 from the conversion coating could act as inhibitor and cause a decrease of R_p. The polarization resistance R_{pit}/F (in ohm) for the pitted area decreased with exposure time. This result could be due to an increase of F and/or a decrease of R_{pit}. A separate determination of R_{pit} and F was not possible when these data were analyzed.

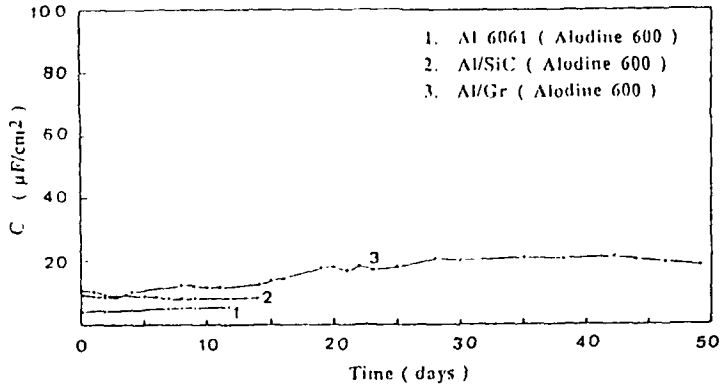

Fig.7.a Capacitance C for Alodine 600 coated Al 6061, Al/SiC, and Al/Gr as a function of exposure time to 0.5 N NaCl.

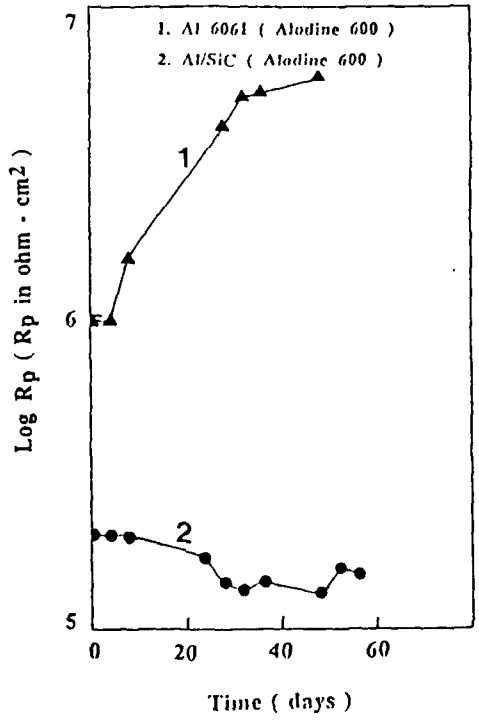

Fig.7.b Polarization resistance R_p for Alodine 600 coated Al 6061 and Al/SiC as a function of exposure time to 0.5 N NaCl.

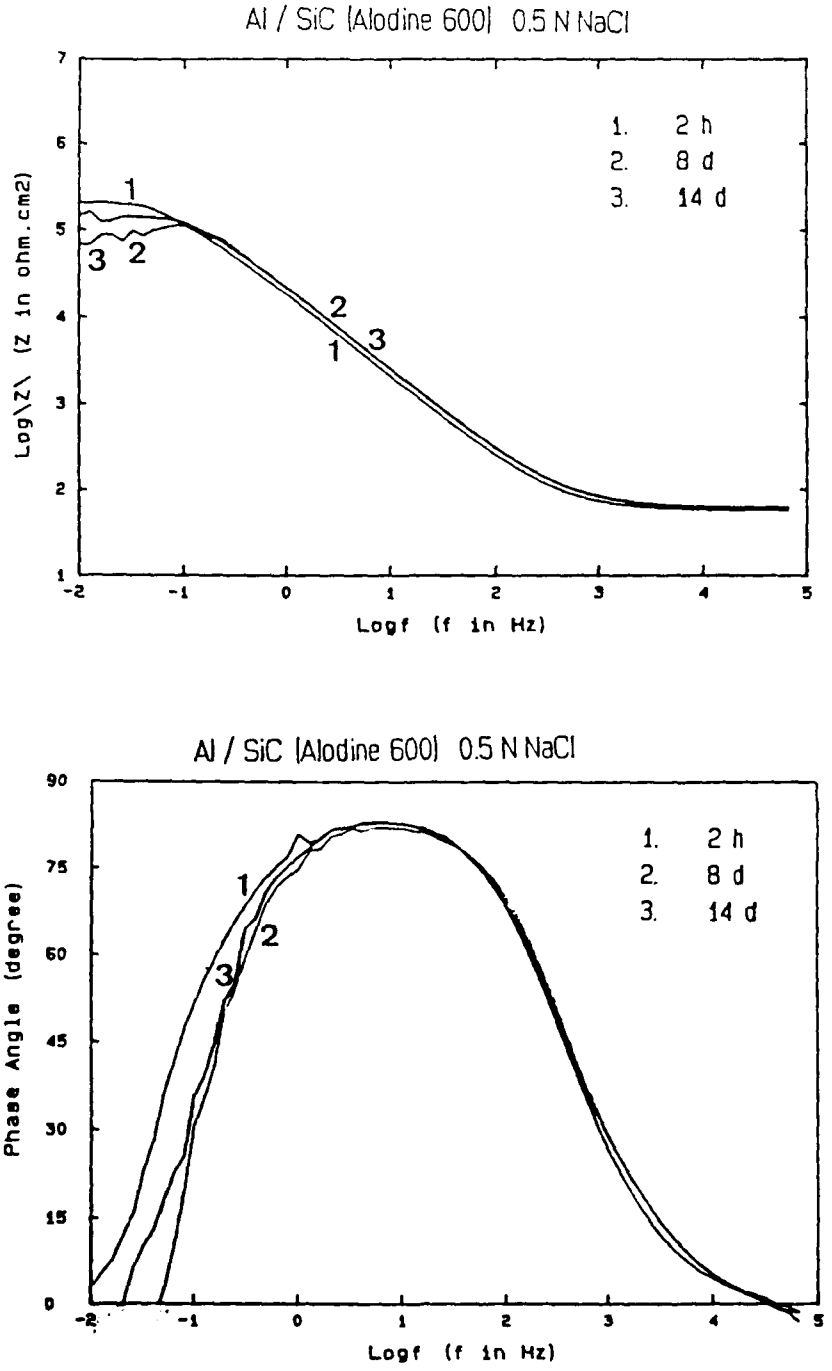

Fig.8.a and b Bode-plots for chromate conversion (Alodine 600) coated Al/SiC as a function of exposure time to 0.5 N NaCl.

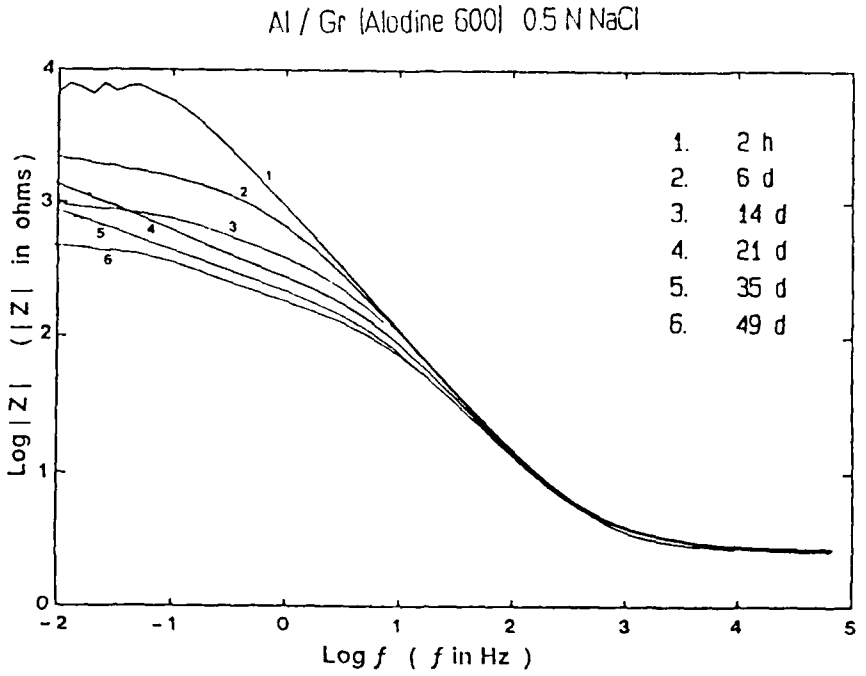

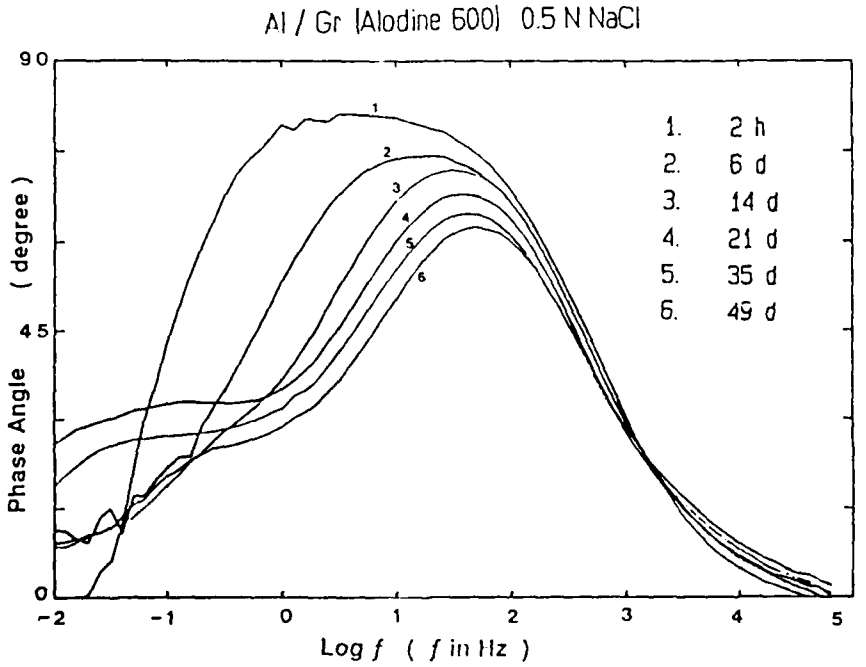

Fig.9.a and b Bode-plots for chromate conversion (Alodine 600) coated Al/Gr as a function of exposure time to 0.5 N NaCl. (A = 20 cm^2)

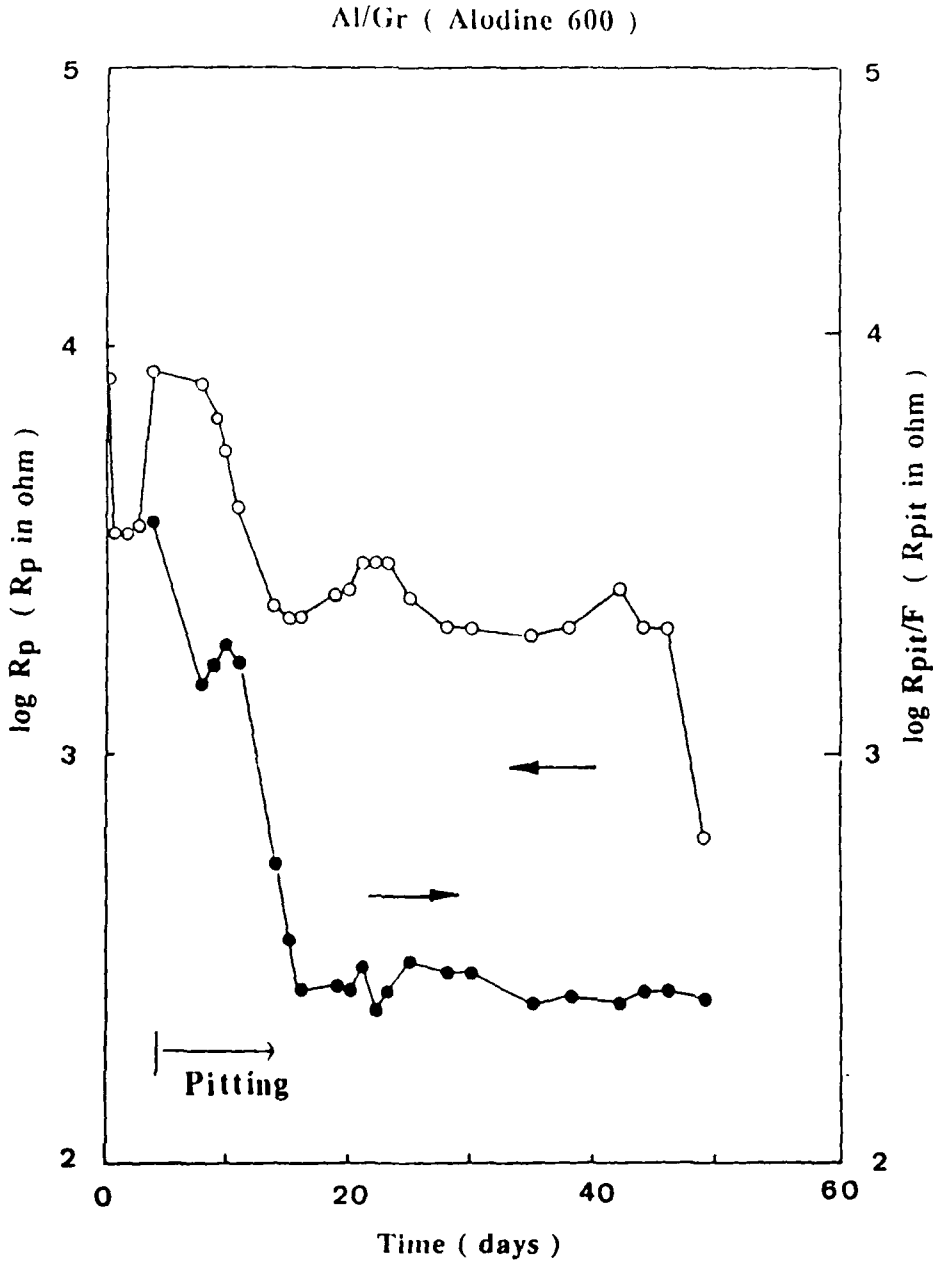

Fig.9.c Time dependence of the polarization resistance Rp and R_{pit}/F for chromate conversion (Alodine 600) coated Al/Gr during exposure to 0.5 N NaCl.

3.1.4 Mg

Fig.10 shows impedance spectra for bare MgAZ31B and MgAZ31B with a dichromate conversion coating (Dow #7), a stannate immersion coating (Dow #23) or a Cr-Mn conversion coating after immersion in 0.5 N NaCl for 2 hr. Fig.10.c shows Nyquist-plots for the data in Fig.10.a and b. All curves show an inductive loop which is the result of the change in the sign of the imaginary part of the impedance and the decrease of the real part of the impedance with increasing frequency in the low-frequency range. The resistive component at a phase angle of zero degree in the low-frequency range of 0.8 to 2 Hz (Fig.10.a.b) or at a value of $Z_{imag} = 0$ (Fig.10.c) corresponds to the transfer resistance R_t decreased in the order Dow #7 > Dow #23 > Cr-Mn conversion coating > as-received Mg. For curve 1, a dc limit can be extrapolated at the lowest frequencies which corresponds to the polarization resistance R_p. Severe pitting was observed for the bare and all conversion coated MgAZ31B samples within 2 hr, indicating that very little improvement in the resistance to NaCl had been achieved by the conversion coatings.

Fig.11.a and b show Bode-plots for bare MgAZ31B exposed to 0.5 N NaCl, 0.5 M Na_2SO_4, deionized water, and ASTM corrosive water (100 ppm each of NaCl, Na_2SO_4 and $NaHCO_3$). The spectra show an inductive loop during exposure to 0.5 N NaCl (curve 1) and capacitive behavior during exposure to the three other solutions. The spectra also show the ohmic component R_s at the highest frequencies corresponding to the solution resistance between the tip of reference electrode and the test electrode surface, the capacitive region between 5 and 50 Hz (curve 2) or between 1 and 5 Hz (curve 3 and 4), and the resistive component at the lowest frequencies corresponding to the polarization resistance R_p for curve 2, 3, and 4. The conductivity of the test solutions decreased in the order 0.5 M Na_2SO_4 > 0.5 N NaCl >> ASTM corrosive water > deionized water. R_p -values were $1 * 10^2$, $1 * 10^4$, $1.9 * 104$, and $5.1 * 10^4$ ohm-cm^2 for MgAZ31B exposed to 0.5 N NaCl, 0.5 M Na_2SO_4, ASTM corrosive water, and deionized water, respectively, after 1 day, indicating that MgAZ31B was much less susceptible to corrosion in Na_2SO_4, ASTM corrosive water, or deionized water than in NaCl. For MgAZ31B exposed to 0.5 N NaCl for 1 day, severe pitting was observed. R_p =100 ohm-cm^2 corresponds to a corrosion rate of about 4.6 mm/year, which shows that it is not possible to expose Mg to NaCl without corrosion protection [40]. On the other hand, for MgAZ31B exposed to 0.5 M Na_2SO_4, ASTM corrosive water, and deionized water, uniform corrosion occurred. The $R_p = 10^4$ ohm-cm2 corresponds to a corrosion rate of about 46 μm/year.

3.2 Anodic Coatings

For the purpose of producing a protective oxide film, anodic coatings were applied to Al and Mg alloys. For Al 6061, the anodizing treatment in sulfuric acid produces an inner continuous barrier layer and an outer porous layer which has to be sealed in hot water to increase its corrosion resistance [20,41]. The application of anodic coatings was also studied for the Al/SiC MMC. An anodic coating (Dow # 17) was applied to MgAZ31B and was sealed in hot water glass solution.

3.2.1 Al 6061

Fig. 12 shows impedance spectra obtained during exposure to 0.5 N NaCl for 77 days at 20°C for Al 6061 with the conventional anodizing treatment in sulfuric

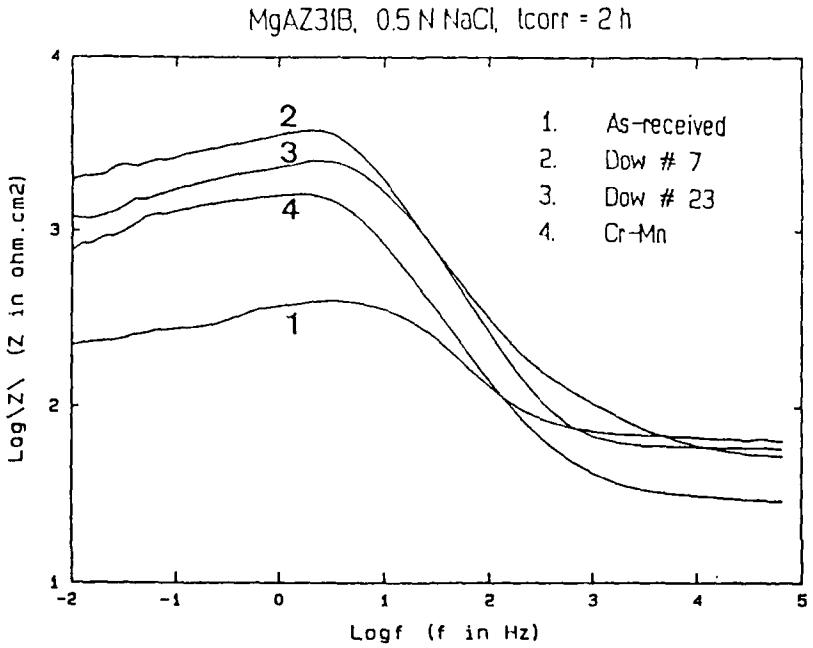

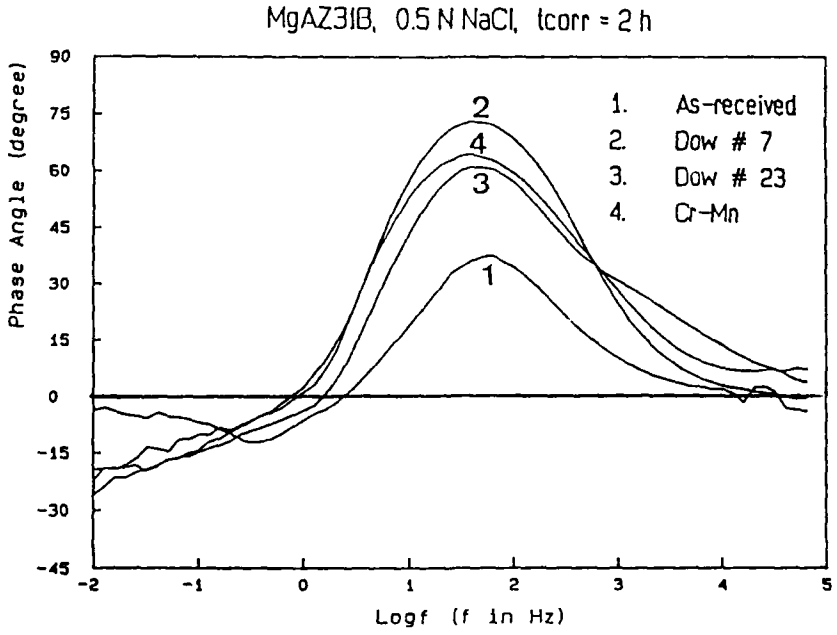

Fig.10.a and b Bode-plots for bare (curve 1), Dow #7 (curve 2), Dow #23 (curve 2), and Cr-Mn coated (curve 4) Mg as a function of exposure time to 0.5 N NaCl.

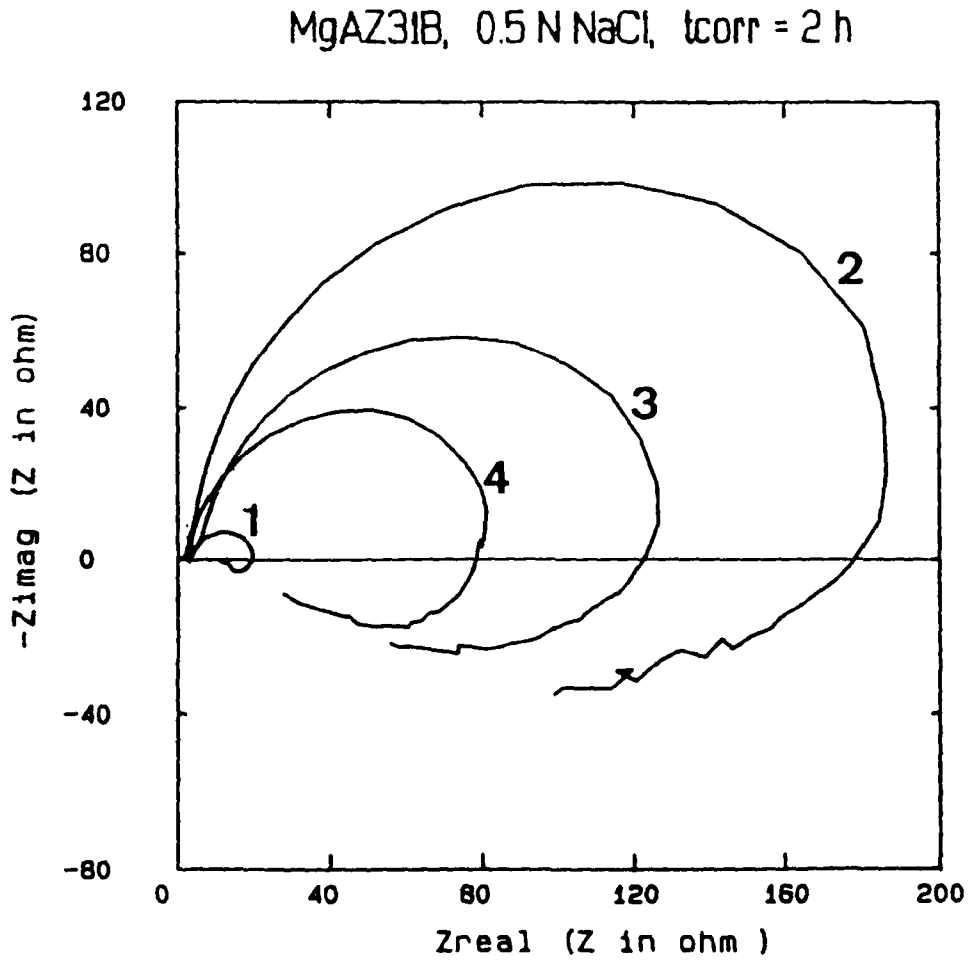

Fig.10.c Nyquist-plots for bare (curve 1), Dow #7 (curve 2), Dow #23 (curve 3), and Cr-Mn coated(curve 4) Mg as a function of exposure time to 0.5 N NaCl.

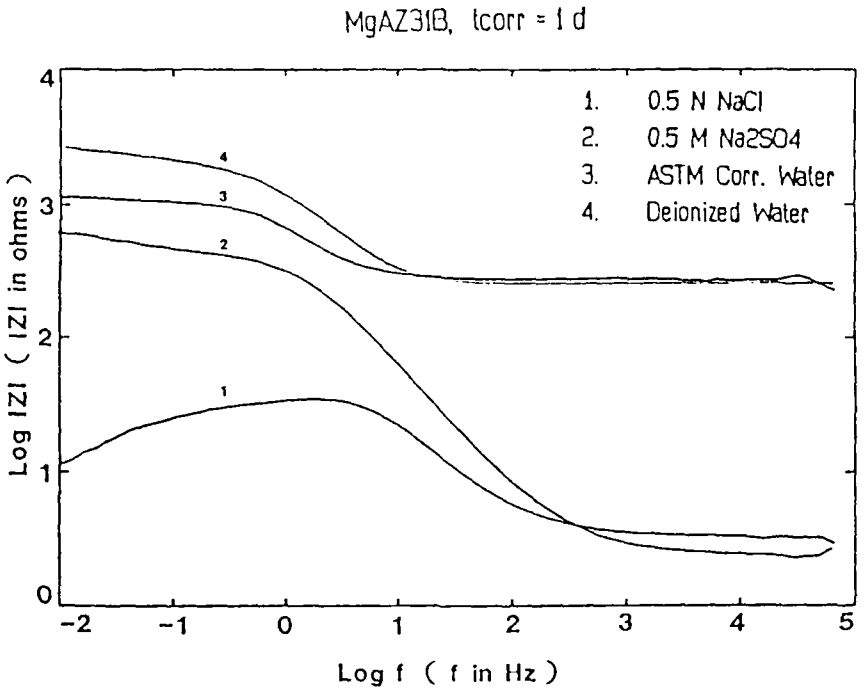

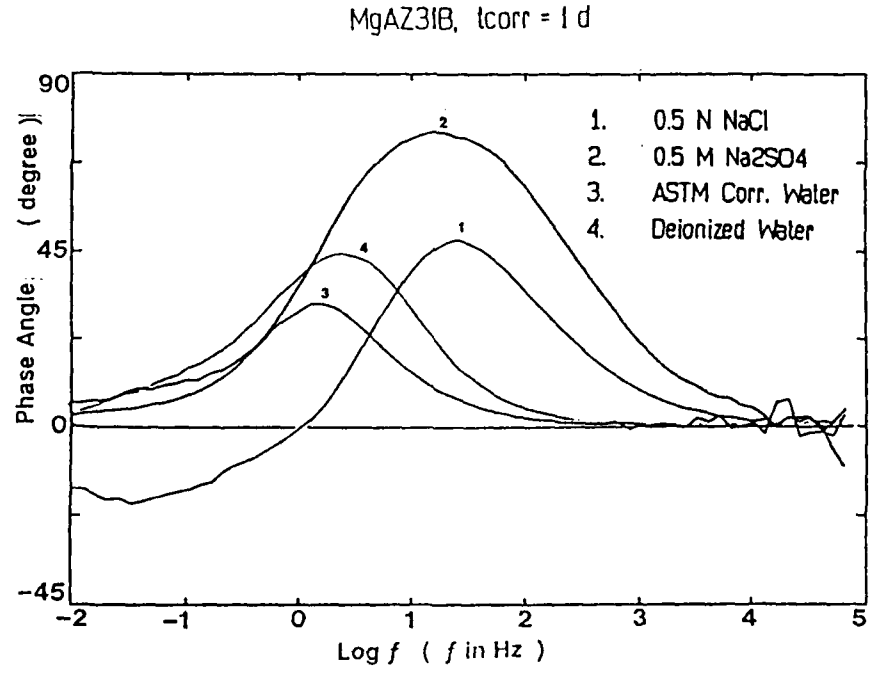

Fig.11.a and b Bode-plots for bare Mg exposed to 0.5 N NaCl, 0.5 M Na_2SO_4, ASTM corrosive water and deionized water after one day. (A = 20 cm^2)

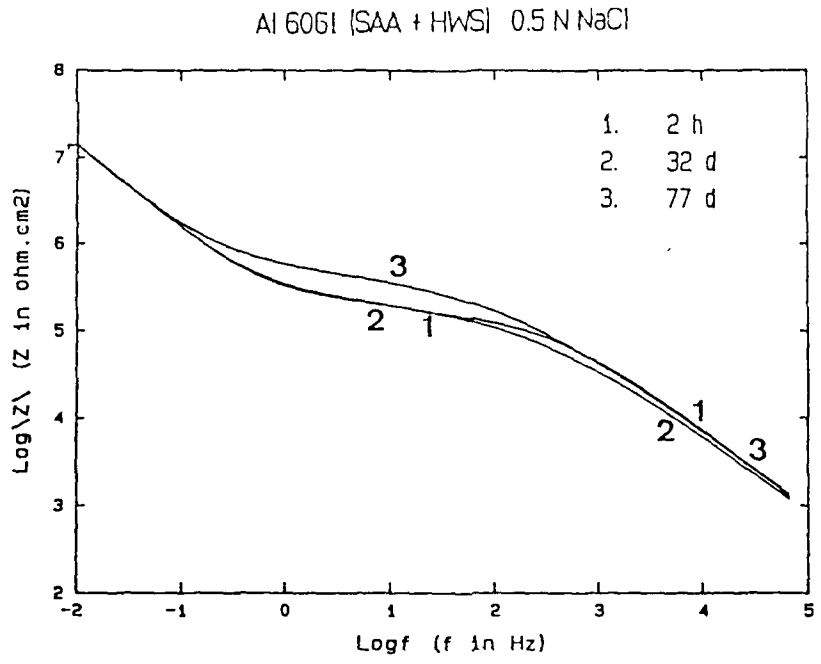

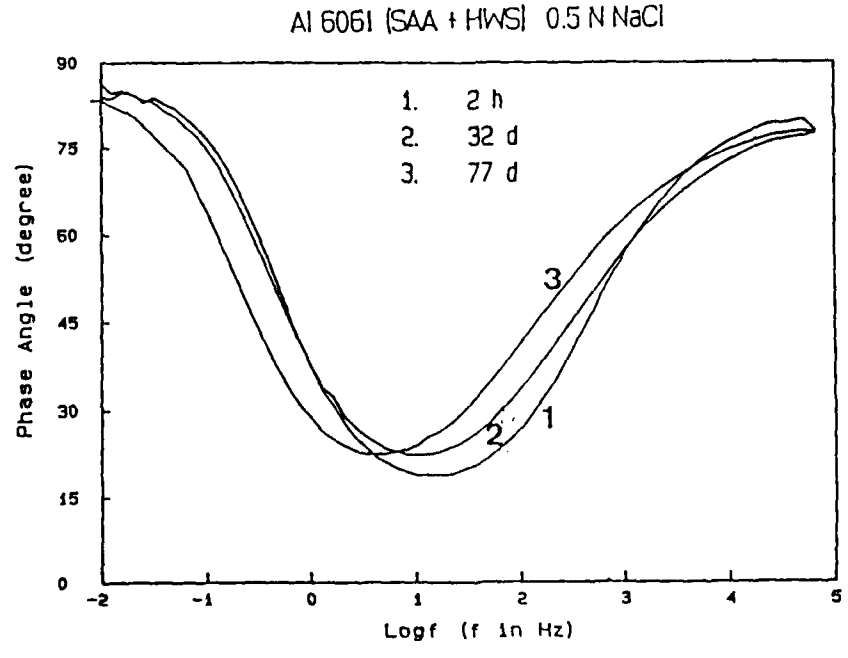

Fig.12.a and b Bode-plots for anodized Al 6061(SAA + HWS) as a function of exposure time to 0.5 N NaCl.

acid (SAA) followed by hot water sealing (HWS). The spectra show the capacitance C_p of the porous layer in the high-frequency region, the capacitance C_b of the barrier layer in the low-frequency region, and the resistive component R_{po} of the porous layer in the frequency range of 5 to 50 Hz. Similar impedance data have been reported by other investigators [42-45]. The resistance of the barrier layer is too large to appear in the measured frequency range. The capacitance of the barrier layer did not change with exposure time, but the capacitance of the porous layer increased somewhat with exposure time as shown in Fig 13. The surface did not show any pits after exposure for 77 days.

The spectra in Fig.14 for hard anodized Al 6061 (SAA and HWS) also show the capacitance C_p of the porous layer in the high frequency region, the capacitance C_b of the barrier layer in the low frequency region, and the resistive component of the porous layer R_{po} in the frequency range of 10 to 100 Hz. The capacitances of barrier layer and porous layer for the hard anodized Al 6061 were less than those for the conventionally anodized Al 6061 (Fig.13) due to the larger thicknesses of the barrier layer and the porous layer for the hard anodized Al 6061. The capacitance of the barrier layer for hard anodized Al 6061 remained constant during 102 days of exposure (Fig.13). However, the capacitance of the porous layer slightly decreased with exposure time (Fig.13). The surface of hard anodized Al 6061 did not show pits during the exposure time of 102 days. These results demonstrate that anodic coatings produced in sulfuric acid followed by hot water sealing provide excellent corrosion resistance for Al 6061.

The capacitance of a parallel-plate capacitor with a dielectric between its plates is

$$C = e\, e_o\, A/d \qquad (3.1)$$

where C is the capacitance (in farads), e is the dielectric constant, e_o is the permittivity of empty space· A is the area of the plates (in meters), and d is the distance between the parallel plates (in meters). For the tested samples A was 20 cm^2, the dielectric constant of the porous layer has been reported as e = 55 and that of the barrier layer as 10 [41,44]. Based on the measured capacitance values $C_b = 7.9 * 10^{-7}$ F/cm^2 and $C_p = 8.8 * 10^{-10}$ F/cm^2 for hard anodized Al 6061, the thicknesses of the barrier layer and the porous layer were calculated as 112 Å and 55 μm, respectively. For conventionally anodized Al 6061, for which $C_b = 1.04 * 10^{-6}$ F/cm^2 and $C_p = 2.94 * 10^{-9}$ F/cm^2 (Fig.14), the thickness of the barrier layer was calculated to be 86 Å and that of the porous layer was 17 μm.

3.2.2 Al/SiC MMCs

Fig.15 shows impedance spectra obtained during exposure to 0.5 N NaCl at 20°C for Al/SiC with the conventional anodizing procedure in sulfuric acid (SAA) and hot water sealing (HWS). The spectra shown in Fig.15 are quite different from those for anodized Al 6061 in Fig.12. The surface showed pits after 22 days and severe general corrosion damage after 34 days. Crevice corrosion was observed at the end of the corrosion test under the O-ring which sealed the test cell (Fig.1). This might have occurred after 7 days when an increase of the capacitance was observed without the observation of pitting (Fig.15, curve 2). The spectra were in agreement with a two-time-constant-model at the beginning of exposure and then changed to essentially capacitive behavior after 29 days.

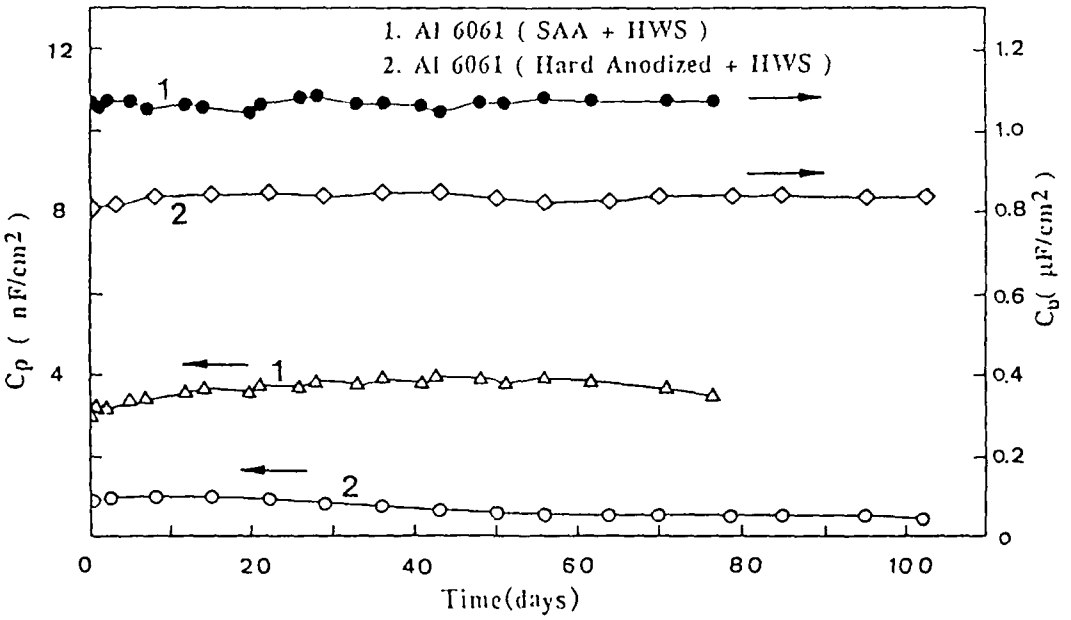

Fig.13 Time dependence of the capacitances C_b and C_p for conventional and hard anodized Al 6061 (SAA + HWS) during exposure to 0.5 NaCl.

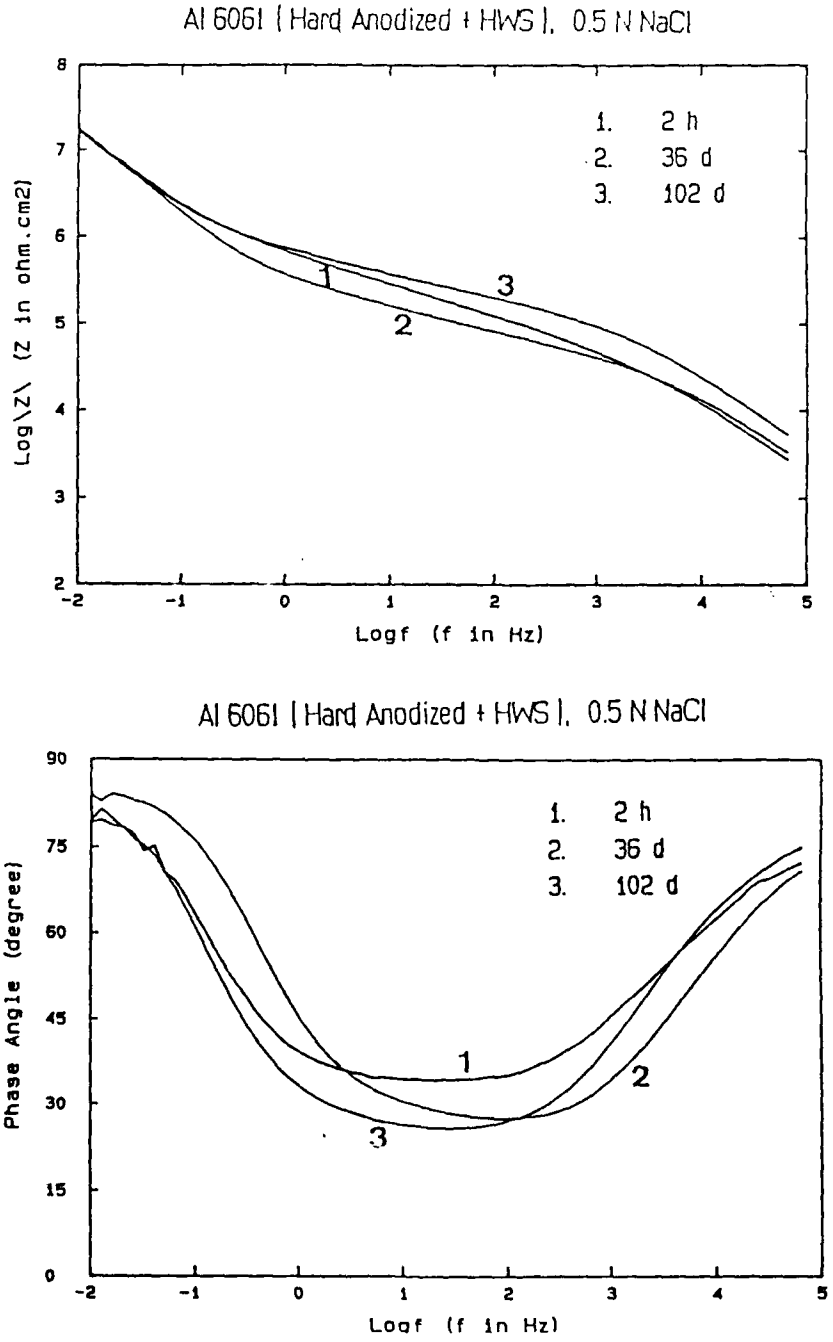

Fig.14.a and b Bode-plots for hard anodized Al 6061 (SAA + HWS) as a function of exposure time to 0.5 N NaCl.

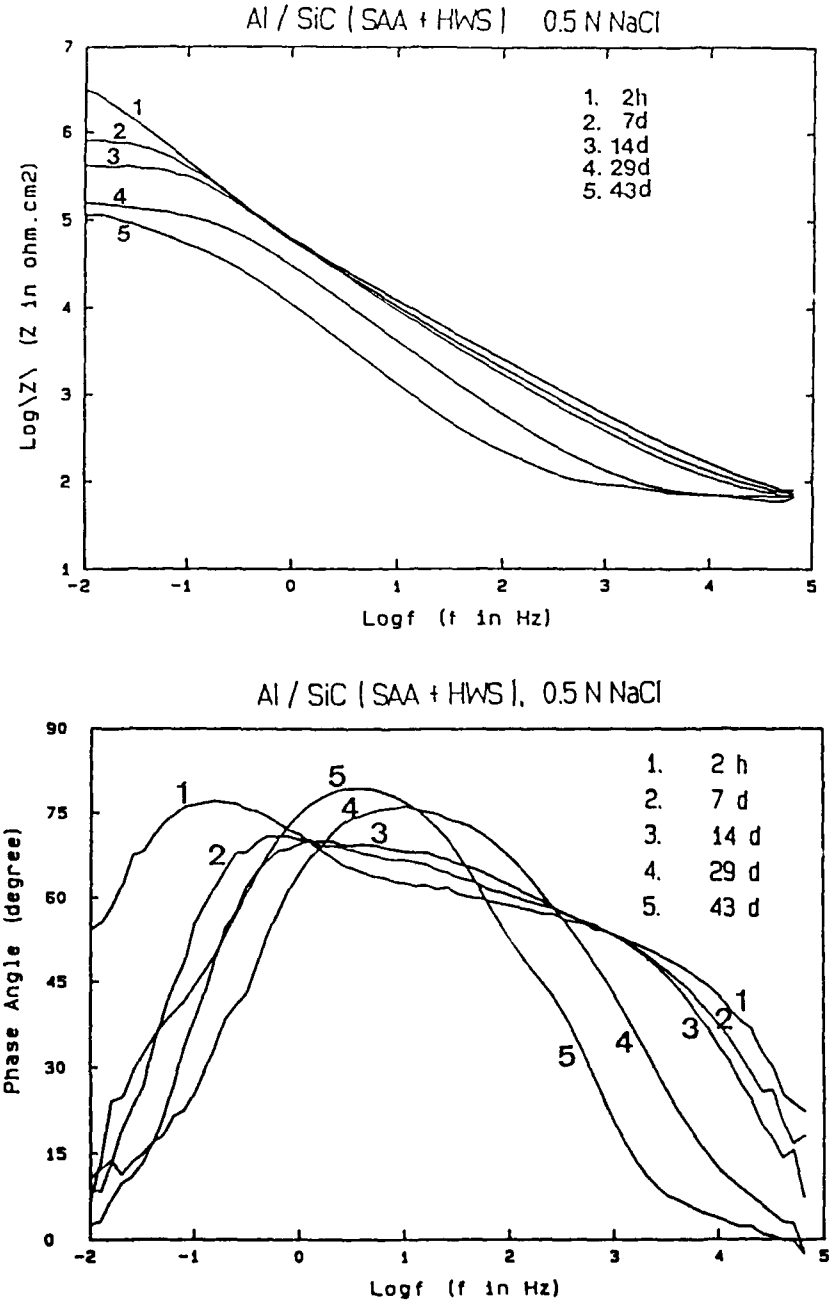

Fig.15.a and b Bode-plots for anodized Al/SiC (SAA + HWS) as a function of exposure time to 0.5 N NaCl.

The severe corrosion damage seems to be reflected in the large increase of the capacitance with time (Fig.15, curve 4 and 5).

Fig.16 shows impedance spectra in 0.5 N NaCl at 20°C for Al/SiC after hard anodizing in sulfuric acid (SAA) and hot water sealing (HWS). The spectra show essentially capacitive behavior and are different from those for Al 6061 (SAA+HWS) in Fig.12 and Fig.13. The surface showed pits after 11 days. Crevice corrosion was observed at the end of test under the O-ring. The increase of the capacitance after 3 days shown in Fig.17 is thought to be due to crevice corrosion. Obviously, the corrosion resistance of hard anodized SiC/Al was even less than that of conventionally anodized SiC/Al. If the presence of SiC particulates prevented the formation of a continuous barrier layer, one can assume that the more SiC particulates are incorporated, the less is the area fraction of the continuous barrier layer. It can be assumed that the oxide layer of the hard anodized SiC/Al contains more SiC particulates than that of the conventionally anodized SiC/Al due to the larger thickness of the hard anodized layer. Hence, it seems likely that because the area fraction of the continuous barrier layer for hard anodized SiC/Al was less than that for conventionally anodized SiC/Al, the corrosion resistance was inferior.

3.2.3 Mg

Fig.18 shows impedance spectra obtained during immersion in 0.5 N NaCl for MgAZ31B prepared with the Dow #17 anodizing treatment and sealed in hot water glass solution. The spectra show the ohmic component at the highest frequencies corresponding to the solution resistance R_s, and the capacitive region in the frequency range of 50 to 100 Hz. The resistive component at the lowest frequencies corresponding to the polarization resistance R_p was observed for an exposure of 2 hr (curve 1). An inductive loop occurred for longer exposure times (curve 2 and 3). The low-frequency part of the impedance had a slope of $n = + 0.1$ in the frequency range of 0.01 to 0.7 Hz (Fig.18.a). The phase angle changed its sign at about 0.7 Hz (Fig.18.b). This inductive loop is considered to be due to pitting which occurred after 1 day. Fig.18.c shows Nyquist-plots for the same data. Curve 2 and 3 show an inductive loop and a decrease of R_t with exposure time. These results demonstrate that the anodic coating (Dow #17) did not produce a very corrosion resistance surface.

3.2.4 Summary

Table II gives a comparison of damage times for the samples studied. For Al 6061, chromate conversion coatings and anodizing (SAA + HWS) provided excellent corrosion protection. Chromate conversion coatings provided significant corrosion protection for Al/SiC and Al/Gr, but were not as effective as for Al 6061. Anodizing provided protection for Al/SiC, but the structure of the anodized layers was affected by the SiC particulates. For Mg, conversion coatings and anodizing did not provide significant corrosion resistance in 0.5 N NaCl.

3.3 Chemical Passivation

Chemical passivation in $CeCl_3$ is simple and non-toxic, and may provide an alternative to the use of chromate conversion coatings for Al alloys and Al-based MMCs. The materials studied were passivated by immersion in 1000 ppm $CeCl_3$ and then exposed to 0.5 N NaCl as a test of the corrosion resistance of the

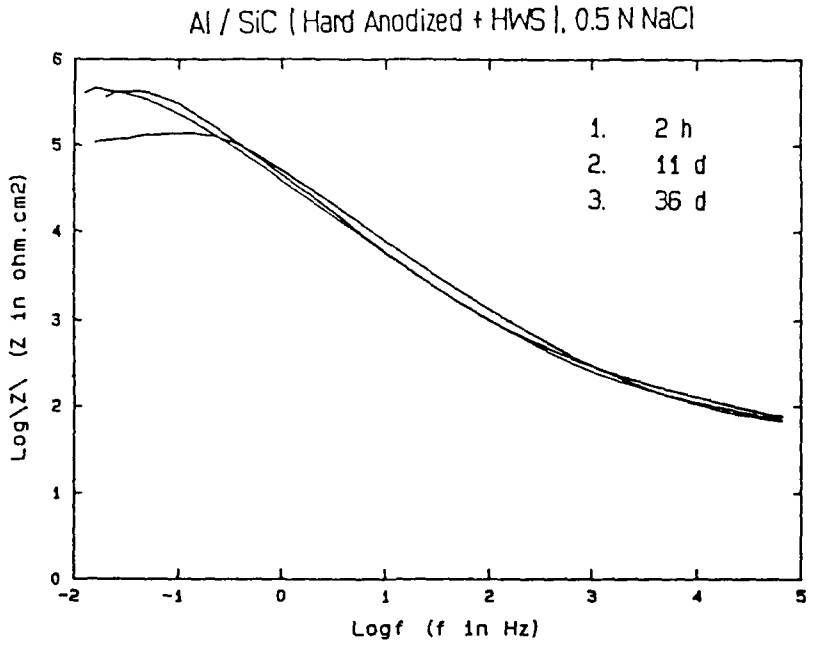

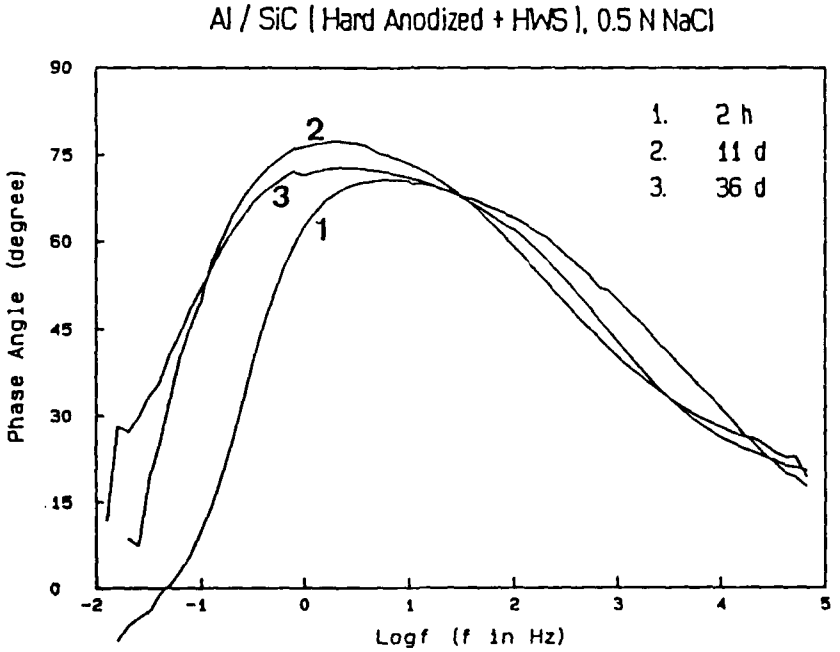

Fig.16.a and b Bode-plots for hard anodized Al/SiC (SAA + HWS) as a function of exposure time to 0.5 N NaCl.

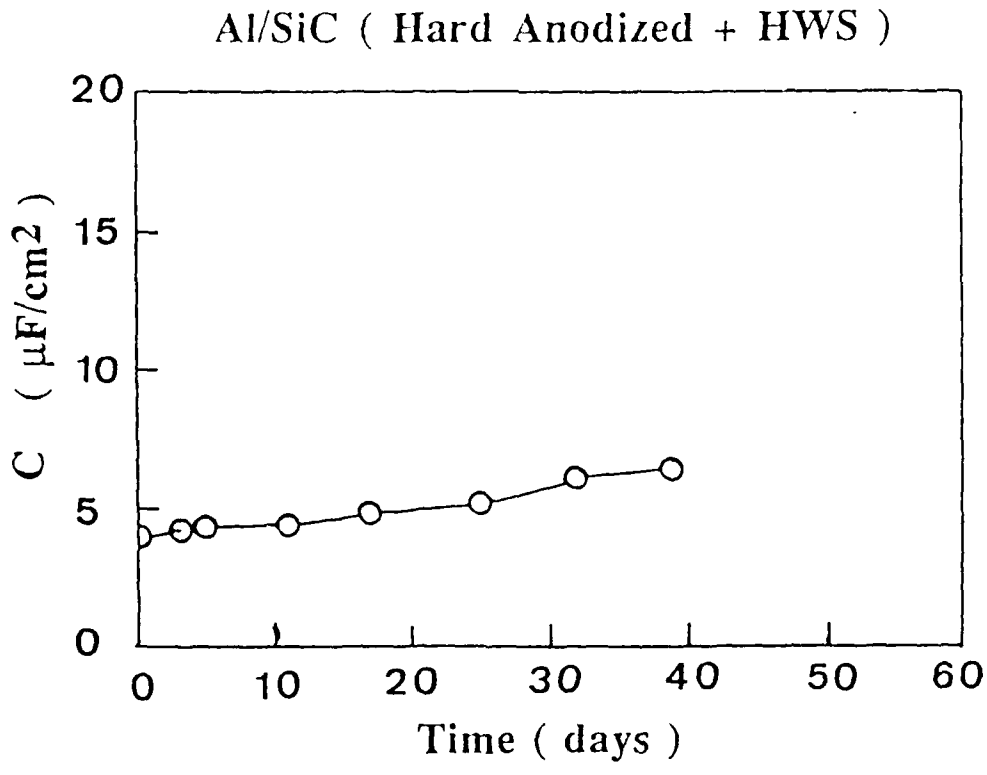

Fig.17 Capacitance C for hard anodized Al/SiC (SAA + HWS) as a function of exposure time to 0.5 NaCl.

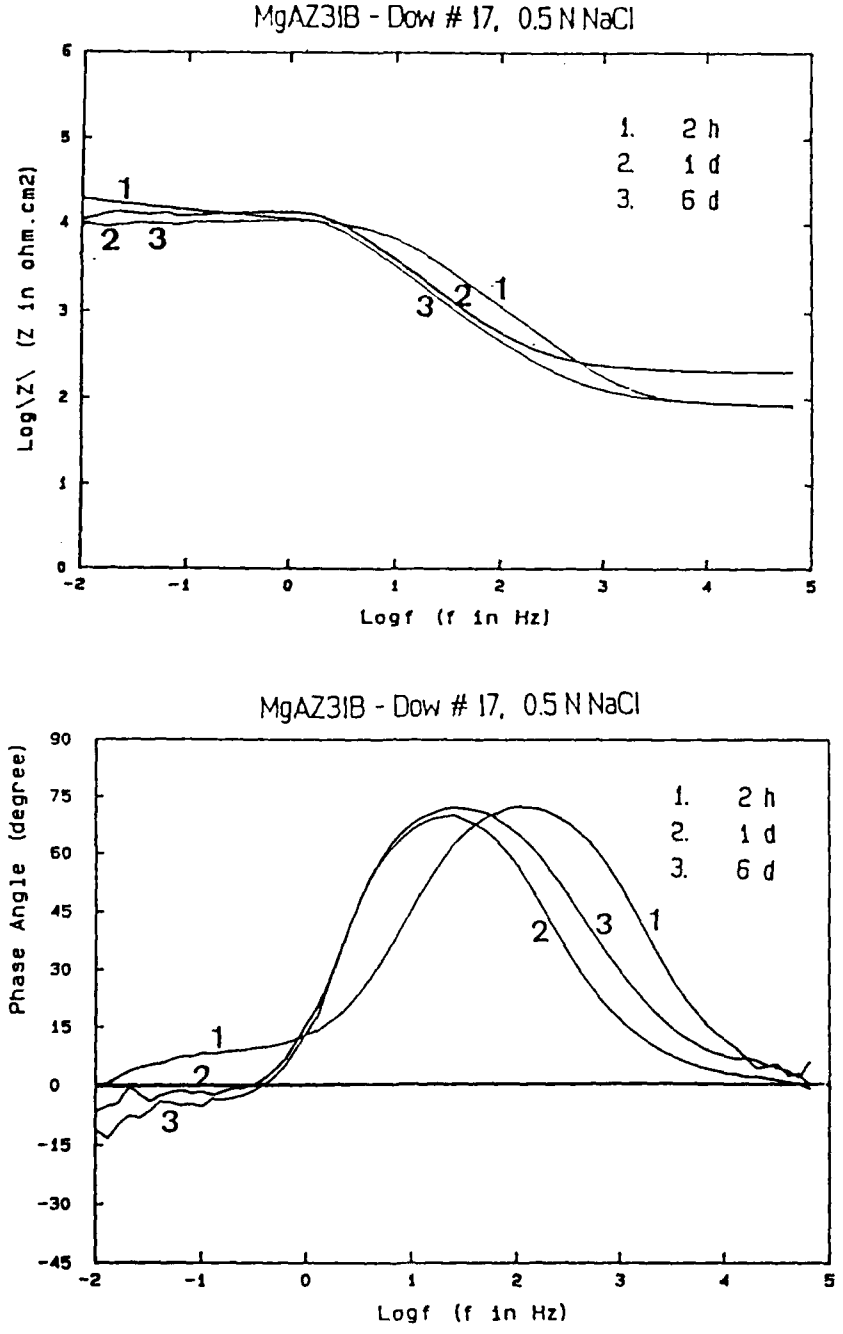

Fig.18.a and b Bode-plots for anodized Mg (Dow #17) as a function of exposure time to 0.5 N NaCl.

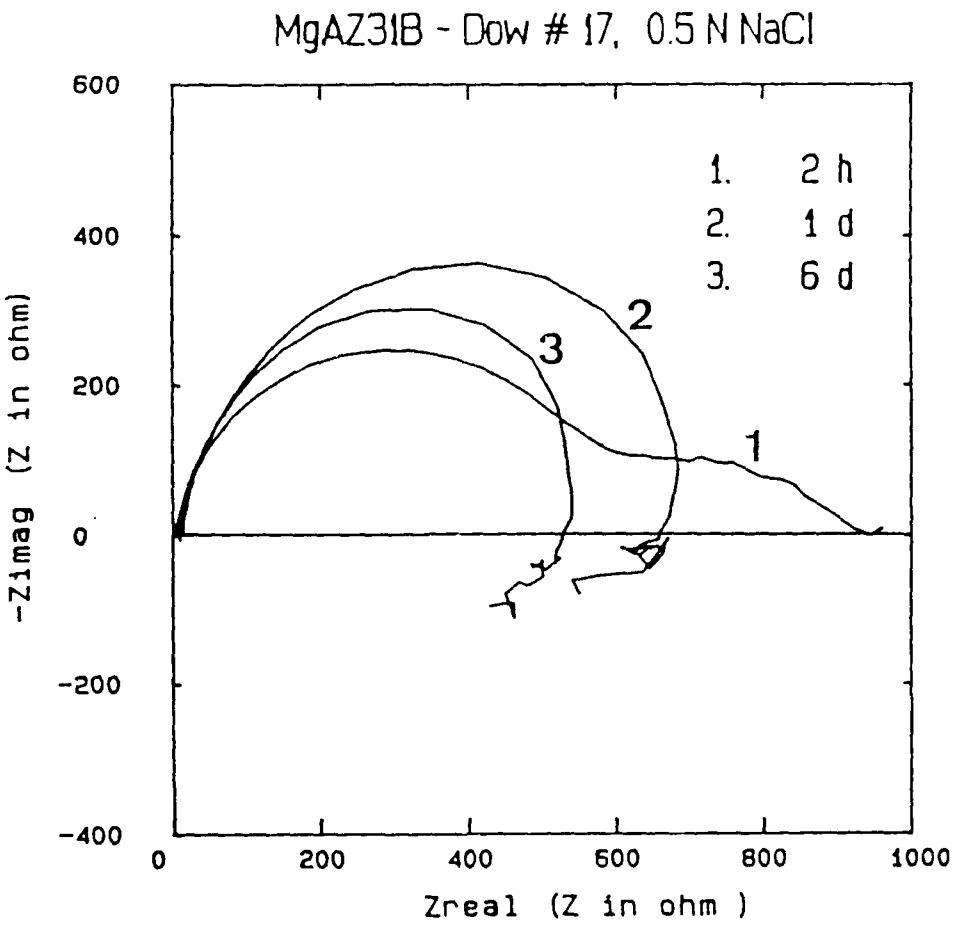

Fig.18.c Nyquist-plots for anodized Mg (Dow #17) as a function of exposure time to 0.5 N NaCl.

Table II Comparison of Pitting Time for Chromate Conversion and Anodized (SAA + HWS) Coated Samples (t_p = pitting time (in days))

Material	Untreated	Conversion Coating	Anodized	Hard anodized
Al 6061	$t_p < 1$	>12 (no pits)	> 77 (no pits)	>102 (no pits)
Al/SiC	$t_p < 1$	$t_p > 5$	$t_p > 22$	$t_p > 11$
Al/Gr	$t_p < 1$	$t_p > 5$	*	*
MgAZ31B	$t_p < 1$ hr	$t_p < 2$ hr (Dow #7) $t_p < 2$ hr (Dow # 23) $t_p < 2$ hr (Cr-Mn)		$t_p < 1$ (Dow #17)

*The Al 6061 face sheet of 50 μm was too thin to be anodized in sulfuric acid.

passive layers. It was observed that it was possible to use EIS to monitor the improvement of the corrosion resistance of the Al alloys and Al-based materials during exposure to the $CeCl_3$ solution. In the following, experimental EIS data and the results of the data analysis will be presented for the materials studied as a function of exposure time in $CeCl_3$ and subsequent exposure in 0.5 N NaCl.

3.3.1 Al 6061

3.3.1.1 Deoxidized Surfaces

Al 6061 was pretreated by hot hexanes, Ridoline 53 and Deoxidizer 7. Fig.19 shows impedance spectra for deoxidized Al 6061 obtained during exposure to $CeCl_3$. The spectra show mainly capacitive behavior in the frequency range of 0.5 to 5 Hz and the ohmic component at the highest frequencies corresponding to the solution resistance R_s. At sufficiently low frequencies a dc limit is observed which corresponds to R_p. An increase of R_p with exposure time in $CeCl_3$ is observed, which suggests that the corrosion resistance was increasing. An small increase of the capacitance after one day exposure to $CeCl_3$ was also observed (Fig.19.a). Fig.20.a shows that the capacitance increased from 5.5 $\mu F/cm^2$ after 2 hr immersion to 6.8 $\mu F/cm^2$ after one day immersion, and then remained unchanged. The dielectric constants for Al_2O_3 and CeO_2 are 12.3 and 21.3, respectively [46]. Hence this result could be due to a thinner film and/or a larger value of its dielectric constant. However, the passive film could not have become thinner because the polarization resistance had increased after 1 day of immersion. Therefore, the observed increase of the capacitance suggests that parts of the Al_2O_3 in the surface layer were replaced by CeO_2 or $Ce(OH)_3$. The polarization resistance was low after 2 hr immersion (Fig. 20.b), because Al alloys still corroded to some extent during the initial stages of passivation. As the passivating film was formed, the polarization resistance increased to $1.6 * 10^6$ ohm-cm^2 after one-day immersion and then remained unchanged. The corrosion potential E_{corr} increased with immersion time (Fig.20.c, curve 1). The passivation process might be completed when the capacitance C, the polarization resistance R_p and the corrosion potential E_{corr} become constant. For deoxidized Al 6061, the termination of the passivation might not be reached for one week immersion, because E_{corr} still had a trend to increase after 7 days. Data such as those shown in Fig.20 can be used to determine the optimal passivation time in $CeCl_3$ for each of the materials studied.

Fig.21 shows impedance spectra for deoxidized Al 6061 which was untreated or passivated for one week in $CeCl_3$ during exposure to 0.5 N NaCl. The spectra show mainly capacitive behavior in the frequency range of 5 to 50 Hz, and a low-frequency dependence of the impedance with a slope of -0.2 to -0.5 starting at about 0.1 Hz. The low-frequency dependence of the impedance with a negative small slope n and the corresponding maximum of the phase angle of 90 * n have recently been identified as being due to pitting [11,12]. Obviously, curves 1-4 in Fig.21 show pitting behavior at the lowest frequencies. However, pitting was not detected visually for passivated Al until the 3rd day of exposure to NaCl. This result suggests that pits initiated after 2 days and that the initial pits were too small to be observed visually. Hence, EIS can serve as a very sensitive monitor to detect the onset of pitting. The capacitive region of curves 1 and 3 changed to that of curve 2 and 4, respectively (Fig.21), because the capacitance increased. These large increases of the capacitance with exposure time are due to severe pitting [11,12]. The corrosion resistance of

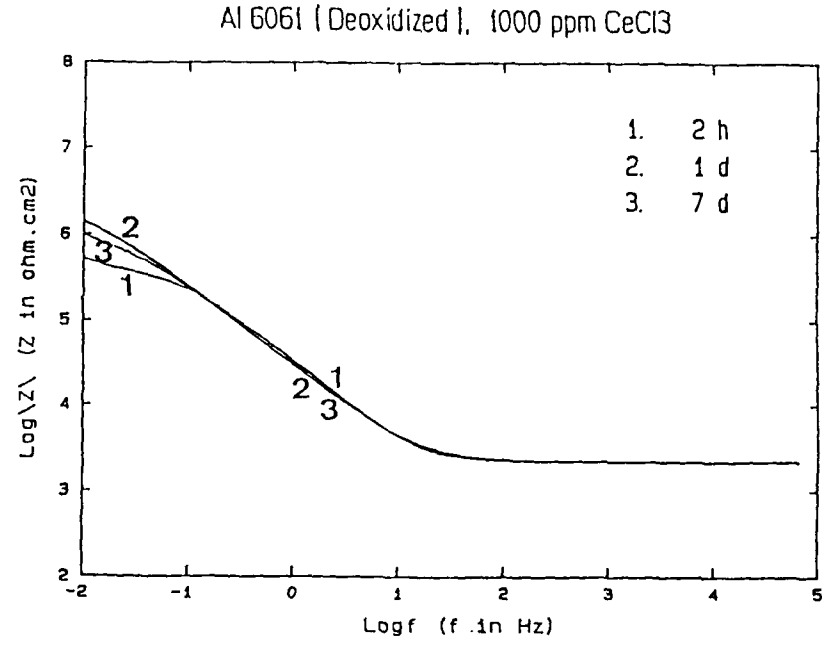

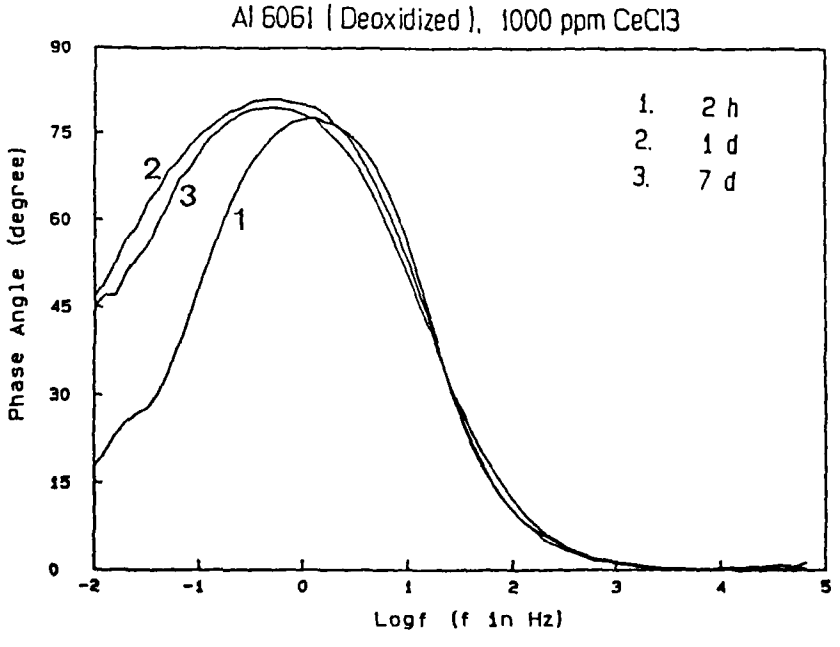

Fig.19.a and b Bode-plots for deoxidized Al 6061 as a function of immersion time in 1000 ppm $CeCl_3$.

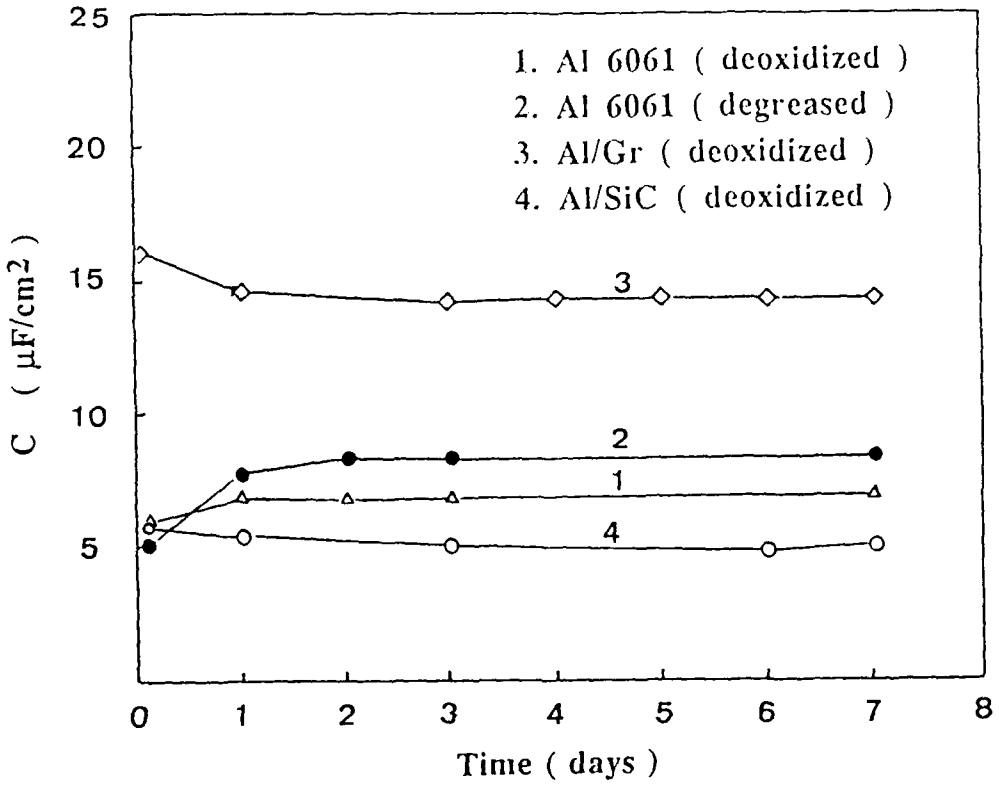

a

Fig.20 Analysis of impedance data for deoxidized Al 6061 (curve 1), degreased Al 6061(curve 2), deoxidized Al/Gr (curve 3), and deoxidized Al/SiC (curve 4) as a function of immersion time in 1000 ppm $CeCl_3$: (a) capacitance C, (b) polarization resistance Rp, (c) corrosion potential Ecorr.

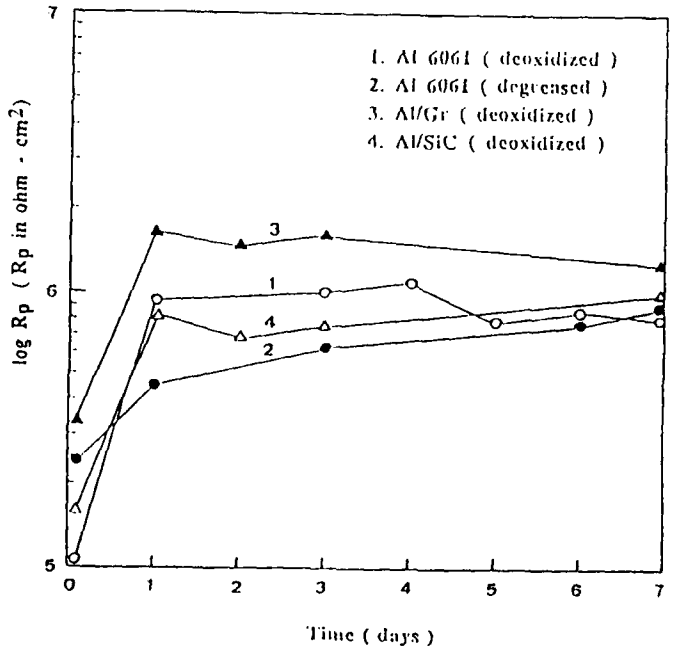
1. Al 6061 (deoxidized)
2. Al 6061 (degreased)
3. Al/Gr (deoxidized)
4. Al/SiC (deoxidized)
log Rp (Rp in ohm - cm2)
Time (days)

b

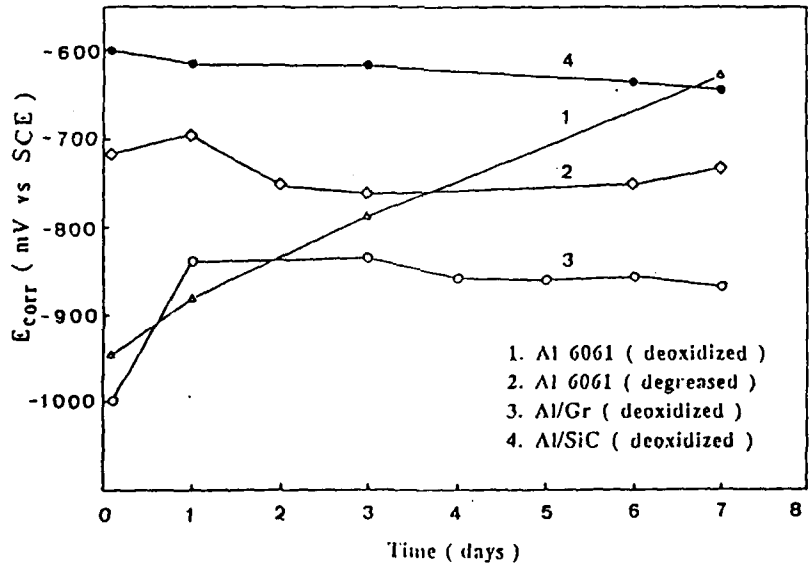
1. Al 6061 (deoxidized)
2. Al 6061 (degreased)
3. Al/Gr (deoxidized)
4. Al/SiC (deoxidized)
Ecorr (mV vs SCE)
Time (days)

c

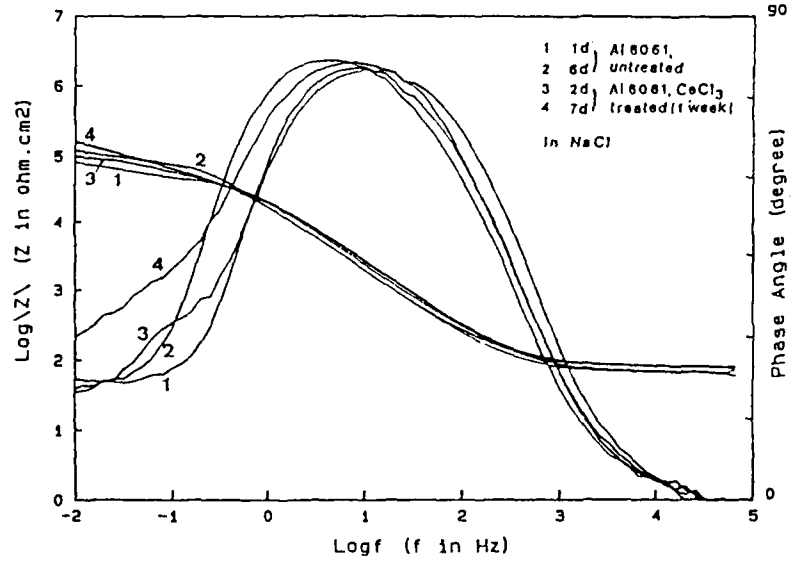

Fig.21 Bode-plots for deoxidized Al 6061 which was untreated (curve 1 and 2) or passivated in $CeCl_3$ for one week (curve 3 and 4) as a function of exposure time to 0.5 N NaCl.

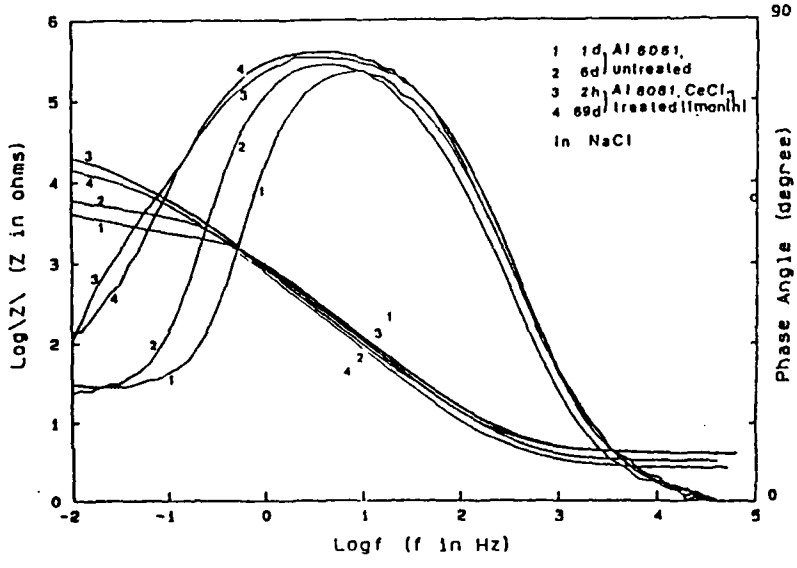

Fig.22 Bode-plots for deoxidized Al 6061 which was untreated (curve 1 and 2) or passivated in $CeCl_3$ for one month (curve 3 and 4) as a function of exposure time to 0.5 N NaCl.
(A = 20 cm^2)

Al 6061 (deoxidized) which had been passivated for one week in $CeCl_3$ was not much better during exposure to 0.5 N NaCl than that of the untreated samples, as can be seen from the fact that the impedance of curve 4 for the passivated sample at 0.01 Hz is not much larger than that of curve 2 for the as-received sample (Fig.21).

In order to evaluate the effect of the immersion time in $CeCl_3$ on the resulting corrosion resistance, deoxidized Al 6061 was passivated in $CeCl_3$ for one month. The spectra in Fig.22 obtained during exposure to 0.5 N NaCl show essentially capacitive behavior between 5 and 50 Hz, and pitting behavior in the low-frequency range for curves 1 and 2. Curve 3 for the passivated sample shows mainly capacitive behavior. One pit was detected visually after 29 days of exposure. Curve 4 shows an increase of the capacitance after 69 days, but did not clearly show the changes in the frequency dependence of the impedance and phase angle in the low-frequency range for a pitted surface. This result suggests that transmission line type impedance should be observed at frequencies below 0.01 Hz. The impedance at 0.01 Hz for curves 1 and 2 is much small than that for curves 3 and 4. Hence the corrosion resistance of deoxidized Al 6061 which was passivated for one month in $CeCl_3$ was much better than that of an untreated sample. Also, deoxidized Al 6061 which had been passivated in $CeCl_3$ for one month was much more corrosion resistant than the sample which had been passivated for only one week (Fig.22 vs. Fig.21). Therefore, an immersion time of one week is not enough for deoxidized Al 6061 to form a stable passivating film. It seems to be necessary to use longer immersion times until E_{corr} reaches a constant value (Fig. 20.c).

3.3.1.2 Degreased Surfaces

Impedance spectra obtained during immersion in 1000 ppm $CeCl_3$ for degreased Al 6061, which was only treated with hot hexanes, show mainly capacitive behavior (Fig.23.). The spectra also show that the impedance increased greatly with exposure time at the lowest frequencies. The capacitance increased from 5 $\mu F/cm^2$ after 2 hr immersion to 8.3 $\mu F/cm^2$ after 2 days immersion, and then remained unchanged (Fig.20.a). This increase of the capacitance might be due to the increase of the dielectric constant of the passivating film as the Al_2O_3 in the oxide film is replaced by Ce oxides and/or hydroxides. The polarization resistance was also low after 2 hr immersion (Fig.20.b). As the passivating film was formed, the polarization resistance increased to about $1.0 * 10^6$ ohm-cm^2 after 1 day immersion, and then remained unchanged. The corrosion potential remained stable after 2 days (Fig.20.c). Hence, the passivation process might be completed already after only 2 days.

Fig.24.a and b show impedance spectra between 10^{-3} Hz and 65 kHz obtained in 0.5 N NaCl for 90 days for passivated Al 6061 with the degreasing pretreatment. The spectra show mainly capacitive behavior and a resistive component of the passivated film at the lowest frequencies as well as a symmetric phase angle, indicating that this system is very stable during exposure to NaCl. The capacitance did not change significantly and the polarization resistance gradually increased with time (Fig.24.a). The surface did not show pitting after 90 days. Fig.24.c shows impedance spectra obtained between 10^{-2} Hz and 65 kHz for degreased Al 6061 which was untreated (curves 1-3) or passivated (curves 4-6). For the untreated sample pits were observed in less than one day of exposure to 0.5 N NaCl. The impedance showed essentially capacitive behavior and the low-frequency dependence of the impedance and the phase angle which is

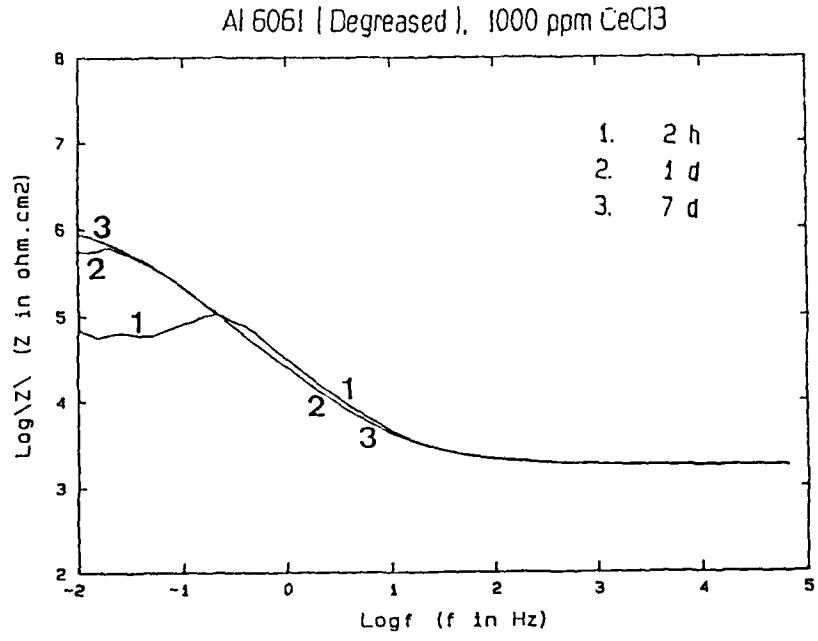

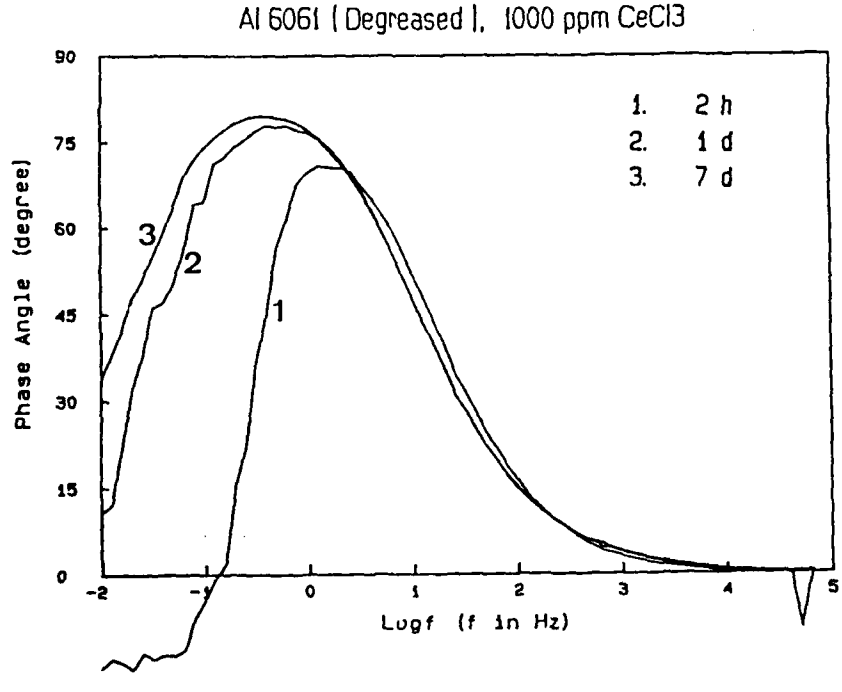

Fig.23.a and b Bode-plots for degreased Al 6061 as a function of immersion time in 1000 ppm $CeCl_3$.

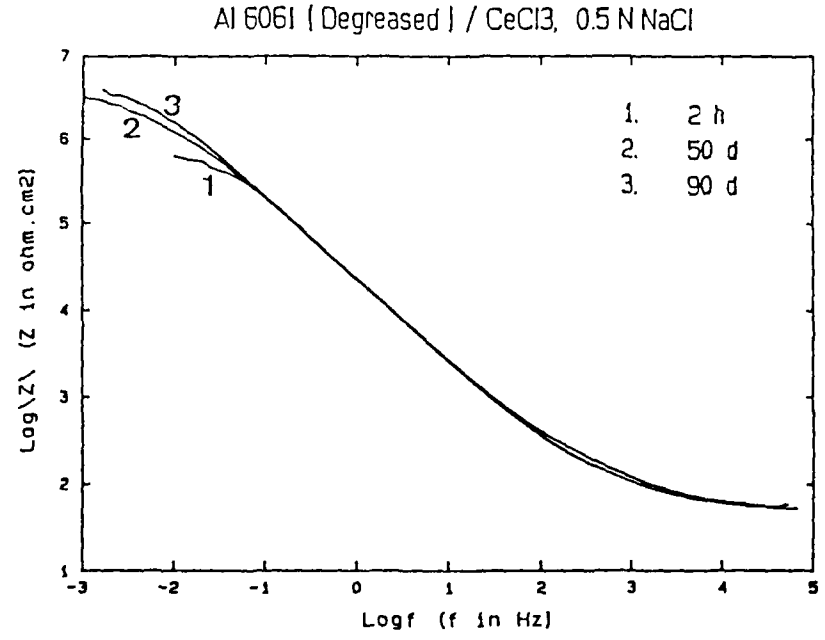

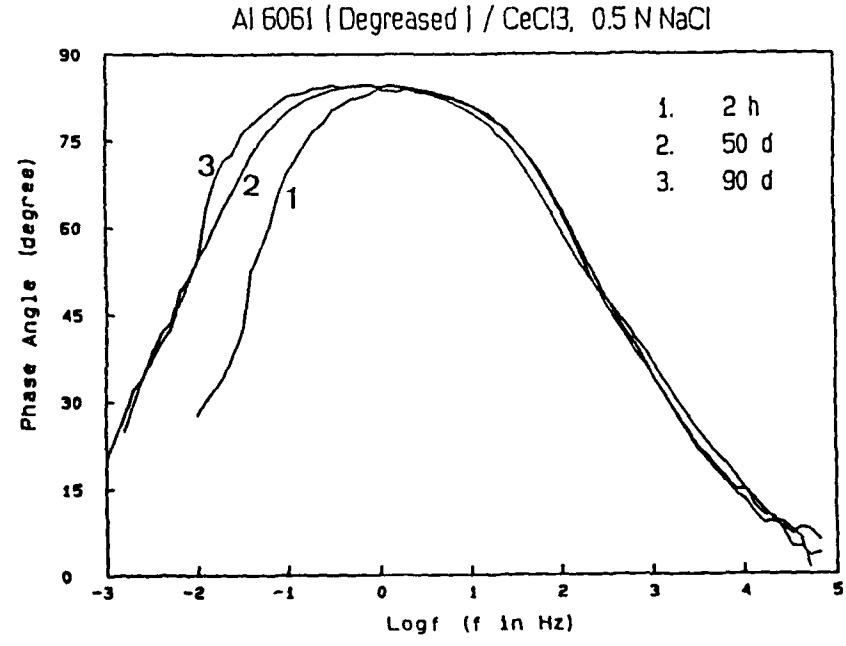

Fig.24.a and b Bode-plots for degreased Al 6061 which was passivated in $CeCl_3$ for one week as a function of exposure time to 0.5 N NaCl.

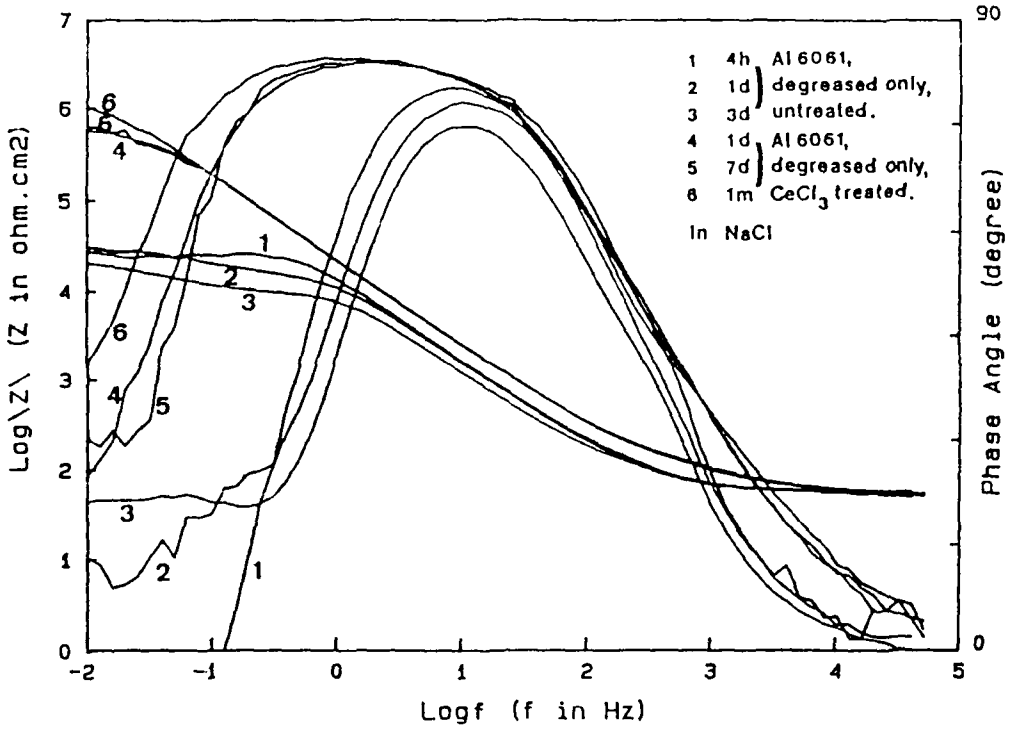

Fig.24.c Bode-plots for degreased Al 6061 which was untreated (curve 1, 2 and 3) or passivated in $CeCl_3$ for one week (curve 4, 5 and 6) as a function of exposure time to 0.5 N NaCl.

characteristic of pitting (curves 1-3 in Fig.24.c). These results demonstrate that passivated Al 6061 which was degreased, but not deoxidized, exhibits excellent corrosion resistance in 0.5 N NaCl.

The results of the analysis of the impedance data which were obtained by fitting to the one-time-constant-model before pitting occurred and to the pitting model after pitting was indicated are plotted in Fig.25, Fig.26, and Fig.27 for as-received and for $CeCl_3$ treated Al 6061. Since it was impossible with the present fit procedure to determine the values of F, C_p and C_{pit} separately, the fit data are plotted as R_{pit}/F (Fig.25.a) and C_t (Fig.25.b). For the as-received Al 6061 Fig.25 shows that both R_{pit}/F and R_p are lower for the degreased samples than for the deoxidized samples (Fig.25.a), while $C_t = C_p(1-F) + C_{pit}\,F$ is higher (Fig.25.b). The large increase in the polarization resistance R_p for the passive surface when pitting occurred (Fig.25.a) could be due to the cathodic protection of the passive surface by the growing pits. The increase of the total capacitance C_t was probably due to the contribution from the capacitance of the pit C_{pit}, when pitting was first observed. These results suggest that the pitting process, which started during the first day of exposure, was more severe for the degreased as-received surface. However, for the $CeCl_3$ treatment, degreased Al 6061 obtained the most corrosion-resistant surface of all materials studied (Table III).

Fig.26.a and b demonstrates the effect of the immersion time in $CeCl_3$ on the corrosion resistance of Al 6061 which was deoxidized before passivation. For the sample passivated in $CeCl_3$ for 7 days, pitting occurred in NaCl in less than 3 days, the values of R_{pit}/F were very low (Fig.26.a) and C_t increased sharply with exposure times (Fig.26.b) because of the large increase of the pitted area. On the other hand, for the sample immersed in $CeCl_3$ for 1 month, pitting was detected visually only after 29 days, at which time an increase of C_t could also be observed (Fig.26.b). When pitting initiated, R_p increased sharply due to cathodic protection of the passive surface by the growing pits and then stayed constant. During immersion in 0.5 N NaCl for 2 hr, the initial value of C_t for the one-month $CeCl_3$ treated Al 6061 was much larger than that for the one-week $CeCl_3$ treated Al 6061 (Fig.26.b). This result suggests that the one-month $CeCl_3$ treated Al 6061 should have a larger dielectric constant assuming that the thickness of passive film of the one-month $CeCl_3$ treated Al 6061 was equal to or larger than that of the one-week $CeCl_3$ treated Al 6061. For Al 6061, the passive film which was obtained by immersion in $CeCl_3$ for one month might contain CeO_2 and $Ce(OH)_4$, while the passive film which was produced in $CeCl_3$ for one week contained mainly $Ce(OH)_3$ which would dissolve in the neutral solution. For the one-week $CeCl_3$ treated Al 6061 (degreased) which had only been pretreated with hot hexanes, the polarization resistance R_p gradually increased with exposure time (Fig.27.a) and the capacitance remained constant during exposure to 0.5 N NaCl for 90 days (Fig.27.b). This steady behavior demonstrates that the $CeCl_3$ treatment provided excellent corrosion resistance for degreased Al 6061. The increase of the corrosion resistance of degreased Al 6061 through the treatment in $CeCl_3$ is comparable to that produced by chromate conversion coatings. For degreased Al 6061 which had been passivated in $CeCl_3$ for one week, the value of R_p was between $6 * 10^5$ and $4 * 10^6$ ohm-cm^2 for 90 days exposure in NaCl (Fig.27.a). For Al 6061 with a chromate conversion coating (Alodine 600) the value of R_p was between $9 * 10^5$ and $9 * 10^6$ ohm-cm^2 for 12 days exposure (Fig.7.b). This similar result suggests that passivation in $CeCl_3$ is an alternative to the use of chromate conversion coatings for Al 6061.

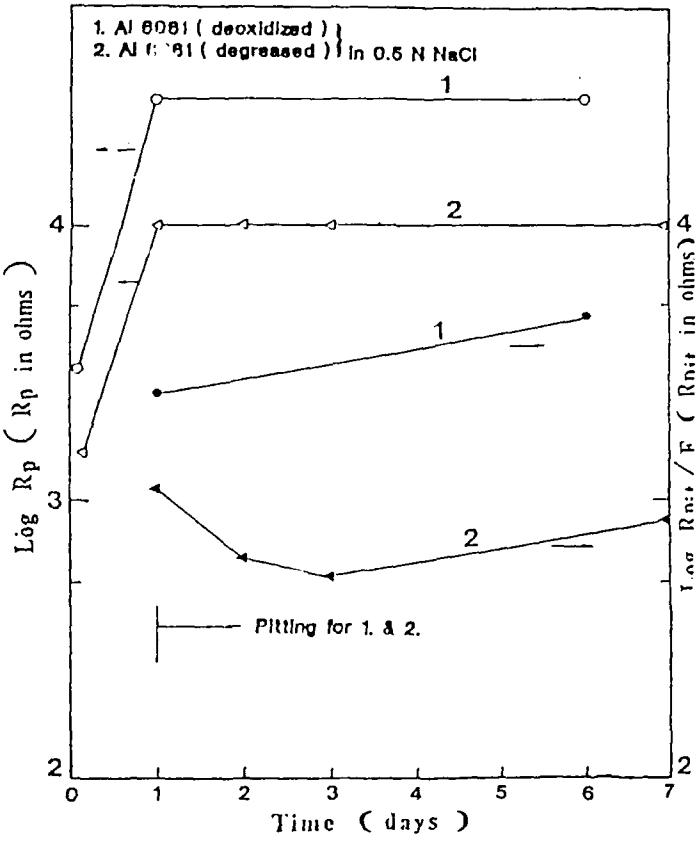

a

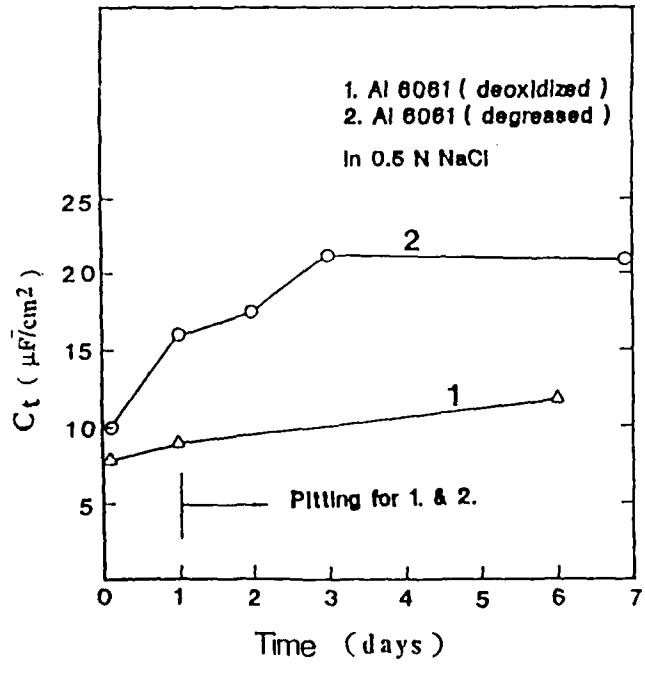

b

Fig.25 Analysis of impedance data for deoxidized Al 6061 (curve 1) and degreased Al 6061 (curve 2) as a function of exposure time to 0.5 N NaCl :
(a) polarization resistance Rp and R_{pit}/F,
(b) capacitance C_t.

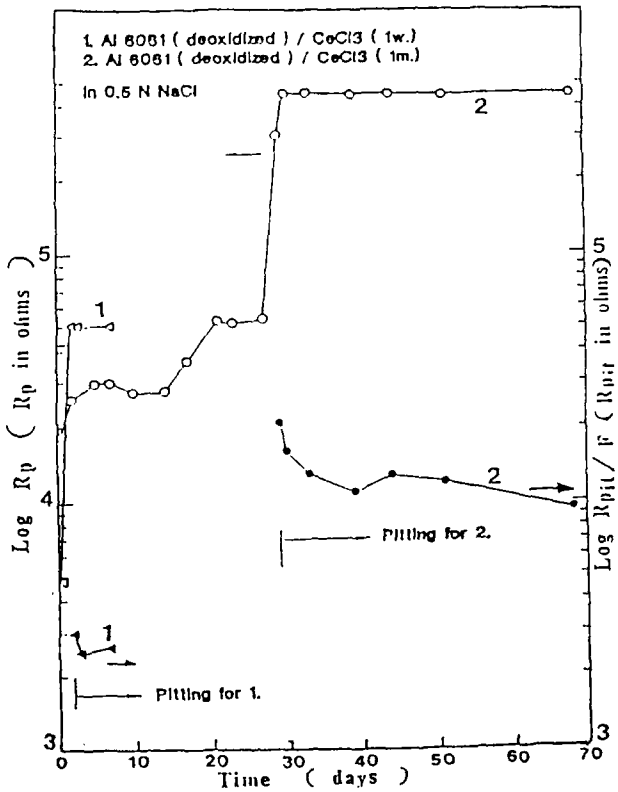

a

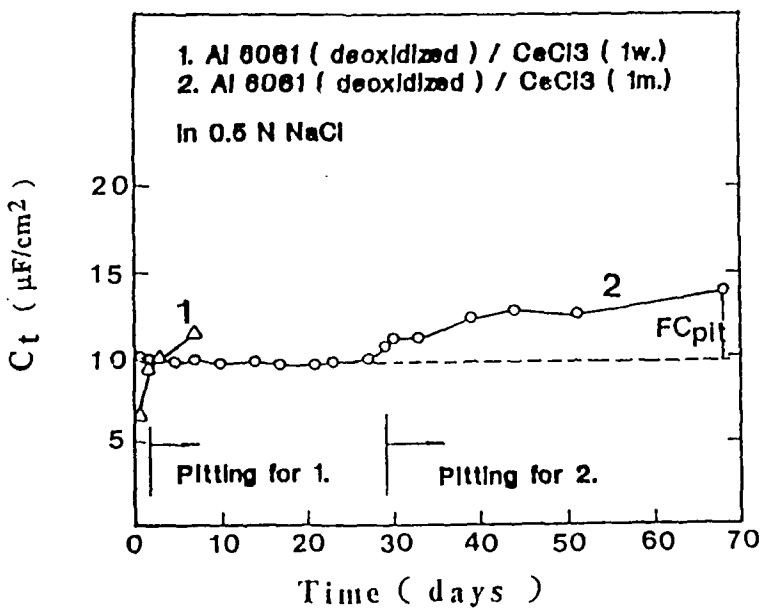

b

Fig.26.a and b Analysis of impedance data for deoxidized Al 6061 which was passivated in $CeCl_3$ for one week (curve 1) or for one month (curve 2) as a function of exposure to 0.5 N NaCl :
(a) polarization resistance R_p and R_{pit}/F,
(b) capacitance C_t.

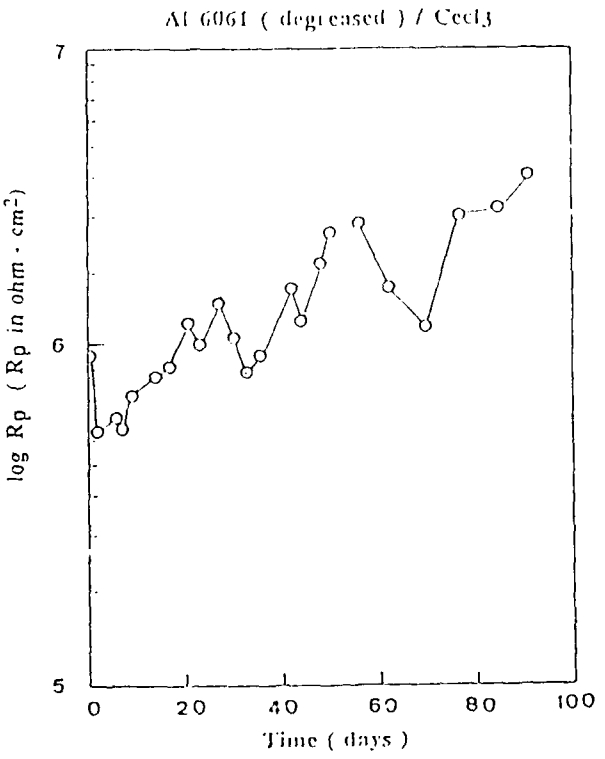

a

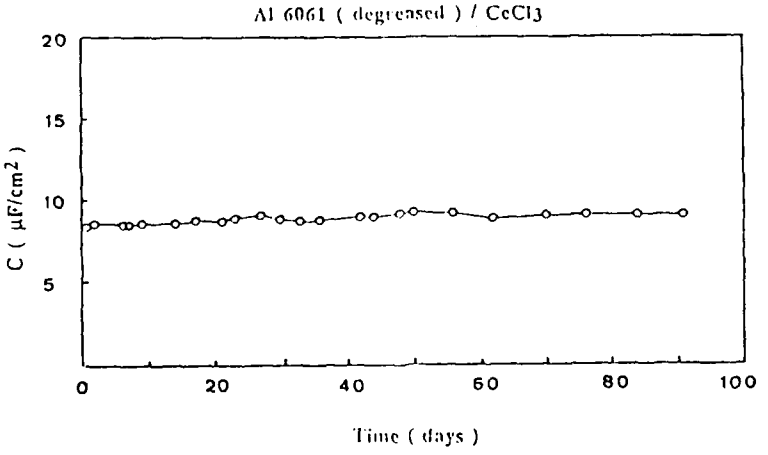

b

Fig.27.a and b Analysis of impedance data for degreased Al 6061 which was passivated in $CeCl_3$ for one week as a function of exposure time to 0.5 N NaCl : (a) polarization resistance Rp, (b) capacitance Ct.

3.3.2 Al 7075

Fig.28 shows the impedance spectra for Al 7075 in the T6 and T73 condition obtained during immersion in 1000 ppm $CeCl_3$. At sufficient low frequencies a dc limit is observed for curves 1 and 3 which corresponds to polarization resistance R_p. For the simple spectra in Fig.28, the phase angle has a maximum at intermediate to low frequencies. The capacitance decreased with exposure time for both heat treatments, indicating that a passive film was formed. For both heat treatments a significant increase of the impedance with exposure time in $CeCl_3$ was observed at the lowest frequencies, which suggests that R_p and the corrosion resistance have increased. For Al 7075-T6, the capacitance decreased from 10 $\mu F/cm^2$ after 2 hr to 8.6 $\mu F/cm^2$ after 2 days of exposure and then remained unchanged (Fig.29.a). The polarization resistance increased from $1 * 10^6$ ohm-cm^2 after 2 hr to $6 * 10^6$ ohm-cm^2 after 3 days and then remained unchanged (Fig.29.b). E_{corr} shifted from -730 mv to -682 mv during the first 3 days of exposure and then remained unchanged(Fig.29.c). These results suggest that passivation was completed after 3 days of immersion.

For Al 7075-T73 during immersion in $CeCl_3$, the capacitance decreased from 8.7 $\mu F/cm^2$ after 2 hr to 8.2 $\mu F/cm^2$ after 3 days of exposure and then decreased to 6.9 $\mu F/cm^2$ after 7 days of exposure (Fig.29.a). The polarization resistance increased from $3.2 * 10^5$ ohm-cm^2 after 2 hr to $2.4 * 10^6$ ohm-cm^2 after 3 days and then remained unchanged (Fig.29.b). E_{corr} gradually shifted from -810 mV to -665 mV during 7 days of exposure, bit did not reach a constant value (Fig.29.c). These results suggest that passivation was not completed after 7 days of immersion.

When the Al 7075 samples with the two different heat treatments were immersed in 0.5 N NaCl after the passivation treatment in $CeCl_3$, it was found that the corrosion resistance had increased, but the beneficial effect was quite different for the T6 (Fig.30) and T73 (Fig.31) conditions. Only small changes in the corrosion resistance of the passivated Al 7075-T6 occurred over a period of 23 days (Fig.30), while large changes in the spectra and severe corrosion were observed for the passivated Al 7075-T73 in only one day (Fig.31, curve 4). The impedance spectra for the passivated Al 7075-T6 after 2 hr immersion in NaCl (Fig.30) were essentially the same as those recorded in $CeCl_3$ (Fig.28). No changes in capacitive region of the spectra for passivated Al 7075-T6 were observed for 23 days, which is an extraordinary result considering that the untreated sample pitted after a few days (Fig.30). For the untreated Al 7075-T6, the impedance spectra (Fig.30) showed essentially capacitive behavior for curve 1 and the changes in the low-frequency dependence of the impedance with a slope of $n = -0.3$ for curve 2, which is a characteristic feature of the pitting model. Large increases of the capacitance were observed for the untreated Al 7075-T6 after 4 days (Fig.30). These large increases of the capacitance with exposure time and the changes in the frequency dependence of the impedance and the phase angle are due to severe corrosion and pitting.

Pitting was observed visually after 2 hr for the untreated Al 7075-T73 and after 1 day of exposure for passivated Al 7075-T73. Fig.31 shows that the impedance spectra changed rapidly in one day for both the passivated (curve 3 and 4) and the untreated (curves 1 and 2) Al 7075-T73. The spectra in curve 2 are typical for those predicted by the pitting model. A comparison of the spectra for the same exposure time shows that the $CeCl_3$ treatment has improved the corrosion resistance of the Al 7075-T73, but only to a degree which is much less

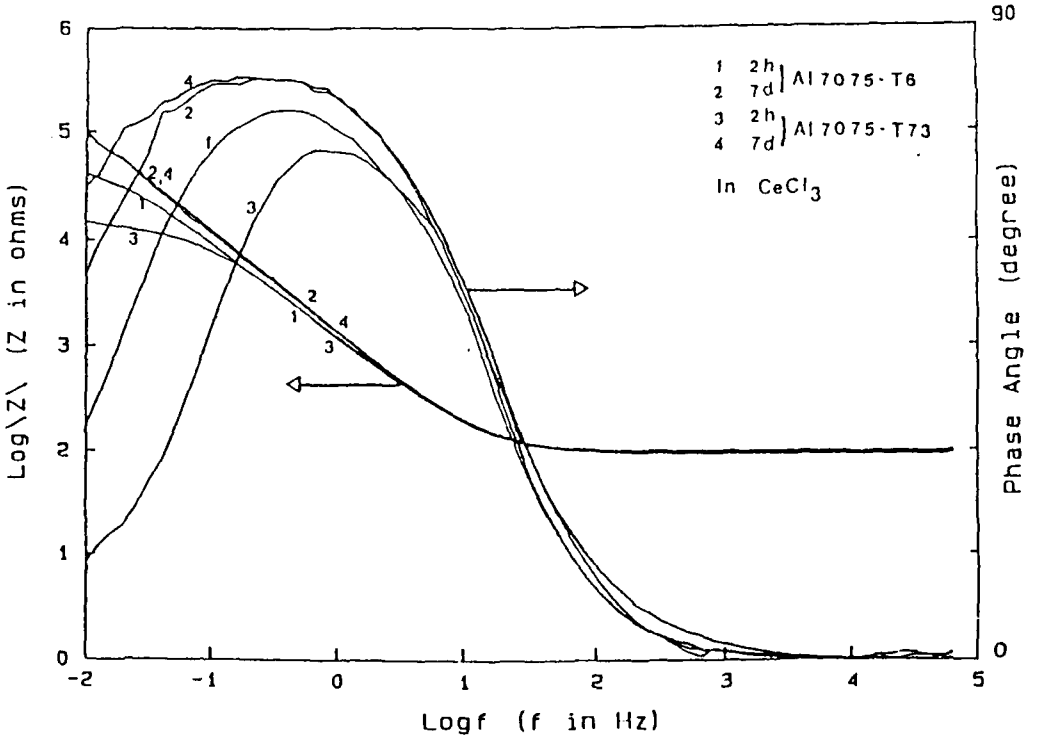

Fig.28 Bode-plots for deoxidized Al 7075-T6 and Al 7075-T73 as a function of immersion time in 1000 ppm $CeCl_3$. ($A = 20\ cm^2$)

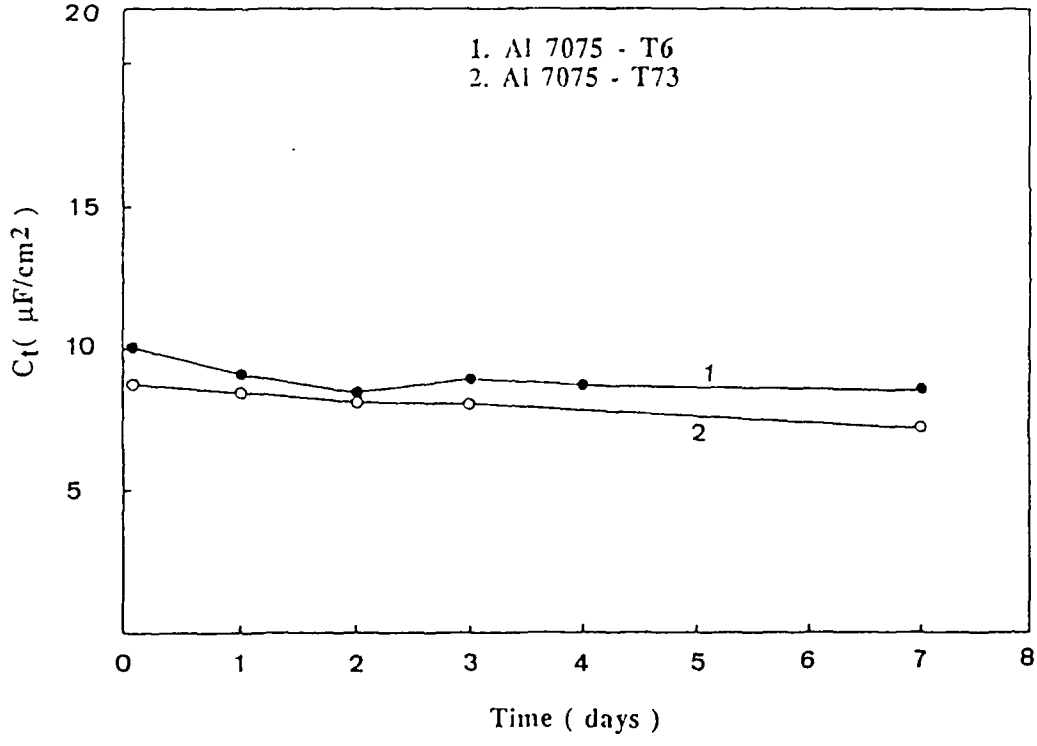

a

Fig.29 . Analysis of impedance data for deoxidized Al 7075-T6 (curve 1) and Al 7075-T73 (curve 2) as a function of immersion time in 1000 ppm $CeCl_3$:
(a) capacitance C,
(b) polarization resistance R_p,
(c) corrosion potential E_{corr}.

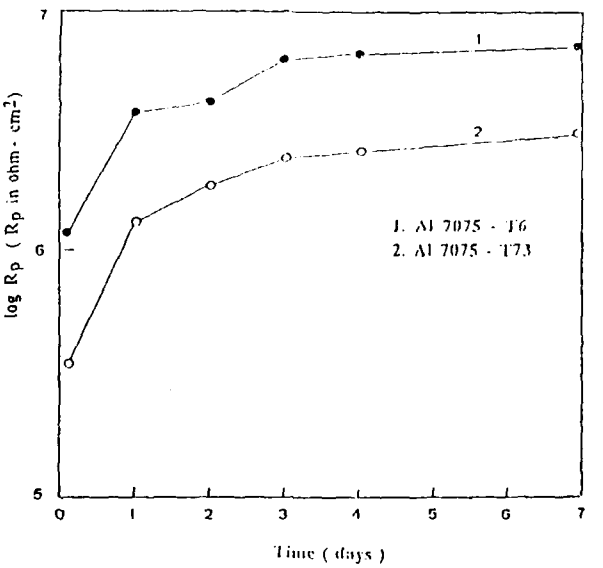
log Rp (Rp in ohm - cm²)
Time (days)
1. Al 7075 - T6
2. Al 7075 - T73
1
2
7
6
5
0
1
2
3
4
5
6
7

b

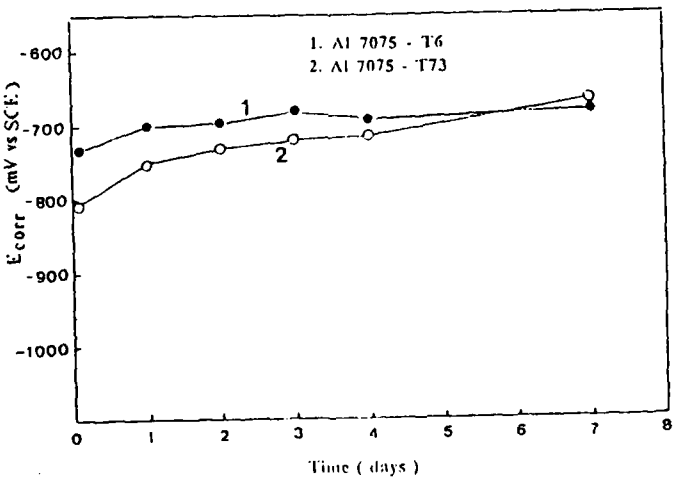
1. Al 7075 - T6
2. Al 7075 - T73
E corr (mV vs SCE)
Time (days)
-600
-700
-800
-900
-1000
1
2
0
1
2
3
4
5
6
7
8

c

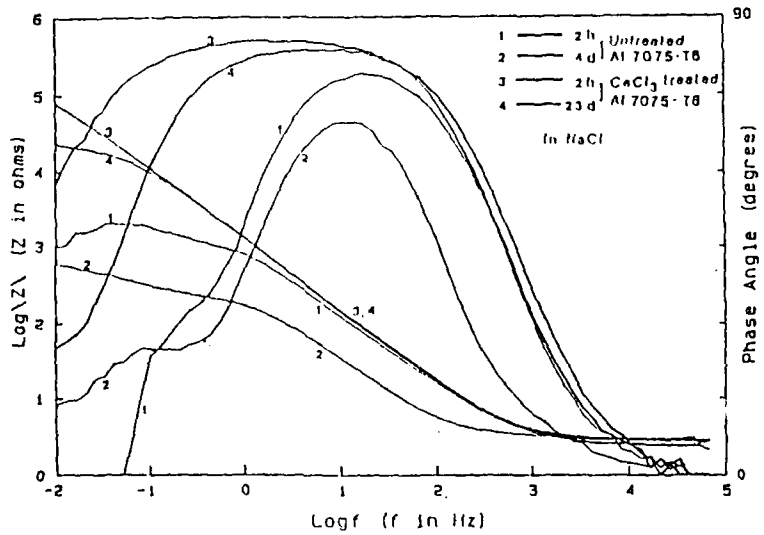

Fig.30 Bode-plots for deoxidized Al 7075-T6 which was untreated (curve 1 and 2) or passivated in $CeCl_3$ for one week (curve 3 and 4) as a function of exposure time to 0.5 N NaCl. (A = 20 cm^2)

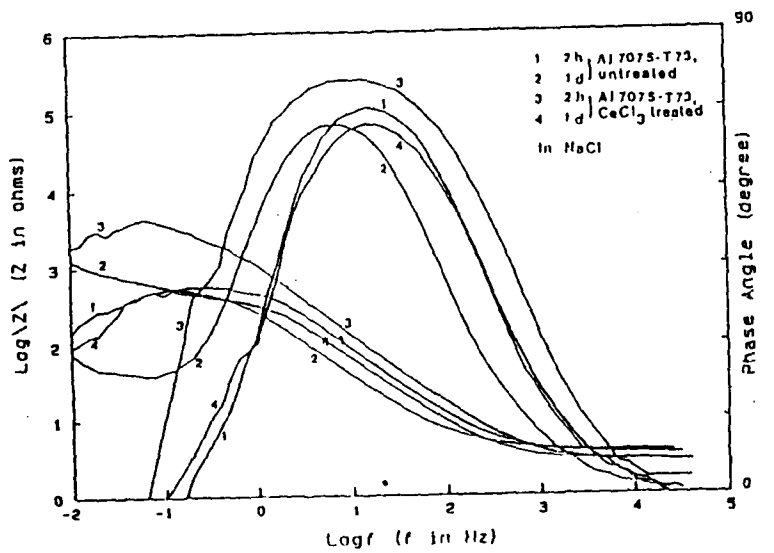

Fig.31 Bode-plots for deoxidized Al 7075-T73 which was untreated (curve 1 and 2) or passivated in $CeCl_3$ for one week (curve 3 and 4) as a function of exposure time to 0.5 N NaCl. (A = 20 cm^2)

significant than for the T6 condition.

The results of the analysis of the impedance data obtained by fitting to the one-time-constant-model before pitting and to the pitting model after pitting for as-received and for $CeCl_3$ treated Al 7075-T6 are plotted in Fig.32. For passivated Al 7075-T6, the polarization resistance R_p for the passive surface and the total capacitance C_t remained more or less constant before pitting and increased after pitting. A small increase of C_t was observed a few days before pits were detected visually, as indicated by the marker in Fig.32.b. This result demonstrates the sensitivity of EIS towards localized corrosion of Al alloys. The polarization resistance R_{pit}/F for the pitted surface decreased with exposure time (Fig.32.a). For the untreated Al 7075-T6, the increase of C_t was much larger and was obviously dominated by the increase of FC_{pit} (Fig.32.b). The polarization resistance R_p of the passive surface for the untreated Al 7075-T6 was much less than for the treated Al 7075-T6, indicating the excellent corrosion resistance achieved by chemical passivation in $CeCl_3$.

In order to obtain further information concerning the pit growth kinetics from the results shown in Fig.32, the value of F was determined visually at the end of the test. Based on the values of F and FC_{pit} as determined from the last data point in Fig.32.b, the constant values of C_{pit} were calculated as 133 $\mu F/cm^2$ for Al 7075-T6 and 105 $\mu F/cm^2$ for Al 6061. Assuming that C_{pit} (in $\mu F/cm^2$) did not change with exposure time, it was then possible to calculate F as a function of exposure time. R_{pit} (in ohm-cm^2) can be calculated from R_{pit}/F. The results of this procedure are shown in Fig.33.a for $1/R_{pit}$ and K and in Fig.33.b for F and n. In addition to the results for Al 7075-T6, data are also shown for Al 6061 which was deoxidized and then immersed in $CeCl_3$ for one month. For both samples the rate of the pit growth $1/R_{pit}$ decreased with exposure time. A value of R_{pit} = 1000 ohm-cm^2 corresponds to a pit growth rate of about 0.2 mm/yr assuming a Tafel parameter B = 20 mV. The parameter K of the transmission line term seems to be independent of time, but dependent on material (Fig.33.a). F increased from about 1 % to about 4 % in both cases, while n, a factor which is assumed to depend on pit geometry, had values close to -0.5, which implies that the shape of the pits is cylindrical [47].

3.3.3 Al/SiC MMCs

The impedance spectra for Al/SiC (deoxidized) obtained during immersion in 1000 ppm $CeCl_3$ showed mainly capacitive behavior. R_p increased with exposure time and the capacitance decreased slightly after one day (Fig.20.a). The polarization resistance increased from 2 * 10^5 ohm-cm^2 after 2 hr to 1 * 10^6 ohm-cm^2 after six days (Fig.20.b). E_{corr} decreased from -600 mV to -635 mV (Fig.20.c). These results suggest that passivation was completed after 6 days of immersion.

After 3 months of exposure to NaCl, the spectra for the passivated samples (curves 3 and 4 in Fig.34) showed the frequency dependence of the impedance and the phase angle at the lowest frequencies which is characteristic of pitting behavior. The capacitance of the $CeCl_3$-treated Al/SiC increased after 3 month exposure to 0.5 N NaCl due to pitting. The spectra for as-received Al/SiC (curves 1 and 2) indicated pitting behavior as evidenced by the large increase of the capacitance with exposure time (Fig.34). The capacitance of the as-received SiC/Al after 1 day (curve 1 in Fig.34) is larger than that of the $CeCl_3$-treated Al/SiC after 2 hr (curve 3 in Fig.34) due to pitting for the as-received Al/SiC. An increase of the corrosion resistance in 0.5 N NaCl due

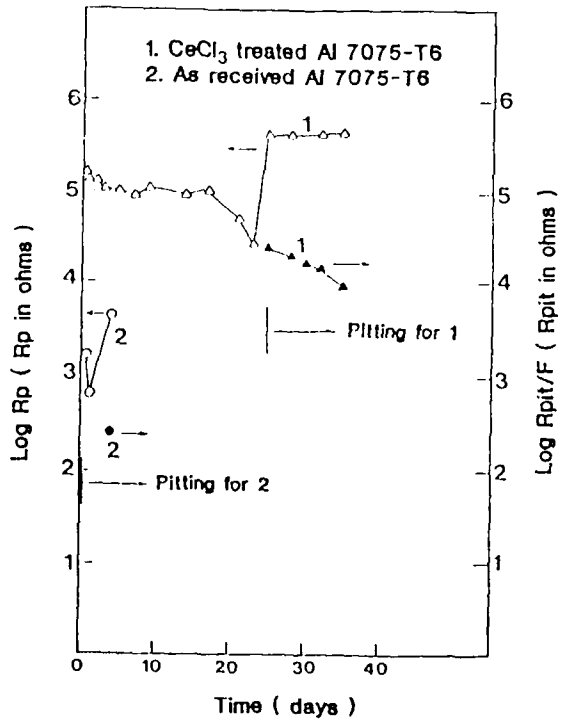

a

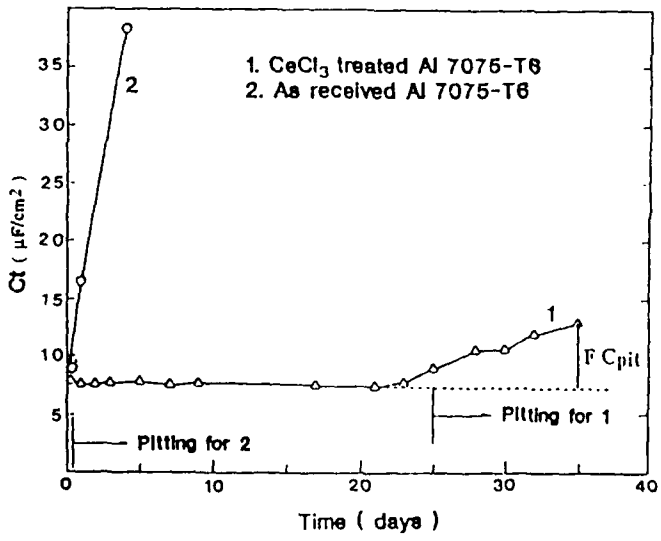

b

Fig.32 Analysis of impedance data for deoxidized Al 7075-T6 which was passivated in $CeCl_3$ for one week (curve 1) or untreated (curve 2) as a function of exposure time to 0.5 N NaCl.
(a) R_p and R_{pit}/F,
(b) C_t.

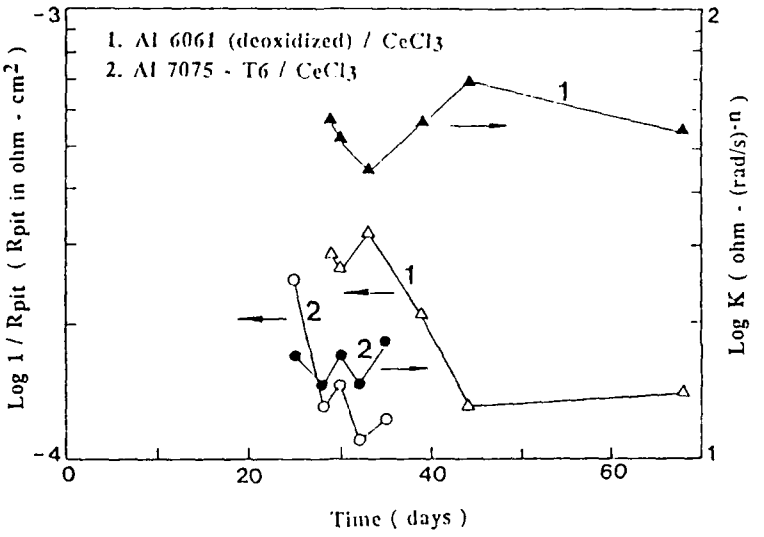

a

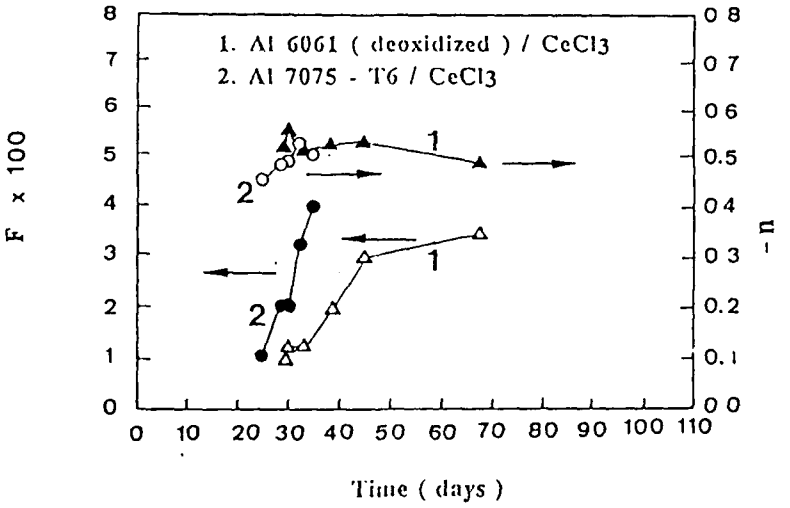

b

Fig.33 Analysis of impedance data for deoxidized Al 6061 which was passivated in $CeCl_3$ for one month (curve 1) and Al 7075-T6 which was passivated in $CeCl_3$ for one week (curve 2) as a function of exposure time to 0.5 N NaCl.
(a) $1/R_p$ and K , (b) n and F.

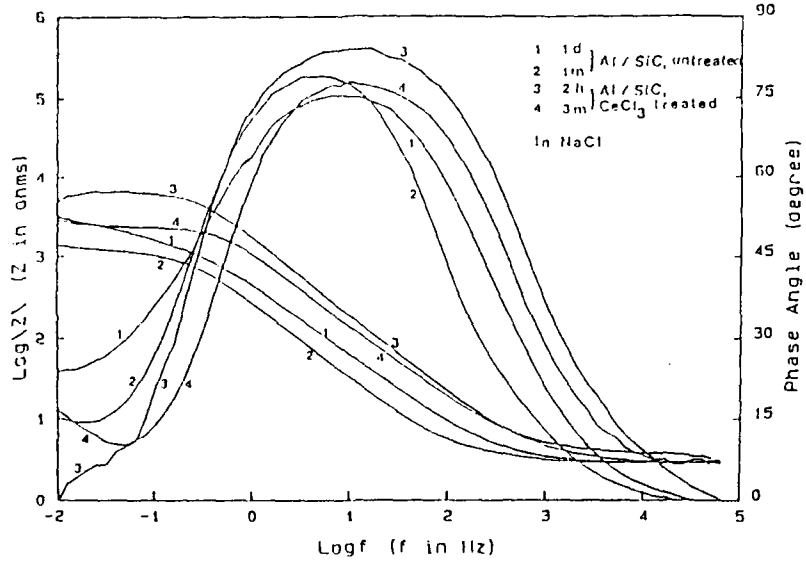

Fig.34 Bode-plots for Al/SiC as a function of exposure time to 0.5 N NaCl;
Curve 1 and 2 : as-received
Curve 3 and 4 : $CeCl_3$, 7 days
(A = 20 cm^2)

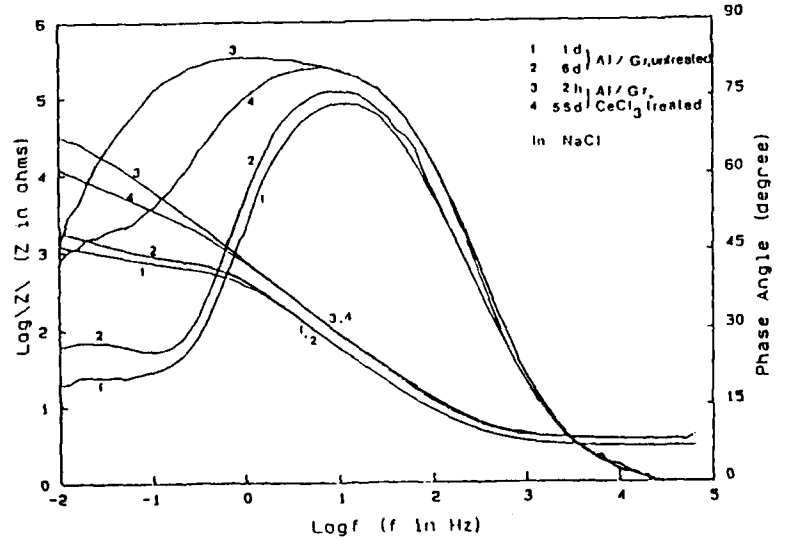

Fig.35 Bode-plots for Al/Gr as a function of exposure time to 0.5 N NaCl;
Curve 1 and 2 : as-received
Curve 3 and 4 : $CeCl_3$, 7 days
(A = 20 cm^2)

to the passivation in $CeCl_3$ was observed for Al/SiC because the impedance of the curve 4 was larger than that of the curve 2 at the lowest frequencies (Fig.34). The corrosion resistance of the passivated Al/SiC decreased with exposure time and pits were detected visually after 81 days. This shows that the resistance of the passivated Al/SiC to pitting was much improved in comparsion to that of bare Al/SiC. At the end of the corrosion test after three months, crevice corrosion was detected under the O-ring which provided a seal between the test cell and the sample. Since crevice corrosion did not occur for any of the other Al alloys and Al-based MMCs, it was concluded that it was the result of the presence of the SiC particulates. For passivated Al/SiC, the impedance spectra showed changes in the frequency dependence of the impedance and the phase angle at low frequencies after 8 days of exposure, but pits was not detected visually until 81 days of exposure. This result suggests that the observed crevice corrosion occurred after 8 days.

3.3.4 Al/Gr MMCs

The impedance spectra for Al/Gr obtained during immersion in 1000 ppm $CeCl_3$ show that the impedance at the lowest frequencies increased and that the capacitance decreased after 6 days of exposure.

For passivated Al/Gr, pits were detected visually after 42 days. The impedance spectra for passivated Al/Gr exposed to NaCl showed mainly capacitive behavior before pitting (curve 3 in Fig.35) and pitting behavior at the lowest frequencies between 0.01 and 0.1 Hz after pitting (curve 4 in Fig.35.a and b.). When pits penetrated the Al face sheet and reached the graphite fibers, blistering of the Al face sheet was observed and evolution of the hydrogen gas occurred occasionally from some isolated spots on the blistered surface. The frequency dependence of the impedance and the impedance in the capacitance region did not change very much for curves 3 and 4, indicating that the corrosion process at the Al/Gr galvanic couple did not produce a large value of C_{pit}. Fig.35 shows a large increase of the corrosion resistance for Al/Gr in 0.5 N NaCl due to the passivation in $CeCl_3$ because the impedance in the low-frequency region for passivated Al/Gr (curve 3 and 4) is much larger than as-received Al/Gr (curves 1 and 2). For the untreated Al/Gr pitting corrosion was already indicated after one day of exposure to NaCl. The low-frequency data kept changing during the six-day exposure time and showed a frequency dependence of the impedance and the phase angle which are predicted by the pitting model (Fig.4). Contrary to the large increases of the capacitance for untreated Al 6061, Al/SiC, Al 7075-T6 and T73, the impedance in the capacitance region for untreated Al/Gr did not change very much during 6 days of exposure (curves 1 and 2 in Fig.35). This result might be due to a small value of C_{pit} for the Al/Gr galvanic couple.

The results of the analysis of the impedance data obtained by fitting to the one-time-constant-model before pitting and to the pitting model after pitting for as-received and for $CeCl_3$ treated Al/Gr and Al/SiC are plotted in Fig.36 and Fig.37. The pitting process for untreated Al/Gr and Al/SiC is characterized by lower values of R_{pit}/F than R_p before pitting (Fig.36.a) and an increase of C_t with exposure time (Fig.36.b). When pitting initiated, the polarization resistance R_p of the passive surface increased and then remained constant probably due to cathodic protection by the growing pit. For the passivated Al/SiC, small changes of C_t and large increases of R_p were observed when crevice corrosion apparently occurred after about 8 days (Fig.37.a and b). At this time

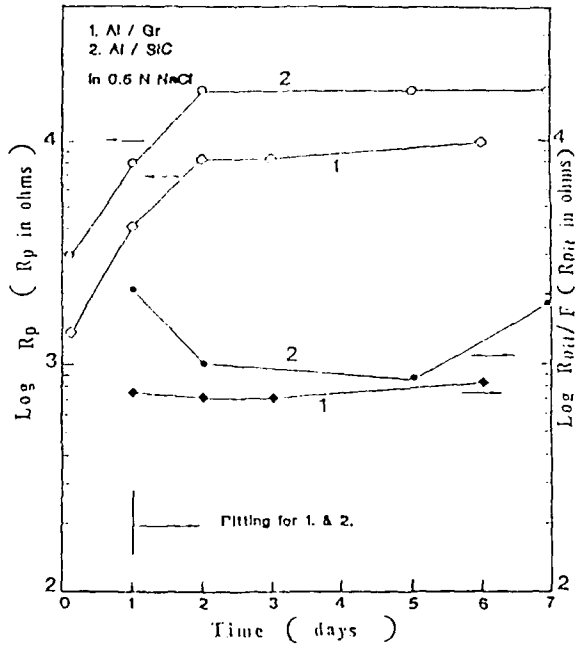

a

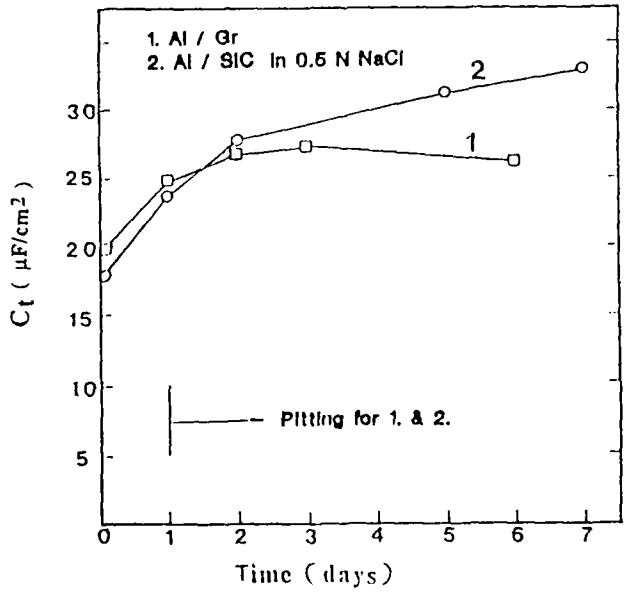

b

Fig.36.a and b Analysis of impedance data for untreated Al/Gr and untreated Al/SiC as a function of exposure time to 0.5 N NaCl :
(a) R_p and R_{pit}/F
(b) C_t.

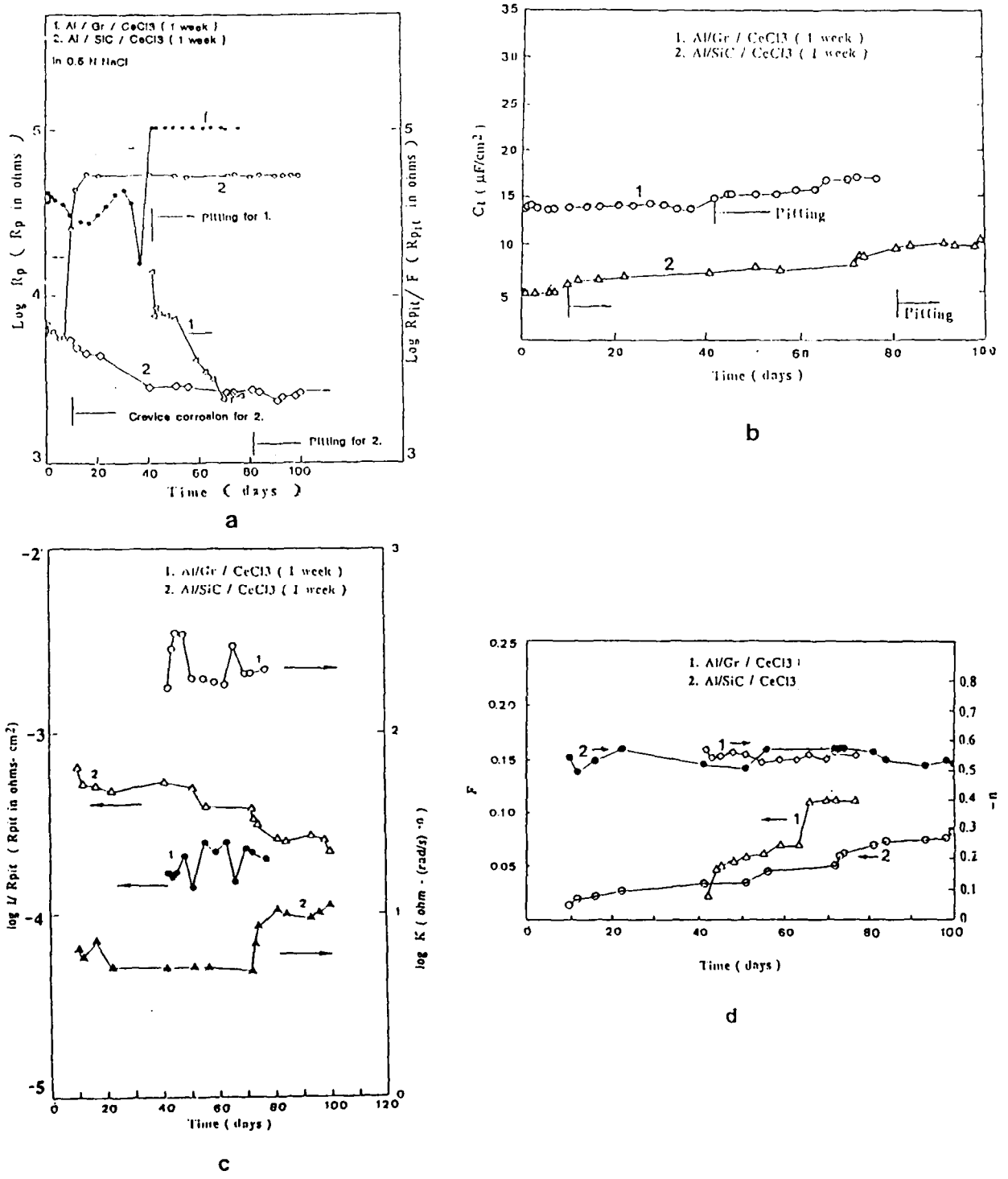

Fig.37 Analysis of impedance data for $CeCl_3$ treated (one week) Al/Gr (curve 1) and $CeCl_3$ treated (one week) Al/SiC (curve 2) as a function of exposure time to 0.5 N NaCl :
(a) R_p and R_{pit}/F
(b) C_t , (c) $1/R_p$ and K , (d) n and F.

C_t showed a small increase with another increase after about 72 days. This second increase of C_t might be due to pitting, which was detected visually only after 81 days. After crevice corrosion occurred, R_{pit}/F showed a small decrease due to an increase in F (Fig.37.a). When the first pits were observed after 81 days, R_{pit}/F decreased slightly. The localized corrosion process for passivated Al/SiC is obviously dominated by crevice corrosion. For passivated Al/Gr, R_{pit}/F decreased sharply when blistering of the Al face sheet and evolution of hydrogen gas were observed due to the penetration of the Al face sheet and galvanic interaction of the Al matrix with the graphite fibers. R_p increased after pitting occurred and then remained constant (Fig.37.a). An increase of the capacitance C_t was observed after pitting occurred(Fig.37.b, curve 1). Although the impedance spectra showed only slight changes in the capacitive region (Fig.35), a significant increase of the capacitance C_t was calculated by the fitting program (Fig.37.b) due to the high polarization resistance of the passive surface R_p and the changes of the slope of the log /Z/ vs. log f curve in the capacitive range.

Using the same assumptions and calculations as for the passivated Al 7075-T6 and the passivated Al 6061 the kinetics of the pit growth for the passivated Al/Gr and Al/SiC are shown in Fig.37.c for $1/R_{pit}$ and K and in Fig.37.d for F and n. For passivated Al/SiC, the rate of pit growth $1/R_{pit}$ decreased with exposure time, but for passivated Al/Gr $1/R_{pit}$ increased slightly with exposure time presumably due to galvanic coupling of Al to Gr. A value of $R_{pit} = 10^3$ ohm-cm^2 corresponds to a pit growth rate of about 0.2 mm/yr. The parameter K of the transmission line term seems to be independent of time, but is material dependent. F increases from about 2 % to about 11 % for passivated Al/Gr and from about 1 % to about 8 % for passivated Al/SiC, while n, a factor related to pit geometry, had values close to -0.55 which implies that the shape of pit is cylindrical [47]. The constant values of C_{pit} used for these calculation were 38 μF/cm^2 for passivated Al/Gr and 69 μF/cm^2 for passivated Al/SiC.

The dramatic effects of passivation in 1000 ppm $CeCl_3$ on the corrosion resistance are shown in Table III which compares the times at which pitting was first detected visually for untreated and treated samples. Without the passivation treatment pits initiated in less than one day for all materials, while passivated samples could survive exposure to 0.5 N NaCl for one to three months without pitting. For passivated SiC/Al crevice corrosion was indicated after 8 days, but pits were not observed in 81 days.

3.4 Polymer Coatings

Delamination of polymer coatings and filiform corrosion have been observed on aluminum and magnesium surfaces covered by polymer coatings [3,11-13,40]. Delamination of polymer coatings is a consequence of the cathodic reaction. For Al in 0.5 N NaCl, oxygen reduction:

$$2H_2O + O_2 + 4e^- \text{-----> } 4OH^- \qquad (3.2)$$

occurs under the coating or in a defect in the coating. The high hydroxyl ion concentration dissolves the oxide and the Al metal and attacks the polymer at the interface between the polymer and the substrate. For polymer coatings without defects, it is necessary for water and oxygen to penetrate through the coating and reach the interface for delamination to occur. Also, the diffusion of Cl^- may accelerate the rate of delamination and cause pitting under the

Table III Comparison of Pitting Times for Chemical Passivation in $CeCl_3$ and for Untreated samples (t_p = pitting time; tc = crevice time (in days))

Materials	Pretreatment	CeCl3 treated	Untreated
Al 7075-T6	deoxidized	$t_p > 24$	$t_p < 1$
Al 7075-T73	deoxidized	$t_p < 1$	$t_p < 1$
Al 7075-T73	degreased	$t_p < 1$	$t_p < 1$
Al 6061	deoxidized	$t_p > 3$	$t_p < 1$
Al 6061*	deoxidized	$t_p > 29$	$t_p < 1$
Al 6061	degreased	> 90 (no pits)	$t_p < 1$
Al 6061/SiC	deoxidized	$t_p > 81$ $t_c > 8$	$t_p < 1$
Al 6061/Gr	deoxidized	$t_p > 40$	$t_p < 1$

* one-month CeCl3 treatment

coating.

For Mg in 0.5 N NaCl, the cathodic reaction is

$$2H_2O + 2e^- \text{-----> } 2OH^- + H_2 \qquad (3.3)$$

The alkali is generated under the coating directly by reduction of H_2O without oxygen penetrating through the coating. Also, the diffusion of Cl^- may accelerate the rate of delamination and cause pitting in the coating due to the high pressure of hydrogen gas which is produced by the cathodic reaction and accumulates under the coating.

Hysol CG7-4102, which is an epoxy resin made by Dexter Corporation, has excellent wetting properties and good adhesion to most metals. It provides excellent chemical resistance for steel in 10 % hydrochloric acid for 30 days according to the technical information from the Dexter Co. Hence, epoxy coatings of 25-30 μm thickness as measured by a micrometer were applied to Al 6061, Al/SiC, Al/Gr, Al-Li 2091-T6, and MgAZ31B.

3.4.1 Al 6061

For the purpose of estimating the adhesion between the polymer coating and the substrate, the coated Al 6061 panels were t .ted at R.T. (20°C) and 35°C since adhesion loss increases with increasing temperature. Impedance spectra for 25 μm epoxy coatings on Al 6061 exposed to 0.5 N NaCl at 20°C and at 35°C are shown in Fig.38 and Fig.39, respectively. The spectra show essentially capacitive behavior and a resistive component of about 10^9 ohm-cm^2 at the lowest frequencies which could be due to the polymer film or the potentiostat input. Fig 40 shows that the coating capacitance increased by 3 % in 73 days at 20°C and by 3.5 % in 55 days at 35°C. The coated surface did not show any damage, such as pits, delamination or filiform corrosion. Hence the increases of the capacitance must be due to the water uptake of the coating which can be estimated approximatively by the Brasher and Kingsbury equation [48] which was based on the assumption that the swelling of the polymer coating can be ignored:

$$x = \log(C_t/C_o)/\log 80 \qquad (3.4)$$

In Eq.3.4 x is the volume fraction of water in the coating, C_t is the capacitance of the polymer coating at time t, C_o is the capacitance of the polymer coating at time zero, and 80 is the dielectric constant of water at 20°C.

Based on the assumption that C_o in Eq.3.4 is the capacitance of the polymer coating measured after 2 hr immersion in 0.5 N NaCl, the water uptake of the coatings was calculated as 0.7 % after 73 days at 20°C and 1.0 % after 55 days at 35°C. The very stable behavior observed in the impedance data demonstrates the excellent corrosion resistance of the epoxy coated Al 6061 and the excellent adhesion between the epoxy coating and Al 6061.

3.4.2 Al 6061/SiC

Fig.41 shows impedance spectra for a 25 μm epoxy coating during exposure to 0.5 N NaCl for 109 days. The spectra show essentially capacitive behavior and a resistive component of 10^9 ohm-cm^2 at the lowest frequencies. Not much change was observed in linear capacitive range (Fig.41). The surface of coating did

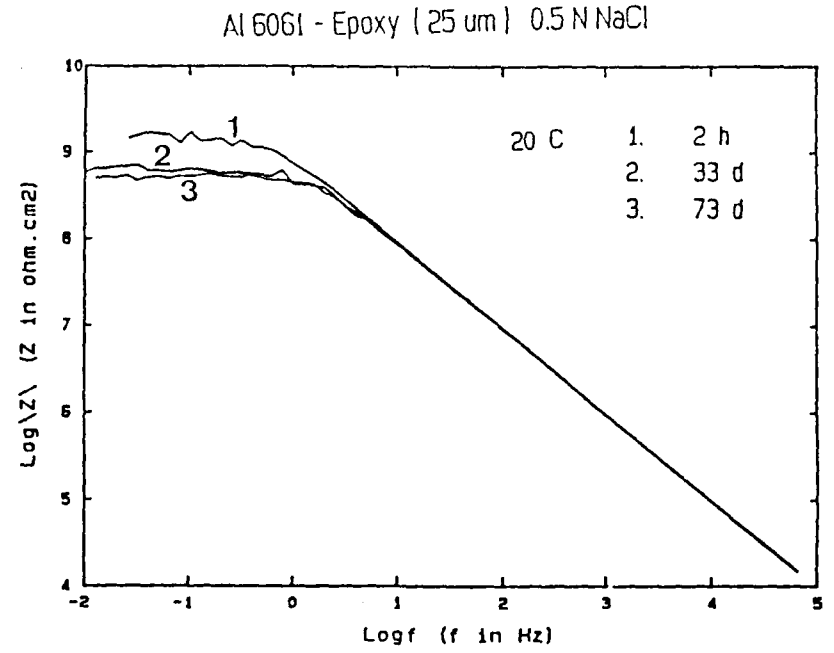

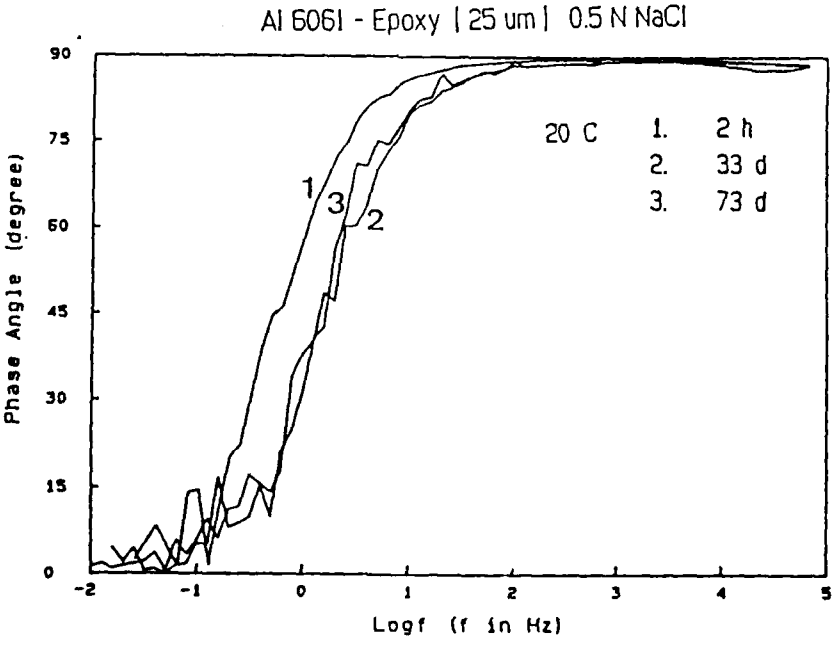

Fig.38.a and b Bode-plots for Al 6061 with a 25-µm epoxy coating as a function of exposure time to 0.5 N NaCl at 20°C.

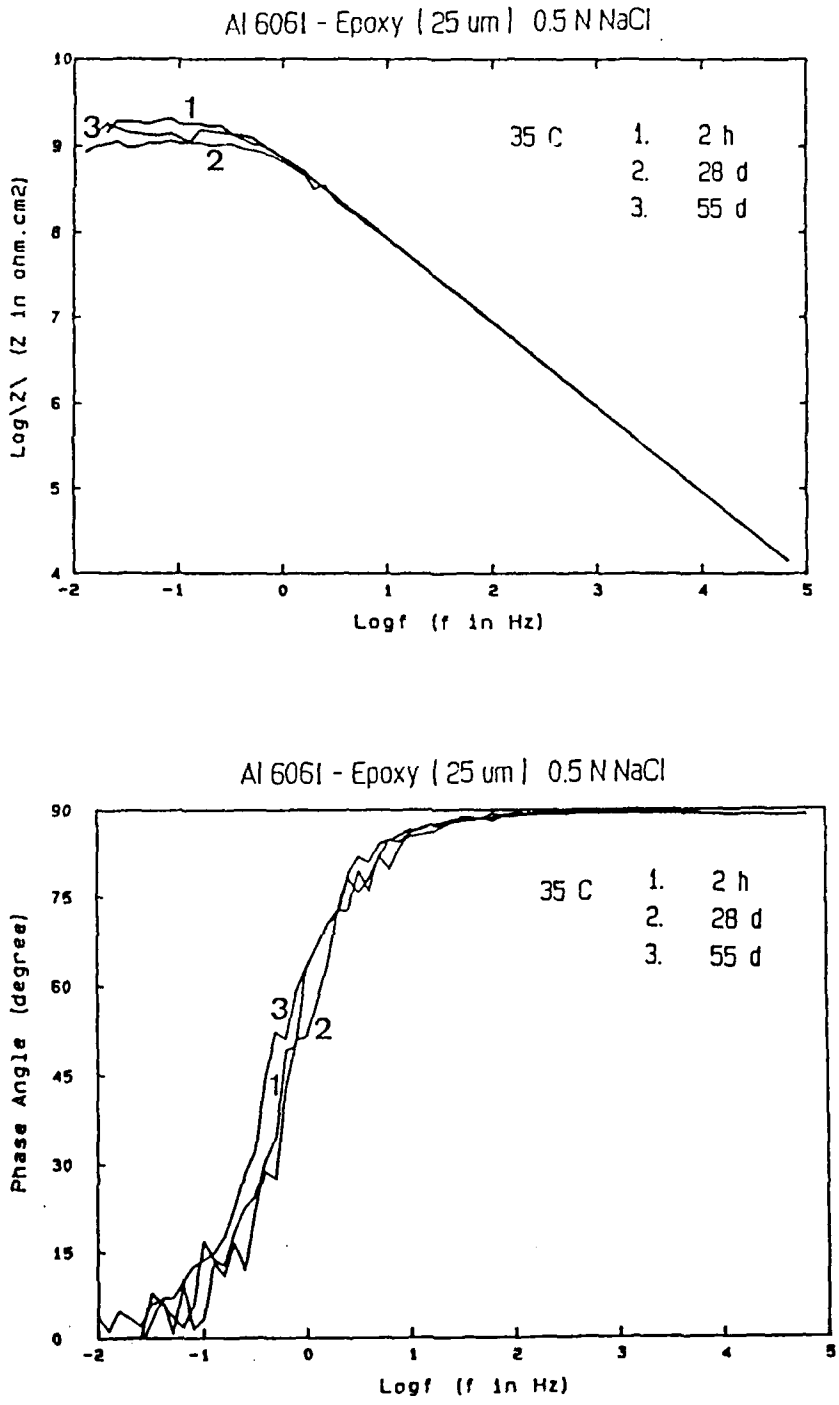

Fig.39.a and b Bode-plots for Al 6061 with a 25-µm epoxy coating as a function of exposure time to 0.5 N NaCl at 35°C.

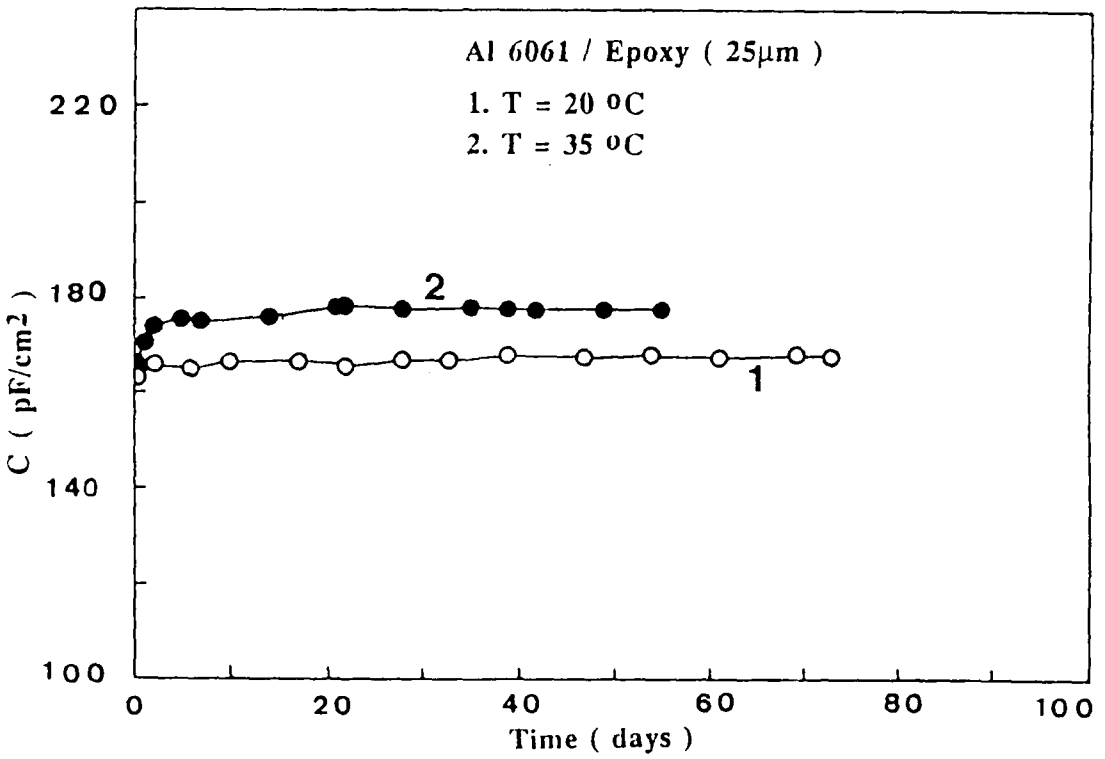

Fig.40 Time dependence of the capacitance C_C for Al 6061 with a 25-μm epoxy coating during exposure to 0.5 N NaCl at 20°C and 35°C.

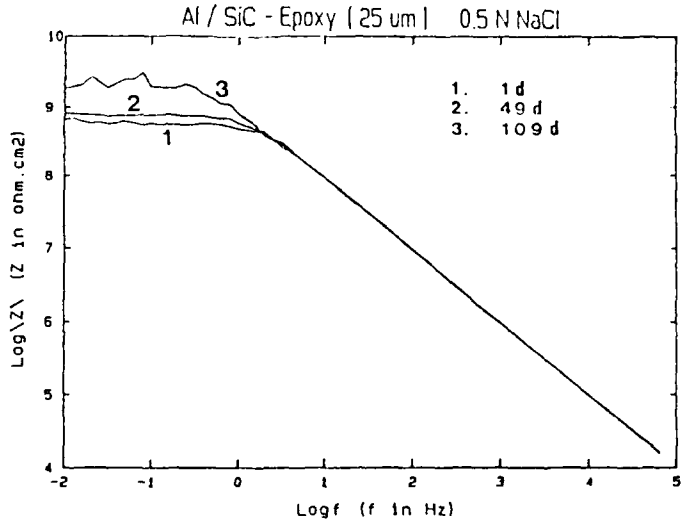

Fig.41 Bode-plots for Al/SiC with a 25-µm epoxy coating as a function of exposure time to 0.5 N NaCl.

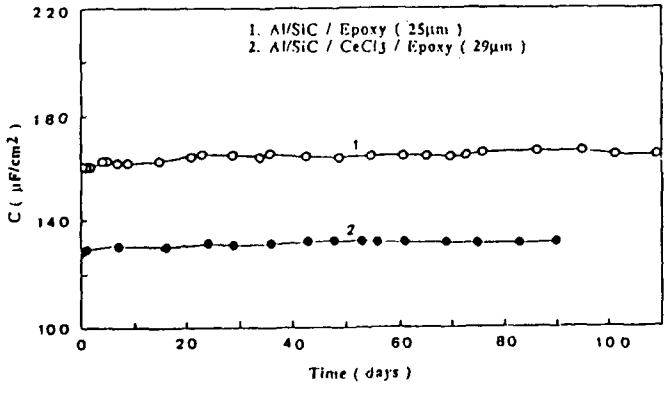

Fig.42 Time dependence of the capacitance C_C for Al/SiC with a 25 µm epoxy coating (curve 1) and Al/SiC which had been pretreated by immersion in $CeCl_3$ and coated with a 29-µm epoxy coating (curve 2) during exposure to 0.5 N NaCl.

not show any damage, such as pits, delamination or filiform corrosion. Fig.42 shows that the capacitance gradually increased with increasing exposure time and reached a constant value after 23 days. The capacitance increased by 3% after 102 days and the water uptake of the coating was 0.7%. This very stable behavior demonstrate the excellent corrosion resistance of the epoxy coated Al/SiC and the excellent adhesion between the epoxy coating and the Al/SiC surface.

In order to evaluate the effects of damage to the coating and the resistance to coating delamination, a hole of 0.7 mm diameter was drilled into the sample surface. The spectra in Fig.43.a and b are dominated by the reactions in the damaged area (curves 2-5). The spectra also show the solution resistance in the hole R_h between 10^4 Hz and 10^5 Hz, the capacitance C_{pit} of the damaged area at 10 to 100 Hz, the polarization resistance R_{pit} of the damaged area at about 0.01 to 1 Hz and transmission line-type behavior at about 0.01 to 1 Hz. The capacitance of coating, C_c, cannot be observed in curves 2-5 because it occurs at frequencies above 100 kHz and is consistent with curve 1. R_h increased with increasing exposure time due to build-up of corrosion products in the hole. C_{pit} also increased with time due to an increase of corroding area. Based on the initial area of the drilled hole, C_{pit} is calculated as 30 $\mu F/cm^2$ and R_{pit} as $3 * 10^3$ ohm-cm^2, which is equivalent to a corrosion rate of 0.66 mm/y for the first 2 hr of exposure time. Fig.44.a shows that the capacitance C_{pit} of the damaged area increased with increasing exposure time. Assuming that the normalized value of C_{pit} = 30 $\mu F/cm^2$ remains constant during the exposure period, then the damaged area increased in a similar manner as C_{pit} in Fig.44.a and R_{pit} (in ohm-cm^2) increased with increasing exposure time as shown in Fig.44.b. Hence, the growth rate of the damaged area in the coating decreased with increasing exposure time presumably due to ohmic control resulting from the increase of the solution resistance in the hole, R_h, as a result of the formation of corrosion products (Fig.44.b). The minimum of the phase angle ϕ_{min} corresponding to R_h and the frequency f_{min} corresponding to the minimum of the phase angle ϕ_{min} decreased with exposure time (Fig.44.c). The initial corrosion rate of the artificial pit was only 0.66 mm/y and delamination did not occur for 93 days. The surface around the damaged area did not show any color change and also passed the delamination test in which the coating around the damaged area was scribed to the substrate to form an "x" and tested with a piece of double adhesion tape. No part of the coating was found on the tape after this pull-test.

3.4.3 Al 6061/Gr

The Al/Gr sample used in these tests had exposed graphite at some areas of the surface. An 32 μm epoxy coating was applied and the corrosion behavior was studied in 0.5 N NaCl. The spectra in Fig.45 for coated Al/Gr show essentially capacitive behavior and a resistive component about 10^9 ohm-cm^2 at the lowest frequencies. Fig.46 shows that the capacitance rapidly increased in the first 3 days and then reached a constant value after about 50 days. The capacitance increased was 7.9 % and the water uptake was calculated to be 1.7 % after 98 days. The coating did not show pits, delamination or filiform corrosion after the exposure test. Therefore, the epoxy coatings provided excellent corrosion protection for Al/Gr in 0.5 N NaCl despite the fact that the face sheet contained some defects which would have caused galvanic corrosion in the absence of the coating. The water uptake of the coating was higher than for coatings on Al/SiC and Al 6061. This result may be due to the shorter curing time which was used for the coating on Al/Gr.

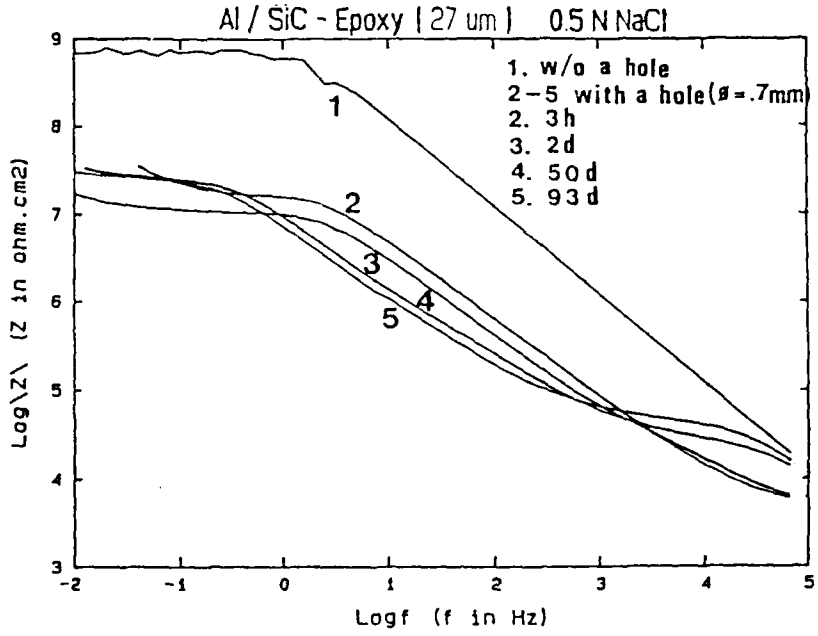

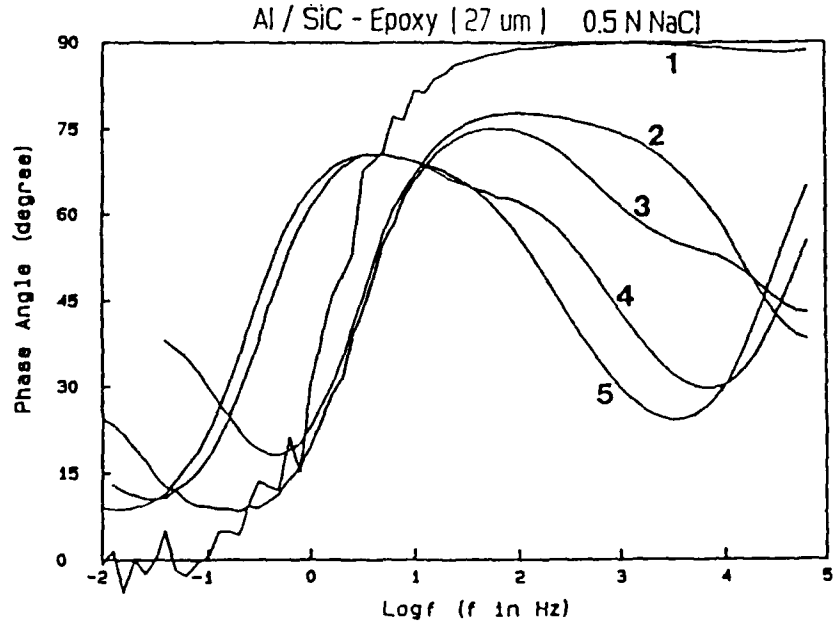

Fig.43.a and b Bode-plots for Al/SiC with a 27-µm epoxy coating containing a hole of 0.7 mm diameter (curve 2-5) and without a hole (curve 1) as a function of exposure time to 0.5 N NaCl.

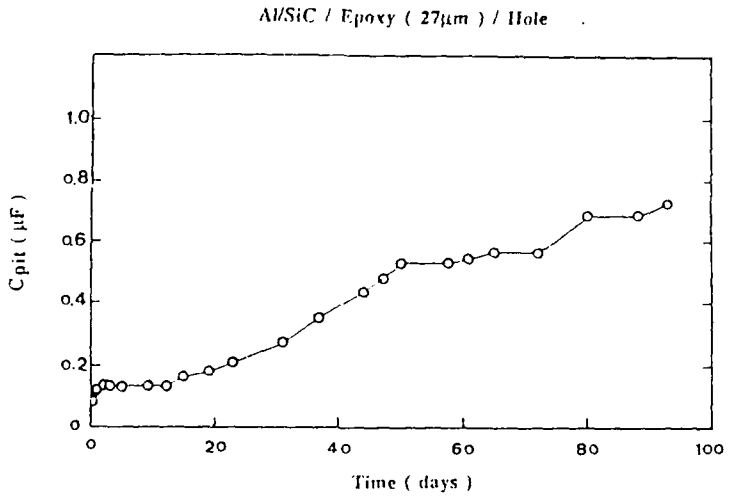

a

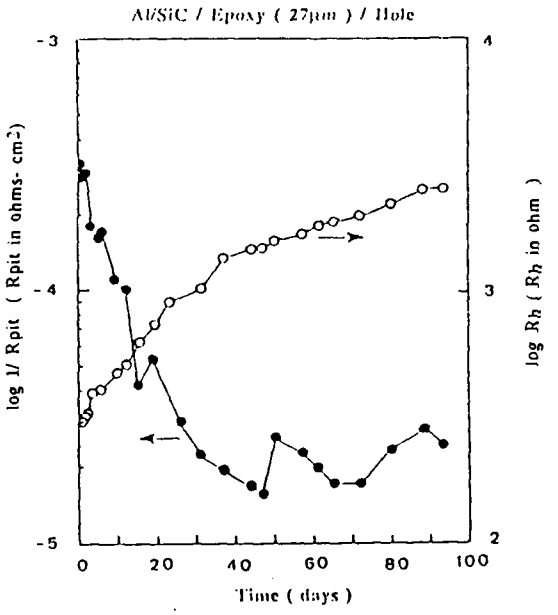

b

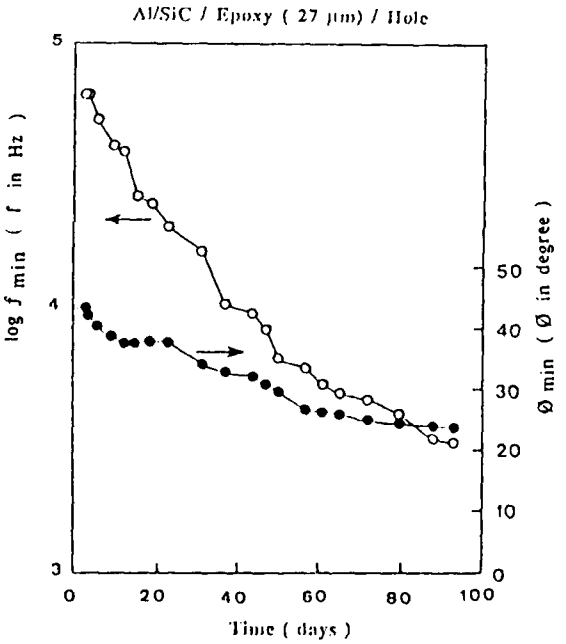

c

Fig.44 Analysis of impedance data for Al/SiC with a 27-μm epoxy coating containing a hole of 0.7 mm diameter as a function of exposure time to 0.5 N . NaCl
(a) C_{pit} , (b) $1/R_{pit}$ and R_h
(c) f_{min} and $Ø_{min}$

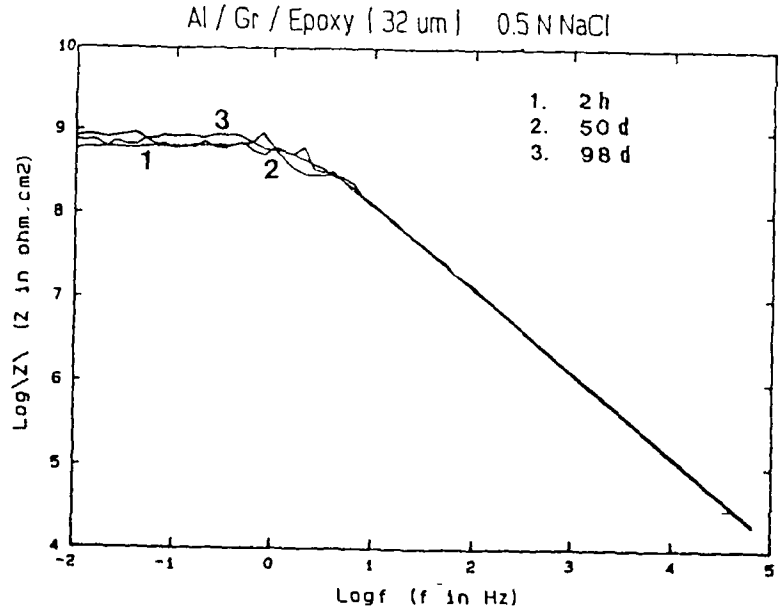

Fig.45 Bode-plots for Al/Gr with 32-µm epoxy coating as a function of exposure time to 0.5 N NaCl.

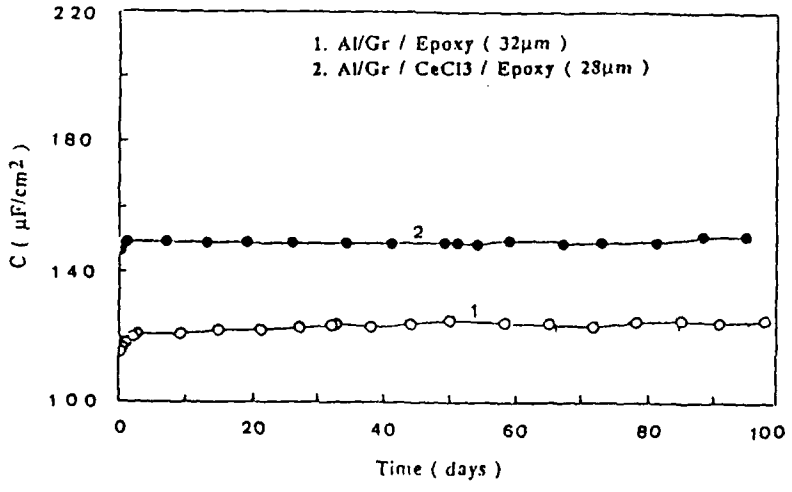

Fig.46 Time dependence of the capacitance C_c for Al/Gr with a 32-µm epoxy coating and Al/SiC which had been pretreated by immersion in $CeCl_3$ and coated with a 28-µm epoxy coating during exposure to 0.5 N NaCl.

3.4.4 Al-Li 2091-T6

Al-Li alloys possess lower density and exhibit a higher stiffness than other Al alloys. The composition of the Al-Li 2091-T6 was given in Table I. The impedance spectra for as-received Al-Li 2091-T6 exposed to 0.5 N NaCl show the changes of the frequency dependence of impedance and phase angle at low frequencies (0.0 1 to 0.1 Hz) which are characteristic of pitting (Fig.47). The surface of the as-received Al-Li 2091-T6 showed pitting within 2 hr. Since Li is one of the most reactive elements, Al-Li alloys possess very poor corrosion resistance.

The results of the analysis of the impedance data for as-received Al-Li 2091-T6 obtained by fitting to the pitting model are shown in Fig.48.a and b. The as-received Al-Li 2091-T6 showed very poor corrosion behavior and pitting occurred within 2 hr. The polarization resistance R_p for the passive surface remained constant, while R_{pit}/F showed a decrease with exposure time (Fig.48.a). The capacitance C_t for as-received Al-Li 2091-T6 increased sharply from 8 $\mu F/cm^2$ to 58 $\mu F/cm^2$ during 5 days of exposure (Fig.48.b) most likely due to a large increase of F with exposure time and a very large capacitance C_{pit}.

Fig.49 shows impedance spectra for Al-Li 2091-T6 with a 30 μm epoxy coating during exposure to 0.5 N NaCl for 90 day. The spectra show essentially capacitive behavior and a resistive component about 10^9 ohm-cm^2 at the lowest frequencies. The capacitance gradually increased with increasing exposure time and reached a constant value after 49 days. The water uptake was calculated as 0.9 % after 90 days. The coating surface did not show pits, delamination or filiform corrosion after 90 days. This very stable behavior demonstrates the excellent corrosion resistance of the epoxy coated Al-Li which is in contrast to the very poor corrosion resistance of the bare surface.

A hole of 0.75 mm diameter was drilled into the surface of epoxy coated Al-Li 2091-T6 to evaluate the effects of damage, such as a scratch, to the coating and the resistance to coating delamination and corrosion of the exposed Al-Li surface. The spectra in Fig 50.a and b are for coated Al-Li 2091-T6 with and without an artificial pit. Curve 1 for the coated sample without an artificial pit shows essentially capacitive behavior. Curve 2 is dominated by the corrosion reactions in the artificial pit. The capacitive behavior at about 10^6 Hz corresponds to the coating capacitance C_c and that at about 100 Hz corresponds to the capacitance C_{pit} of the artificial pit. The ohmic component at about 10^5 Hz corresponds to the solution resistance R_p in the artificial pit and the resistive component at about 0.2 Hz corresponds to the polarization resistance R_{pit} of the artificial pit. The spectra show transmission line-type behavior below about 0.2 Hz. The surface showed delamination and the color of coating surface around the artificial pit changed from light yellow to light brown after 5 days. Curve 3 shows that the capacitance C_{pit} increased markedly and that the resistive component R_{pit} of the artificial pit decreased after 9 days.

3.4.5 MgAZ31B

Fig.51 shows impedance spectra for a 30 μm epoxy coating on Mg during exposure to 0.5 N NaCl for 95 days. The spectra show essentially capacitive behavior and a resistive component about 10^9 ohm-cm^2 at the lowest frequencies for 1 day (curve 1) and 56 days (curve 2). Changes to a transmission line model at the lower frequencies were observed after 82 days (curve 3) and 95 days (curve 4)

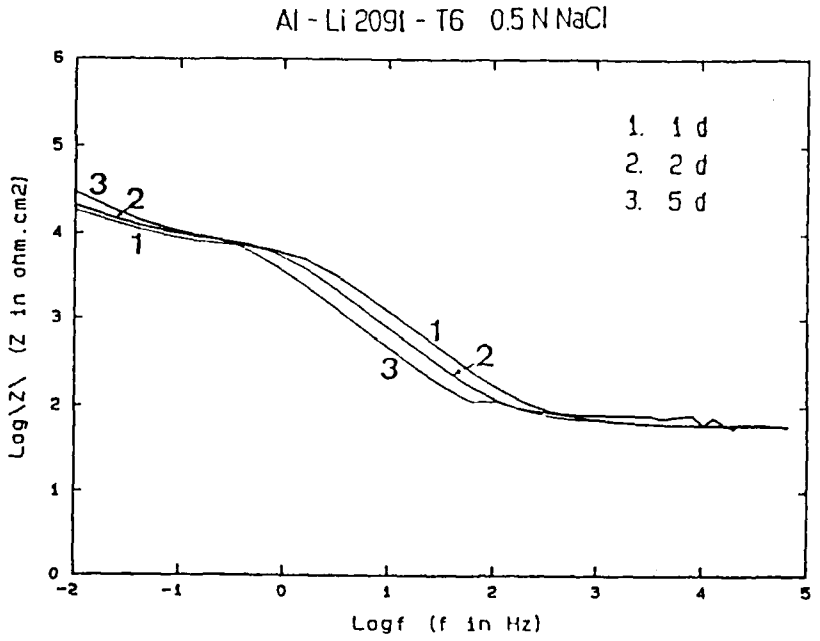

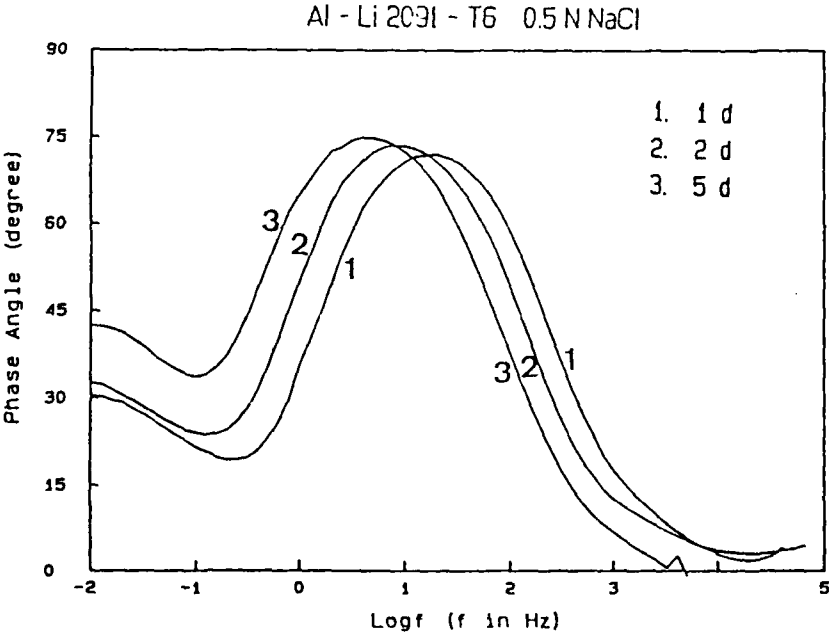

Fig.47.a and b Bode-plots for as-received Al-Li 2091-T6 as a function of exposure time to 0.5 N NaCl.

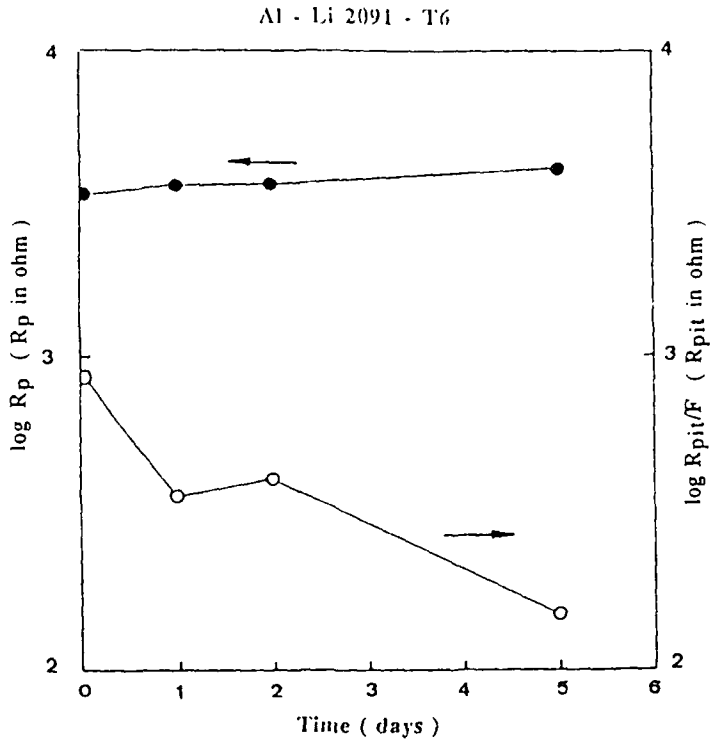

a

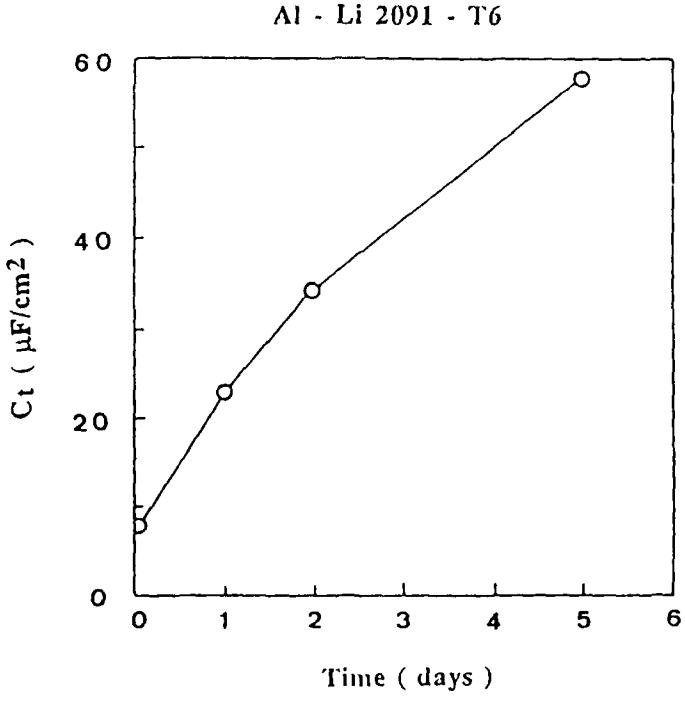

b

Fig.48.a and b Analysis of impedance data for as-received Al-Li 2091-T6 as a function of exposure time to 0.5 N NaCl.
(a) R_p and R_{pit}/F
(b) C_t.

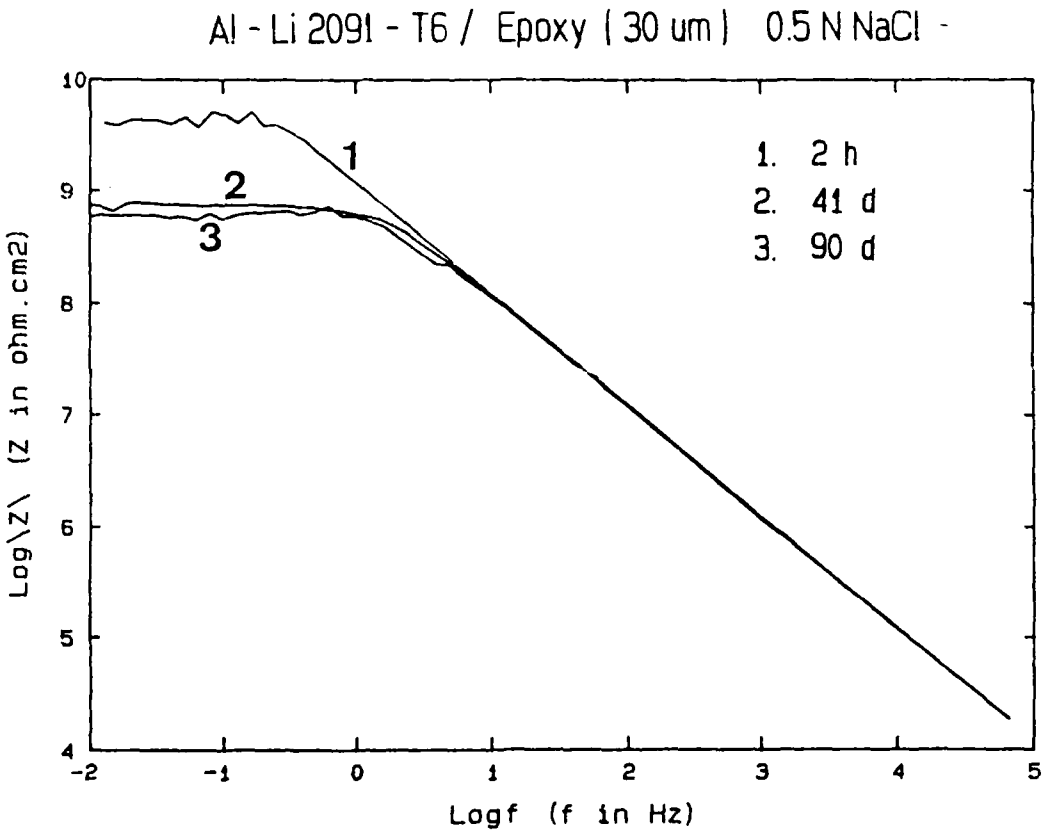

Fig.49 Bode-plots for Al-Li 2091-T6 with a 30 µm epoxy coating as a function of exposure time to 0.5 N NaCl.

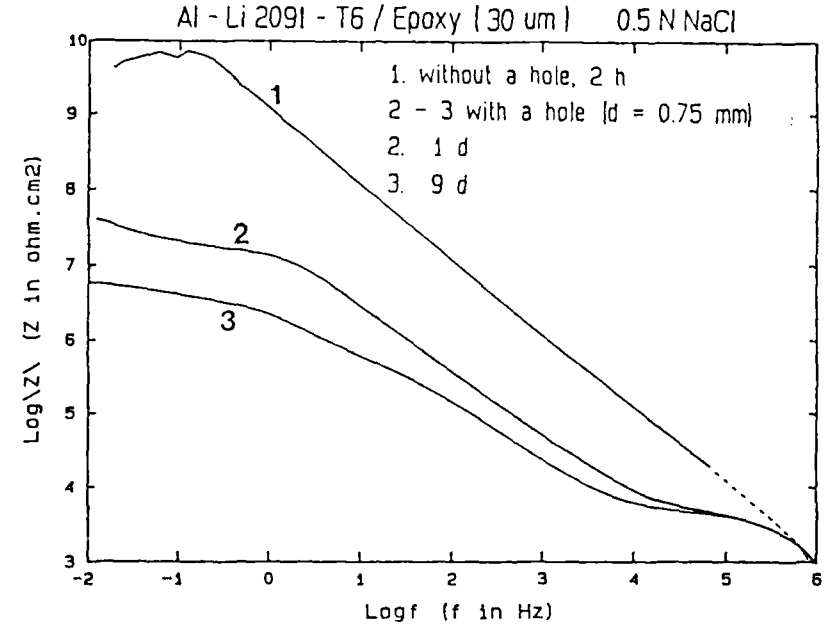

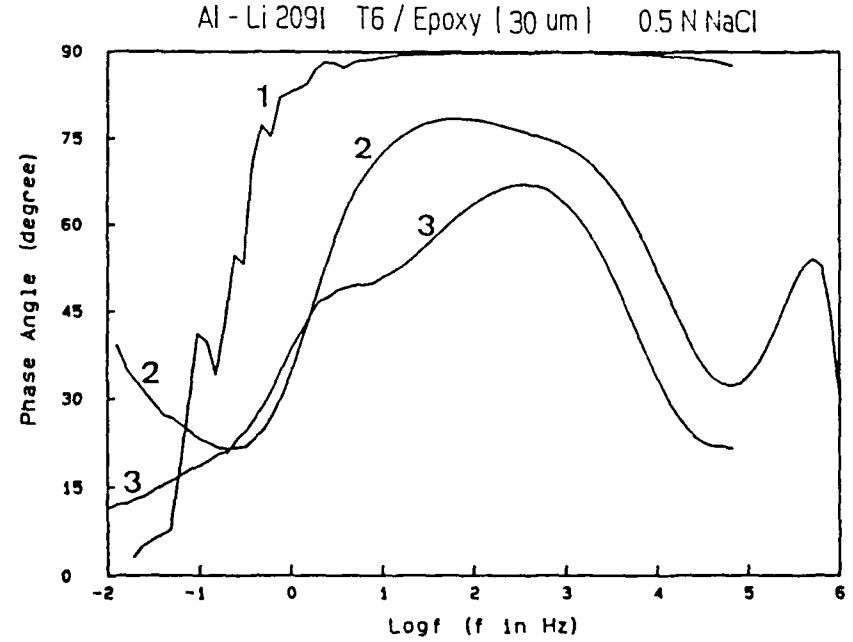

Fig.50.a and b Bode-plots for epoxy (30 μm) coated Al-Li 2091-T6 with a hole of 0.7 mm diameter and without a hole as a function of exposure time to 0.5 N NaCl.

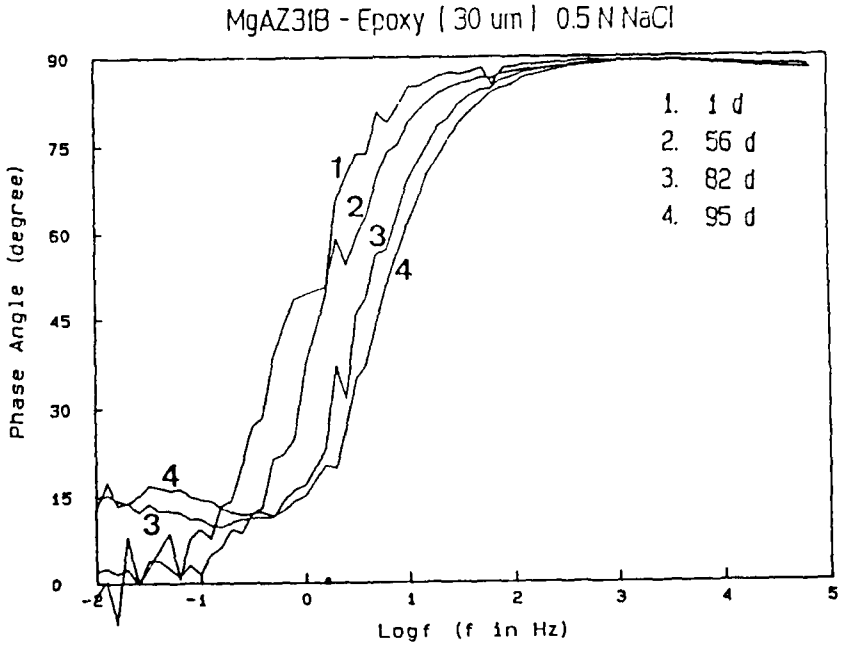

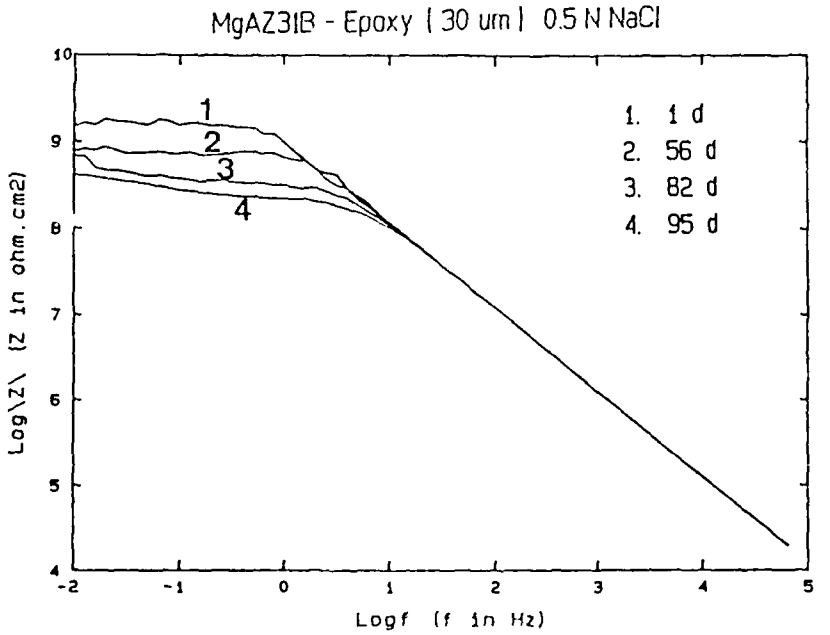

Fig.51.a and b Bode-plots for MgAZ31B with a 30 µm epoxy coating as a function of exposure time to 0.5 N NaCl.

due to filiform corrosion on the surface under the coating. However, the impedance spectra did not indicate the onset of the filiform corrosion after 25 days apparently due to the small area of the active head of the filament. The brown coloration of the inactive tail may be due to the presence of $Mn(OH)_2$ because MgAZ31B contains 0.2 wt % of Mn (Table I). Although filiform corrosion occurred under the epoxy coating, the coating film did not show any damage. Therefore, the observed increase of the coating capacitance must be due to water uptake of the coating. The capacitance increase was 3.4% and the water uptake was 0.8 % after 98 days. Since filiform corrosion only affects the surface appearance, it can be concluded that this epoxy coating provided excellent corrosion protection for MgAZ31B.

3.5 Chemical Passivation Combined with Polymer Coatings

In order to evaluate the adhesive quality between the epoxy coatings and the passive film which contains a mixture of ceric oxides, hydrated cerium oxides and aluminum oxides, degreased samples of Al 6061, Al/SiC, and Al/Gr were passivated by immersion in $CeCl_3$ and then coated with epoxy.

3.5.1 Al 6061

For the purpose of evaluating the effects of the damage to the coating and the resistance to coating delamination, a hole of 0.6 mm diameter was drilled into Al 6061 which had been passivated by immersion in $CeCl_3$ and coated with a 28 μm epoxy layer. After 5 days of exposure to 0.5 N NaCl, the surface of the coated Al 6061 showed filiform corrosion starting from the edge of the hole. The impedance spectra in Fig.52 are for the coated sample without a hole (curve 1) and with a hole (curves 2 - 3). Curve 1 shows essentially capacitive behavior, while curves 2 and 3 are dominated by the corrosion reactions in the artificial pit. The capacitive behavior in the frequency of range of about 10^6 Hz corresponds to coating capacitance C_c and that in the frequency range of 100 to 1000 Hz corresponds to the capacitance C_{pit} for the artificial pit (curves 2 and 3). The ohmic component at about $5 * 10^4$ Hz corresponds to the solution resistance R_h in the artificial pit Not much change of C_{pit} was observed during the first 13 days of immersion. After filiform corrosion occurred, the spectra (curve 2) showed a second time constant in the low-frequency range. Filiform corrosion does not destroy metallic components, but only affects the surface appearance [13,40]. Hence, chemical passivation combined with epoxy coating can provide excellent corrosion resistance for Al 6061.

3.5.2 Al/SiC MMCs

The spectra shown in Fig.53 for Al/SiC which had been pretreated by immersion in $CeCl_3$ and coated with a 29 μm epoxy film are very similar to those for epoxy coated Al/SiC (Fig.41). The three curves measured on the 1st, 48th and 90th day of exposure to NaCl are very similar suggesting that the system is very stable. The capacitance of the coating increased slightly and reached a constant value after 43 days (Fig.42). No filiform corrosion, pits or delamination of the coating was detected visually after 90 days of exposure. The capacitance increased by 2.5 %. and water uptake was 0.6 %. This stable result indicates excellent adhesion between the passive film produced in $CeCl_3$ and the epoxy coating on Al/SiC.

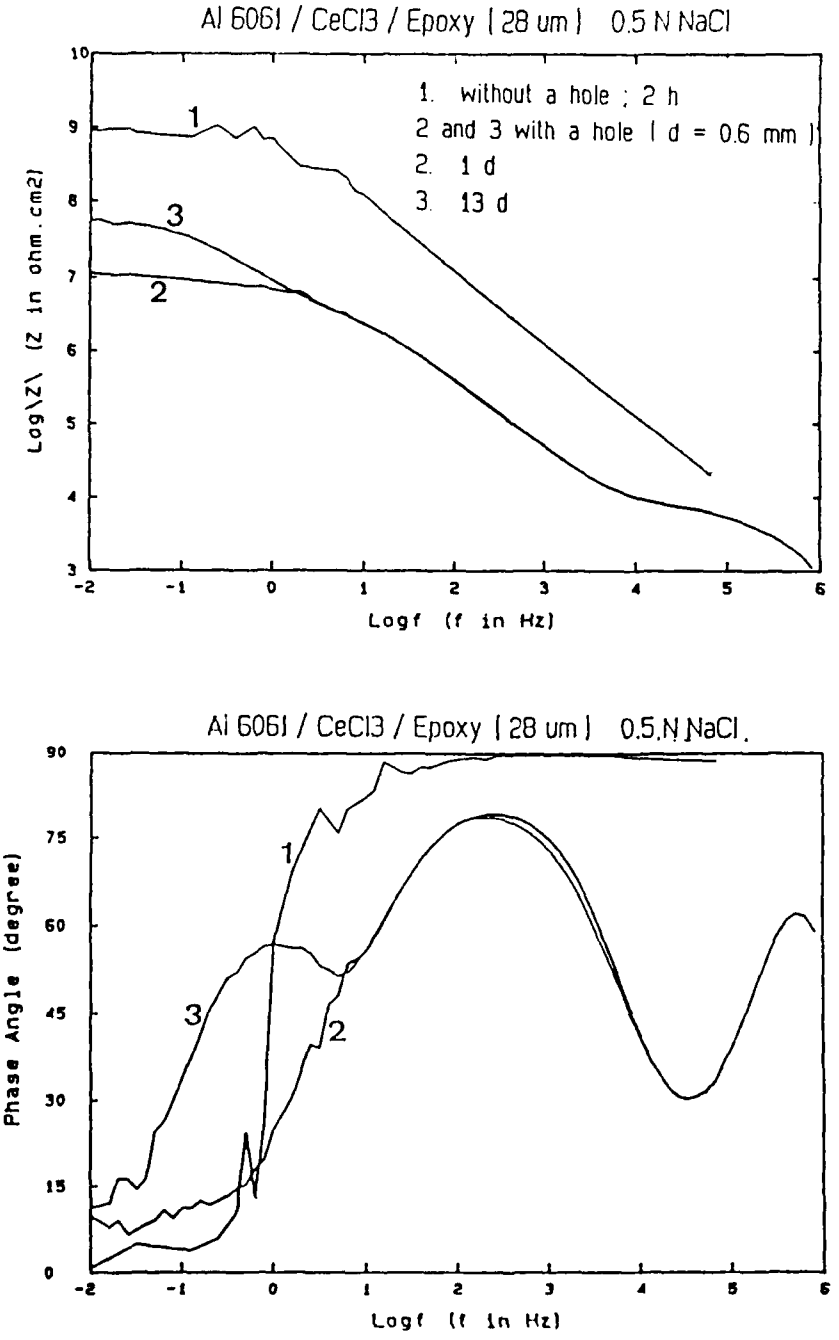

Fig.52.a and b Bode-plots for Al 6061 which had been pretreated by immersion in $CeCl_3$ and coated with a 28 µm epoxy coating containing a hole of 0.6 mm diameter (curve 2 and 3) and without a hole (curve 1) as a function of exposure time to 0.5 N NaCl.

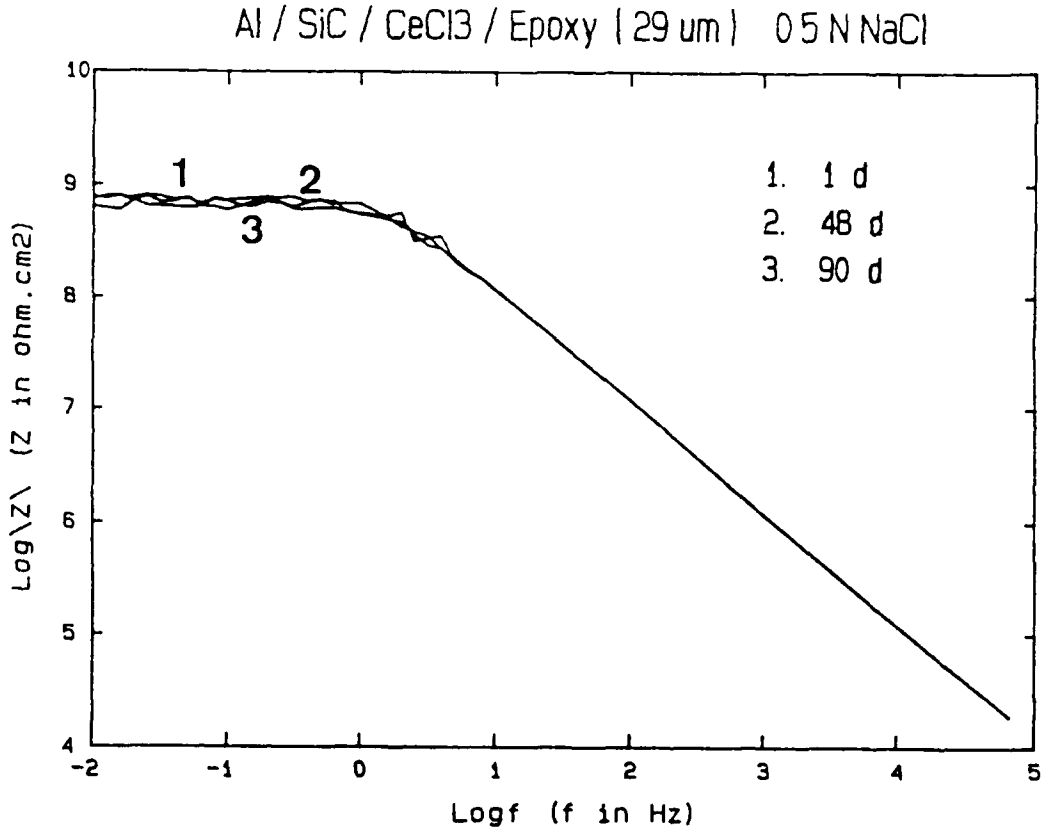

Fig.53 Bode-plots for Al/SiC which had been pretreated by immersion $CeCl_3$ and coated with a 29µm epoxy coating as a function of exposure time to 0.5 N NaCl.

A hole of 0.7 mm diameter was drilled to evaluate the effects of damage to the coating and the resistance to coating delamination. The surface showed slight delamination at the end of the test of 90 days and the color of the coating surface around the hole had changed to yellow. This result suggests that the adhesion between the passive film produced in $CeCl_3$ and the epoxy coating is slightly less than that between the original Al surface and the epoxy coating. The impedance spectra in Fig.54 are for a coated sample without a hole (curve 1) and with a hole (curves 2 - 4). Curve 1 shows essentially capacitive behavior, while Curves 2,3 and 4 are dominated by the corrosion reactions in the artificial pit. C_{pit} changed slightly during the first 7 days of immersion and then increased sharply after 83 day immersion (Fig.54).

3.5.3 Al/Gr MMCs

Fig.55 shows impedance spectra for Al/Gr passivated by immersion in $CeCl_3$ and coated with a 28 μm epoxy film. The spectra shown in Fig.55 for a 90-day exposure period in 0.5 N NaCl are very similar to those for the epoxy coated Al/Gr in Fig.45. The capacitance of the coating gradually increased and reached a constant value after 59 days as shown in Fig.46. Since the surface of the coated sample did not show pits, filiform corrosion, or delamination after 92 days, the increase of the coating capacitance was assumed to be due to water uptake. The increase of capacitance C_c by 3.1 % after 92 days of exposure corresponds to 0.7 % water uptake. This stable behavior suggests excellent adhesion between passive film which was formed in $CeCl_3$ and the epoxy coating.

3.6 Cr-Mn Conversion Coatings Combined with Polymer Coatings

Epoxy coated MgAZ31B showed filiform corrosion after 25 days of exposure to 0.5 N NaCl (Fig.51). In order to enhance the adhesion between the epoxy coating and the substrate, MgAZ31B was pretreated with a porous Cr-Mn conversion coating. This porous film combined with epoxy produced excellent corrosion protection. The Cr-Mn process is described in the British specification, DTD 911C. The Cr-Mn conversion bath consists of sodium dichromate, manganese sulfate, and magnesium sulfate [19].

Fig.56 show impedance spectra for MgAZ31B pretreated with the Cr-Mn conversion coatings and then coated with a 24 μm epoxy film. The surfaces did not show pits, filiform corrosion, or delamination after 92 days exposure to 0.5 N NaCl. The spectra showed mainly capacitive behavior during the entire exposure period. The capacitance increased by 3.3% corresponding to a water uptake of 0.7 % after 92 days. These stable results demonstrate that the porous Cr-Mn conversion coating provides an excellent base for epoxy coatings on MgAZ31B.

A hole of 0.7 mm diameter was drilled into the surface of Mg which had been pretreated with the Cr-Mn conversion coating and coated with 24 μm epoxy. Curve 1 in Fig.57.a and b shows essentially capacitive behavior without an artificial pit, while curves 2 and 3 are dominated by the corrosion reactions in the artificial pit. A large increase of the C_{pit} and a decrease of the R_{pit} were observed after 56 days immersion (Fig.57). The surface did not show delamination or filiform corrosion after 40 days. Based on the double layer capacitance of 10 $\mu F/cm^2$ calculated from the data at 2 hr immersion, the pitted area was determined from the experimental value of C_{pit}. The results of the data analysis are shown in Fig.58 for R_{pit} and C_{pit} as a function of time. C_{pit} increased with exposure time, indicating that the pitted area increased with

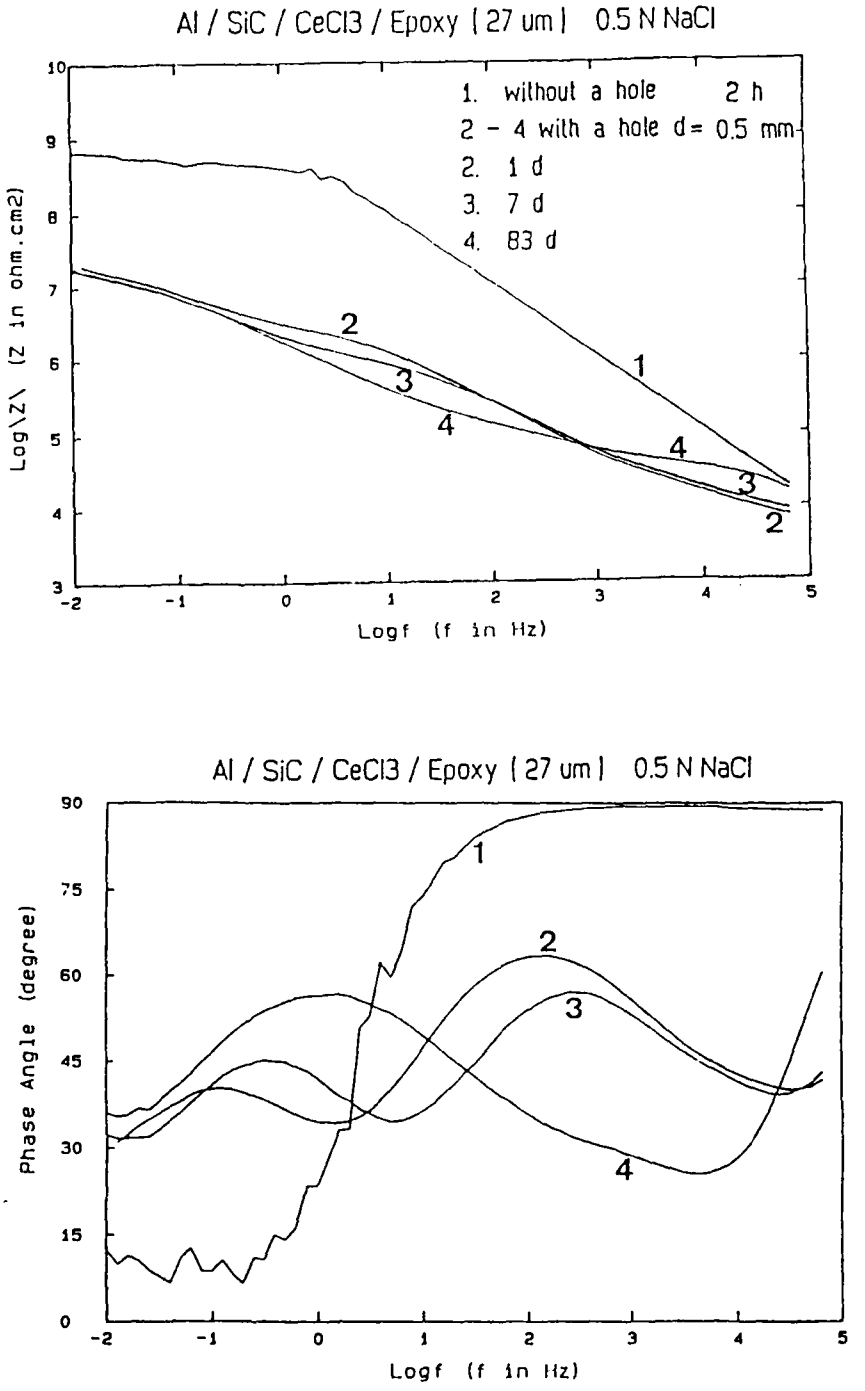

Fig.54.a and b Bode-plots for Al/SiC which had been pretreated by immersion in $CeCl_3$ and coated with a 27 µm epoxy coating containing a hole of 0.5 mm diameter (curve 2-4) and without a hole (curve 1) as a function of exposure time to 0.5 N NaCl.

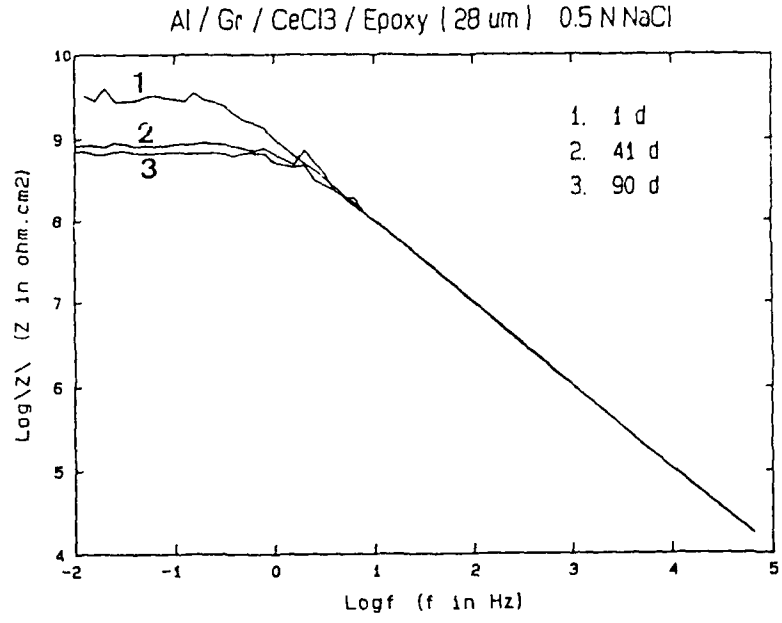

Fig.55 Bode-plots for Al/Gr which had been pretreated by immersion $CeCl_3$ and coated with a 28 µm epoxy coating as a function of exposure time to 0.5 N NaCl.

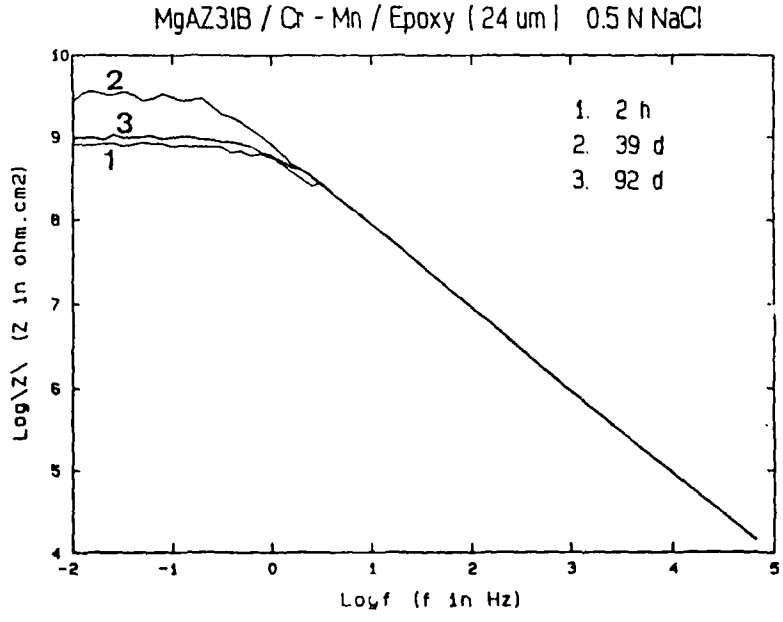

Fig.56. Bode-plots for MgAZ31B which had been pretreated with Cr-Mn conversion coating and coated with a 24 µm epoxy coating as a function of exposure time to 0.5 N NaCl.

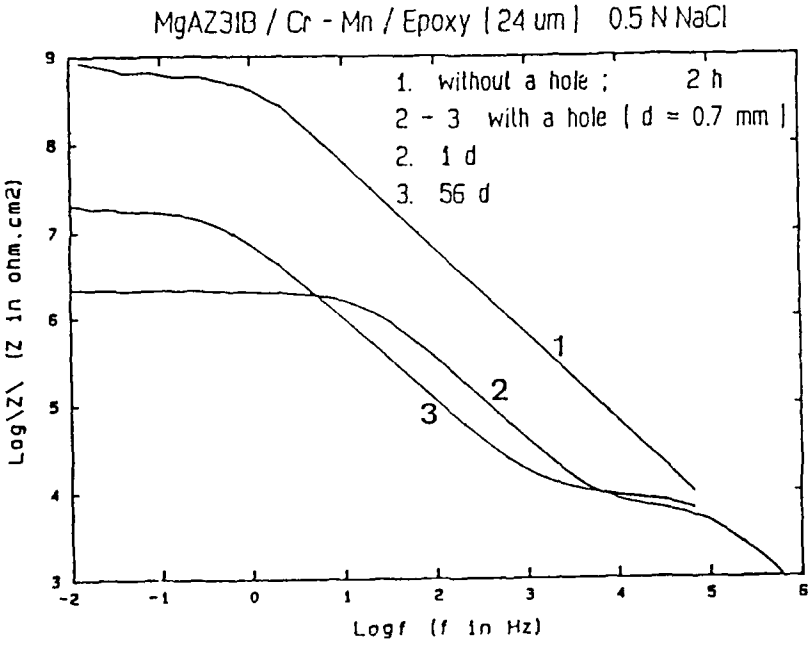

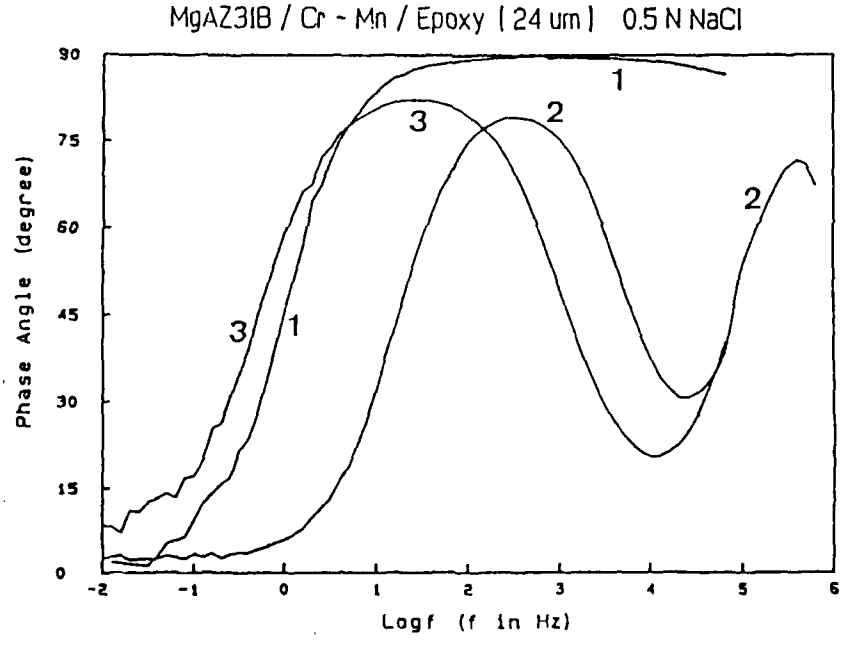

Fig.57.a and b Bode-plots for MgAZ31B which had been pretreated with Cr-Mn coating and coated with a 24 µm epoxy coating containing a hole of 0.7 mm diameter (curve 2-3) and without a hole (curve 1) as a function of exposure time to 0.5 N NaCl.

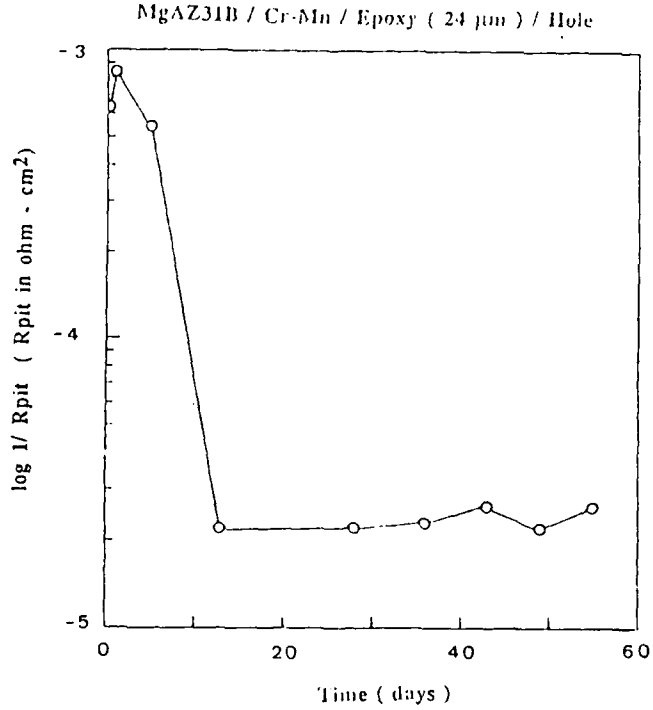

a

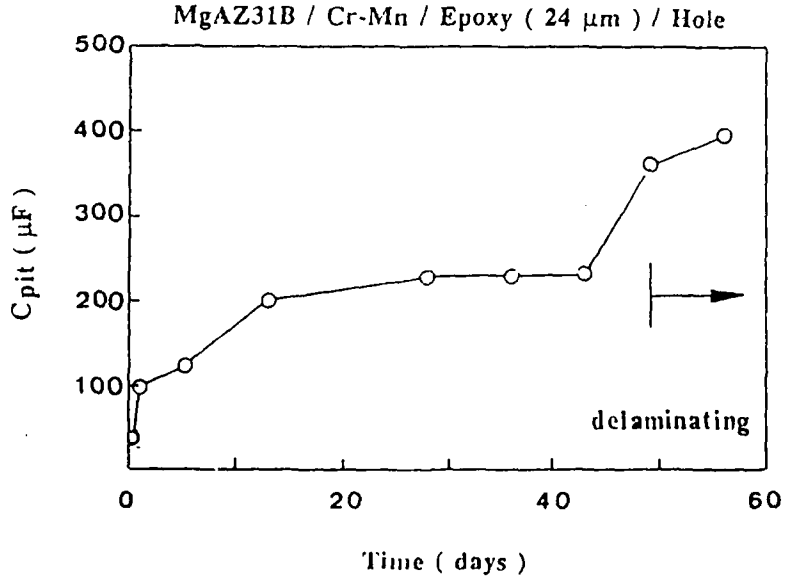

b

Fig.58 Analysis of impedance data for MgAZ31B pretreated with Cr-Mn and coated with a 24 μm epoxy coating containing a hole of 0.7 mm diameter as a function of exposure time to 0.5 N NaCl
(a) $1/R_{pit}$
(b) C_{pit}.

exposure time. R_{pit} (in ohm-cm^2) sharply increased during the first 13 days of exposure and then remained constant (Fig.58.a) which suggests that the corrosion rate of the artificial pit expressed as $1/R_{pit}$ decreased with exposure time. The value of R_{pit} =1.6 * 10^3 ohm-cm^2 during the first 2 hr immersion in Fig.57.a was much larger than that for as-received Mg for which R_{pit} =1 * 10^2 ohm-cm^2. The capacitance C_{pit} increased sharply during the first 13 days of exposure and then showed a more gradual increases (Fig.58.b). After 43 days of exposure, C_{pit} rapidly increased again. Blistering was observed around the artificial pit after 49 days. Delamination may have initiated prior to 49 days of exposure. Evolution of hydrogen gas was not detected visually and the EIS data did not show an inductive loop. Therefore, the corrosion rate of the artificial pit was not as high as that of the bare Mg. This result is due to the smaller cathodic area which drives the corrosion reaction in the artificial pit. The cathodic reaction occurring at the interface between the coating and the substrate around the hole produced high pH levels which decreased the adhesion of the coating. These results show that an artifical pit drilled into the coating surface can serve as an accelerated corrosion test to evaluate the quality of the surface preparation procedure and the corrosion protection provided by the coating.

3.7 Summary

Table IV gives a comparison of the times at which filiform corrosion or delamination were first detected visually for epoxy coated samples. All epoxy coated samples without an artificial hole did not show pits and delamination after exposure to 0.5 N NaCl. These results suggest that epoxy coatings provide excellent corrosion protection for Al 6061, Al/SiC, Al/Gr, Al-Li 2091-T6 and MgAZ31B during exposure to 0.5 N NaCl. For samples with an artificial pit the best adhesion of the epoxy coating was found for epoxy coated Al/SiC. However, for chemically passivated Al/SiC with an epoxy coating containing a hole, delamination occurred after 90 days, indicating that the adhesion between the epoxy coating and passive film produced in $CeCl_3$ was weaker than that between the epoxy coating and Al/SiC. The thickness of the epoxy coatings as measured by a micrometer was in a good agreement with that calculated from coating capacitance using Eq.3.1 and a dielectric constant of 4.3. The water uptake of the coatings was between 0.6 % and 1.0 % for most epoxy coated samples.

4. DISCUSSION

The corrosion protection of Al alloys, Al-based MMCs, and MgAZ31B provided by chromate coatings, anodic layers, polymer coatings and chemical passivation in $CeCl_3$ will be discussed in the following.

4.1 The Corrosion Behavior of Al 6061, Al/SiC, Al/Gr, and MgAZ31B

Six different types of coatings were applied to the materials studied, including chromate conversion coatings, anodized layers, coatings produced by chemical passivation in $CeCl_3$, polymer coatings, chemical passivation combined with polymer coatings, and Cr-Mn combined with polymer coatings. Comparisons of pitting times or damage times for the coated and the untreated samples are shown in Tables II,III, and IV. The untreated Al alloys, Al-based MMCs, Al-Li 2091-T6, and MgAZ31B had a low corrosion resistance and showed pitting within one day of exposure to 0.5 N NaCl. The effects of the coatings on the corrosion resistance will be discussed in the following for the different types of

Table IV Comparison of Damage Time and Water Uptake for Epoxy Coated Samples

Material	Coating	Thickness (μm, *)	Damage Time (days at 20°C)	Water Uptake (%)
Al 6061	epoxy	25 (23)	> 73 [n]	0.7
			55 [n] (35°C)	1.0
Al/SiC	epoxy	25 (23)	>109 [n]	0.7
Al/Gr	epoxy	32 (33)	> 98 [n]	1.7
Al-Li 2091-T6	epoxy	30 (30)	> 90 [n]	0.9
MgAZ31B	epoxy	30 (31)	> 25 [f]	0.8
Al/SiC	$CeCl_3$/epoxy	29 (30)	> 90 [n]	0.6
Al/Gr	$CeCl_3$/epoxy	28 (26)	> 95 [n]	0.7
MgAZ31B	Cr-Mn/epoxy	24 (22)	> 92 [n]	0.7
Al/SiC	epoxy/hole	27 (28)	> 109 [n]	
Al-Li 2091-T6	epoxy/hole	30 (30)	> 5 [d]	
Al 6061	$CeCl_3$/epoxy/hole	28 (30)	> 5 [f]	
Al/SiC	$CeCl_3$/epoxy/hole	27 (28)	> 90 [d]	
MgAZ31B	Cr-Mn/epoxy/hole	24 (22)	> 49 [d]	

* Thickness was measured with a micrometer; values in brackets were calculated from the coating capacitance using a dielectric constant of 4.3.

n : no damage

f : filiform corrosion

d : delamination

material.

4.1.1 Al 6061

For Al 6061, the chromate conversion coating (Alodine 600), conventional and hard anodized layers (SAA + HWS), chemical passivation in $CeCl_3$, the polymer coating, and chemical passivation combined with the polymer coating provided excellent corrosion resistance to 0.5 N NaCl.

4.1.2 Al/SiC

For Al/SiC, the chromate conversion coating (Alodine 600) and anodizing (SAA + HWS) provided significant corrosion protection, but were not as effective as Al 6061. This result suggests that the presence of SiC particulates in the surface layers produced these adverse changes. Chemical passivation in $CeCl_3$ provided much better corrosion resistance of Al/SiC than chromate conversion coatings or anodizing. Polymer coatings and chemical passivation combined with a polymer coating provided excellent corrosion resistance in 0.5 N NaCl. The results obtained in this study for hard anodized Al/SiC, which contained 25 % SiC particulates, are in a good agreement with those reported for Al/SiC which contained 10 % SiC particulates [12].

Trzaskoma et al. [49] anodized Al/SiC which contained 20 vol% SiC whiskers with diameters of 0.5-1 μm and lengths up to 50 μm. The effect of anodizing in sulfuric acid and sealing in hot water on the corrosion resistance of Al/SiC (SAA + HWS) was studied by AC impedance. The impedance spectra [49] for anodized Al/SiC showed a lot of scatter which can be traced back to experimental problems. The impedance at the lowest frequencies was about 10^3 to 10^4 ohm-cm^2 for anodized Al/SiC and 10^3 ohm-cm^2 for bare Al/SiC. Despite the experimental problems with the recording of valid EIS-data, Trzaskoma et al. [49] concluded that the corrosion resistance of Al/SiC can be improved by anodizing. In reference 12, the impedance for anodizing Al/SiC reached 10^4 to 10^5 ohm-cm^2 at the lowest frequencies. For the anodized Al/SiC studied here, which contains 25 vol % SiC particulates, the impedance reached 10^5 to 10^6 ohm-cm^2. These results suggest that the corrosion resistance of Al/SiC can be improved by anodizing. However, anodizing of Al/SiC is not as effective as for the corresponding wrought alloys. Apparently, the presence of the SiC particulates does not allow the formation of a continuous barrier layer as will be discussed below (see 4.3).

4.1.3 Al/Gr

For Al/Gr, the chromate conversion coating (Alodine 600) provided satisfactory corrosion protection, chemical passivation in $CeCl_3$ provided better corrosion resistance than chromate conversion coatings, and the epoxy coating or chemical passivation combined with the epoxy coating produced the best corrosion resistance of all coated surfaces. Compared with an epoxy/polyimide coating which showed delamination of the coating after 12 days exposure to 0.5 N NaCl [12], the epoxy coating and chemical passivation combined with the epoxy coating provided excellent corrosion resistance. The Al/Gr MMC studied in reference 12 contained exposed graphite particules in the surface.

Aylor et al. [50] have applied anodizing to Al 6061/VSB-32 Gr MMCs which contained 35 vol% graphite with three layers each of graphite and Al 6061 and

was covered by a 300 μm thick Al alloy face sheet. An anodic film of 13 μm was formed by anodizing in sulfuric acid and sealing in hot dichromate solution. The corrosion behavior was observed visually by immersing the samples in filtered seawater for 30, 60, 90, and 180 days. The surface showed slight pitting after 180 days of exposure [50]. Aylor et al. [51] also performed hard anodizing in sulfuric acid and sealing in sodium dichromate on Al/Gr which contained 40 vol% graphite and an Al 6061 face sheet of 300 μm thickness. This hard anodized Al/Gr showed slight pitting after 28 months of exposure to filtered seawater [51] which suggests that anodizing can provide excellent corrosion resistance for Al/Gr if the Al face sheet is thick enough to allow formation of a uniform anodic coating as on the anodized wrought Al alloys. For the Al/Gr MMCs studied in this project, which contained 55 vol% of P100 Gr with eight alternating layers of Gr and Al 6061, and was covered with an Al 6061 face sheet of only 50 μm thickness, anodizing in sulfuric acid at 20°C or 0°C and sealing in hot water did not produce a uniform anodic film. The surface of the anodic film showed some small black defects including graphite fibers. The face sheet of 50 μm thickness is too thin to allow satisfactory sulfuric anodizing for Al/Gr. In order to enhance the corrosion resistance of Al/Gr by anodizing, Al 6061 face sheets of at least 75 μm for conventional anodizing and at least 100 μm for hard anodizing are suggested. The resulting increase of the corrosion resistance in hostile environments containing chlorides should more than offset the weight penalty.

For Al/Gr with an Al alloy face sheet of 300 μm, a chromate conversion coating provided less corrosion resistance than hard sulfuric acid anodizing [51]. The conversion coated Al/Gr showed pitting after 9 months of exposure to filtered seawater [51]. For the chromate conversion coated Al/Gr with an Al 6061 face sheet of 50 μm studied here, pitting occurred after 5 days of exposure to 0.5 N NaCl. At the end of the test, a number of graphite fibers in the pits were observed visually. These results suggest that the thickness of the Al face sheet is very important for the corrosion resistance of chromate conversion coatings and anodized layers on Al/Gr MMCs. Therefore, an Al alloy face sheet of 75 μm to 100 μm thickness is suggested for chromate conversion coatings and anodizing of Al/Gr MMCs. However, for chemical passivation in $CeCl_3$ and for the application of epoxy coatings on Al/Gr, the current 50 μm thickness of the Al 6061 face sheet is satisfactory. Similarly, it is likely that if an Al 6061 face sheet would be applied to Al/SiC, a similar degree of corrosion protection as for Al 6061 could be achieved by anodizing and the use of chromate conversion coatings.

4.1.4 MgAZ31B

For MgAZ31B, conversion coatings (Dow #1, Dow #7, Dow #23, chrome-manganese) and anodized layers (Dow #17) did not provide significant protection. However, epoxy coatings and the Cr-Mn conversion coating combined with epoxy coatings provided excellent corrosion resistance in 0.5 N NaCl. Specifically, the Cr-Mn conversion coating combined with an epoxy coating exhibited the best corrosion behavior due to the very good base of the porous Cr-Mn conversion coating for the adhesion of the epoxy coatings. The Cr-Mn coating on the metal surface is discontinuous [11] and the corrosive medium can easily reach the metal surface. Therefore, the main function of the Cr-Mn coating is to provide good adhesion of the epoxy coating on the Mg surface. Similarly, corrosion protection of MgAZ31B can be achieved by proper sealing of an anodized (Dow # 17) surface with an epoxy coating [11]. Compared with epoxy/polyimide coated Mg/Gr MMCs which had

shown blisters and gas evolution after only 2 days of exposure to 0.5 N NaCl [12], the epoxy coating and the Cr-Mn conversion coating combined with an epoxy coating used in this project have improved very much the corrosion resistance of MgAZ31B.

4.2 Chromate Conversion Coatings

For chromate coated Al 6061, pitting did not occur after 12 days exposure to 0.5 N NaCl (Table II). However, pitting occurred after 5 days of exposure for chromate coated Al/SiC and Al/Gr. The reasons for this different behavior will be discussed in the following.

4.2.1 Chromate Conversion Coatings on Al 6061

The chromate conversion coating is self-healing because soluble chromate ions are able to cover small defects such as scratches in the film [18]. Yu et al. [52] have found by using XPS, AES, IR, Ion-beam, and X-ray diffraction that the chemical composition of the chromate conversion coating on Al alloys was mainly $CrOOH \cdot nH_2O$ and that Cr^{+6} existed only in the outer layer of the coating. Agarwala [53] has found by using XPS that the surface composition of a chromate coating on Al 7075-T6 was Cr_2O_3 and Al_2O_3. Asami et al. [54] have concluded by using XPS that the composition of the near surface region of chromate conversion coated Al was mainly Cr in the (III) state and relatively small quantities of Cr in the (VI) state. From these results it can be concluded that the chromate coating contains essentially Cr^{+3} compounds and minor Cr^{+6} and Al^{+3} compounds. The reactions for the formation of the chromate coating are considered to be the following [18,54,55]:

$$2Al + 6H^+ \text{ -----> } 2Al^{+3} + 3H_2 \quad (4.1)$$

$$HCr_2O_7^- + 3H_2 \text{ -----> } 2Cr(OH)_3 + OH^- \quad (4.2)$$

$$2Al^{+3} + 3OH^- \text{ -----> } Al_2O_3 + 3H^+ \quad (4.3)$$

$$2CrO_4^{=} + 10H^+ + 6e \text{ -----> } Cr_2O_3 + 5H_2O \quad (4.4)$$

$$HCr_2O_7^- + H_2O \text{ ------> } 2CrO_4^{=} + 3H^+ \quad (4.5)$$

$$Cr(OH)_3 + CrO_4^{=} + 2H^+ \text{ -----> } Cr(OH)CrO_4 + 2H_2O \quad (4.6)$$

$$2Al + Cr_2O_7^{=} + 2H^+ + 6HF \text{ -----> } 2AlF_3 + 2CrOOH + 3H_2O \quad (4.7)$$

The conversion coating consists of Al_2O_3, Cr_2O_3, $Cr(OH)_3$, $CrOOH$, H_2CrO_4, and $Cr(OH)CrO_4$ and provides excellent corrosion resistance for Al 6061.

4.2.2 Chromate Conversion Coating on Al/SiC

The corrosion resistance of chromate coated Al/SiC was much less than that of chromated Al 6061. This result suggests that the composition of the chromate coating on Al/SiC is different from that on Al 6061 due to the presence of the SiC particulates in the surface of Al/SiC. The chromate coating on Al/SiC may contain SiC particulates in the inner coating film. During the coating process, SiC particulates in the outer surface of Al/SiC may diffuse into the coating solution when Al metal around SiC particulates dissolves due to reaction (4.1) and/or (4.7). Cr^{+6} or Cr^{+3} compounds may cover the surface of SiC particulates due to reactions (4.2), (4.4), (4.5), (4.6), and (4.7).

When chromate coated Al/SiC is exposed to 0.5 N NaCl, some of the chromate in the near surface region of the coating leaches out and SiC particulates are exposed to the electrolyte. The corrosive electrolyte can diffuse through the interface between SiC particulates and the chromate coating. Initiation of pitting may occur when electrolyte has diffused into the interface between Al/SiC and the chromate coating and reached the Al matrix. Therefore, the low corrosion resistance of chromate conversion coated Al/SiC may be due to the presence of SiC particulates in the conversion coating.

4.2.3 Enhancement of the Corrosion Resistance for Chromate Coated Al/Gr

During the coating process, Al corrodes very severely in the coating solution due to the attack by F^- and the low pH (1.7-1.8) of the coating bath according to reactions (4.1) and (4.7). Cr^{+3} and Cr^{+6} compounds are formed, while Al corrodes. It is possible that some Al metal is still exposed to the coating solution when the sample is taken out of the coating bath. A few small defects which included bare Al metal were observed by microscopy on the surface of coated Al 6061, Al/SiC, and Al/Gr. The exposed Al defects may be repaired or healed by leaching chromate ions, which might be the reason that the corrosion resistance of chromate coated Al 6061 increased for the first 7 days of exposure to 0.5 N NaCl (Fig.7.b).

For chromate conversion coated Al/Gr, Cl^- can attack defects in the face sheet and reach graphite fibers during exposure to 0.5 N NaCl. The corrosion resistance sharply decreased during the first 5 days of exposure to 0.5 N NaCl (see Fig.9.c). Therefore, the thickness of the Al face sheet is very important for the satisfactory performance of chromate conversion coatings. An Al 6061 face sheet of at least 75 μm thickness is suggested for Al/Gr.

4.3 Anodic Coatings

The mechanism for the formation of anodic coatings on Al 6061 and Al/SiC, a model for anodized Al/SiC, and suggestions for the improvement of anodized layers on Al/Gr will be discussed in the following.

4.3.1 Anodic Coatings on Al 6061

The principal electrochemical reactions occuring during anodizing of Al-based materials are [41]:

$$Al \text{ -----> } Al^{+3} + 3e^- \qquad (4.8)$$

$$2Al^{+3} + 3O^= \text{ -----> } Al_2O_3 \qquad (4.9)$$

$$2Al^{+3} + 3OH^- \text{ -----> } Al_2O_3 + 3H^+ \qquad (4.10)$$

$$2Al^{+3} + 3H_2O \text{ -----> } Al_2O_3 + 6H^+ \qquad (4.11)$$

The anodic film consists of an outer porous layer with hexagonal columnar cells containing a cylindrical pore with a star-shaped section in its center, and a continuous inner barrier layer which is in contact with the porous outer layer. The anodic film grows at the interface between the oxide and the Al metal by anion (OH^-) transport, and at the interface between the oxide and the electrolyte by cation (Al^{+3}) transport [56]. For sealing in hot water (90°C - 100°C), the reactions are as follows [41]:

$$Al_2O_3 + H_2O \text{ ----> } 2\ AlOOH \text{ -----> } Al_2O_3 \cdot H_2O \text{ (boehmite)} \qquad (4.12)$$

During sealing, the aluminum oxide of the outer porous layer is converted to AlOOH or $Al_2O_3 \cdot H_2O$ which plugs the pores and increases the corrosion resistance of the anodized layer.

4.3.2 Corrosion Resistance for Anodized Al/SiC

Anodizing in H_2SO_4 and sealing in boiling water provides very high corrosion resistance for Al 6061. No pits were observed visually during exposure to 0.5 N NaCl for 102 day. However, for Al/SiC processed with hard anodizing in sulfuric acid and hot water sealing, pitting initiated already after 11 days. Severe pitting and crevice corrosion were observed after 36 days. This low corrosion resistance is considered to be due to the presence of SiC particulates which prevent the formation of a continuous inner barrier layer. Crevice corrosion and pitting may initiate at the SiC particulate/Al oxide interface. For SiC/Al, the larger the thickness of the anodic film, the smaller the area fraction of the barrier layer. Therefore, the corrosion resistance of hard anodized SiC/Al is less than that of conventional anodized SiC/Al.

4.3.3 Model for Anodized Al/SiC

EIS data for hard anodized Al/SiC show mainly capacitive behavior (Fig.16) and are different from those for Al 6061 (Fig.13). A model for the impedance of anodized Al/SiC is shown in Fig.59 and theoretical spectra are plotted in Fig.60 as a function of F, where F is the area fraction of the SiC area, which is normal to the surface of the substrate in the anodic film and 1-F is the area fraction of barrier layer. F increases with increasing thickness of anodic film. The equivalent circuit in Fig.59 consists of the resistance R_b and the capacitance C_b of the barrier layer, the resistance R_{po} and the capacitance C_{po} of the porous layer, the sum of the resistances R_{sic} of the porous layer which is located above the SiC particulates, the sum of the corresponding capacitances C_{sic} and the solution resistance R_s between the tip of the reference electrode and the working electrode. For F = 10 -5 (curve 1 in Fig.60) the spectra are dominated by the capacitances of the porous layer and the barrier layer and the resistive component of the porous layer. For F= 10 -3 (curve 2) the resistive component of the barrier layer appears at the lowest frequencies. For F=0.25 (curve 3), F=0.5 (curve 4) and F=0.75 (curve 5) the spectra are dominated by Csic and Rsic. Curves 3-5 in Fig.60 are similar to the experimental spectra for hard anodized Al/SiC in Fig.16.

4.3.4 Mechanism for the Formation of Anodic Coatings on Al/SiC

The corrosion resistance and the impedance spectra for anodized Al/SiC are quite different from for Al 6061. Therefore, the mechanism for the formation of anodic coatings on Al/SiC must be different from that for Al 6061 as a result of the presence of SiC particulates. It is assumed to consist of the following steps:

(i) Initiation step

The thin barrier layer is first formed on the SiC/Al according to the anodic oxidation reactions (4.9)-(4.11). Then the initial formation of the porous layer occurs due to the dissolution of Al2O3 in the acid used for the anodizing procedure (Fig.61.a).

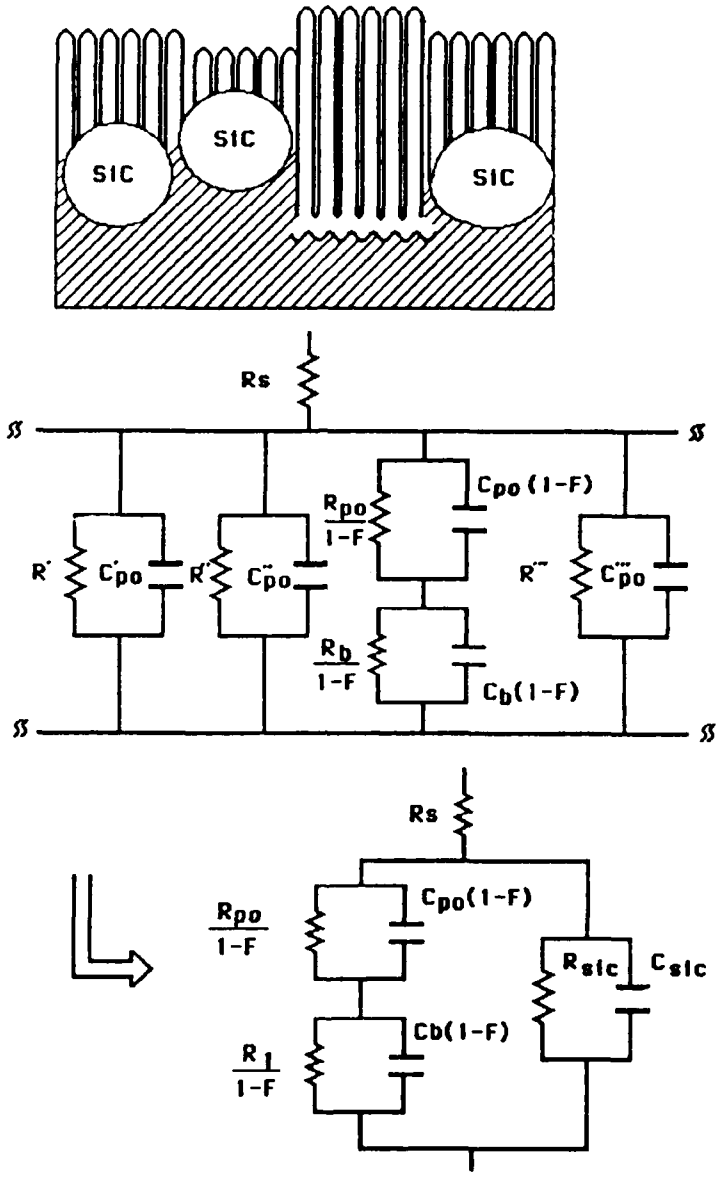

Fig.59 Model and equivalent circuits (EC) for anodized Al/SiC.

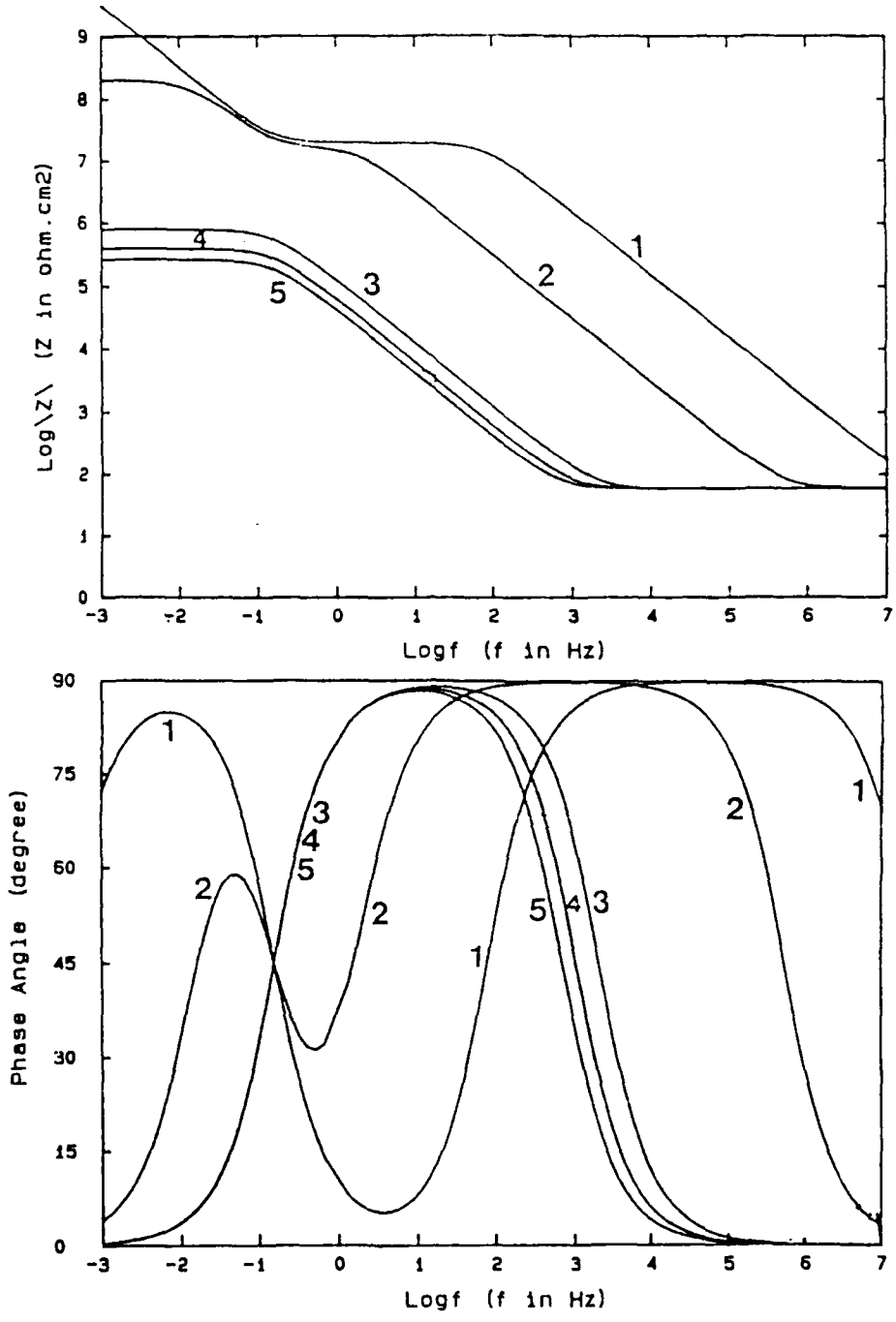

Fig.60 Simulated spectra for anodized Al/SiC.
R_{po} = 10^{6} ohm, R_b = 10^{9} ohm, R_{sic} = 10^{4} ohm
R_s = 3 ohm, C_b = 10^{-6} F, , C_{po} = 10^{-9} F,
C_{sic} = 10^{-4} F, F = 10^{-5} (curve 1),
F = 10^{-3} (curve 2), F = 0.25 (curve 3)
F = 0.5 (curve 4), and F = 0.75 (curve 5)

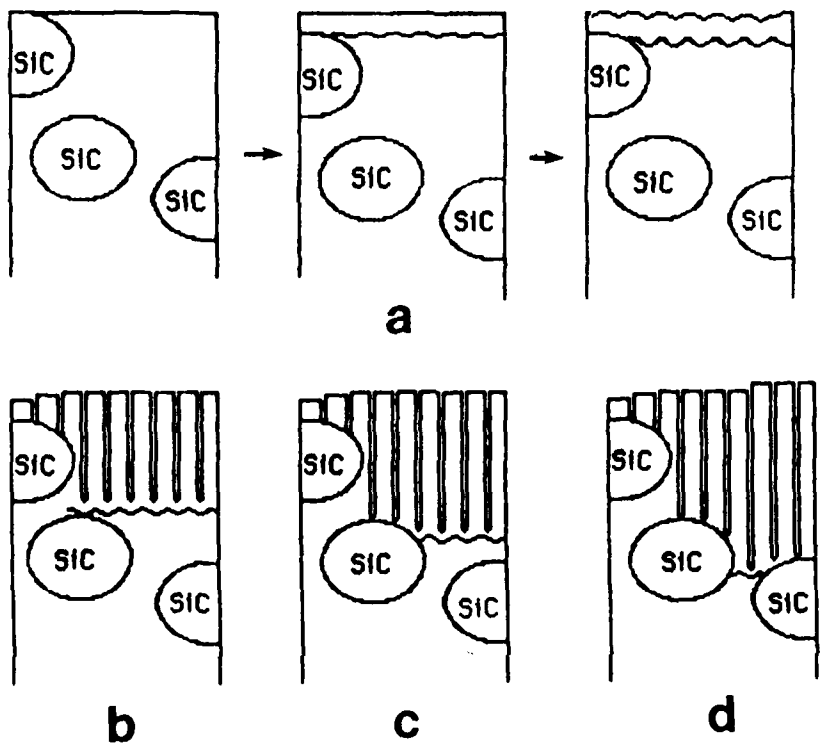

Fig.61 Growth model of anodic oxide film on Al/SiC
(a). Initiation steps of the barrier layer and the pores.
(b), (c), and (d) propagating steps of oxide film

(ii) Propagation step

(a) The anodic oxidation reactions continue to occur at the interface between the Al metal and the barrier layer by anion (OH^-) transport, and at the interface between the electrolyte and the porous layer by cation (Al^{+3}) transport.

(b) The barrier layer grows and reaches the SiC particulates, the base of the porous layer is also going down because the outer side of the barrier layer under the porous layer is dissolved by the acid. Simultaneously, Al^{+3} diffuses into the interface between the electrolyte and the porous layer and reacts with O^{-2}, OH^-, or H_2O to form Al_2O_3. (Fig.61.b)

(c) The barrier layer covering the SiC particulates is converted into a porous layer by the dissolution of Al_2O_3 in the acid. Parts of the barrier layer become thinner and some of it disappear depending on when the applied current is interrupted. (Fig.61.c)

(d) The porous and the barrier layers grow where SiC particulates do not interfere. However, the barrier layer is discontinuous due to the presence of SiC. When the reactions continue, the thickness of the anodic film increases and the interference of SiC particulates in the formation of the barrier layer increases because 25 % of SiC particulates are distributed randomly in the substrate. The larger the thickness of anodic film grows, the smaller will be the area fraction of the barrier layer. (Fig.61.d)

When the voltage reaches the required value, such as 15 V for conventional anodizing or 60 V for hard anodizing, the applied current is interrupted.

4.3.5 Suggested Improvements for Anodizing of Al/Gr

The surface of the anodized layer was observed by microscopy on Al/Gr to contain a few black graphite defects after conventional or hard anodizing due to the thin Al 6061 face sheet. Hence, an Al 6061 face sheet of at least 75 μm for conventional anodizing and at least 100 μm for hard anodizing are suggested. A similar degree of corrosion protection as for anodized Al 6061 would be expected for anodized Al/Gr.

4.4 Chemical Passivation in $CeCl_3$

The mechanism for chemical passivation of Al-based metals in $CeCl_3$ and the reasons for the stability of the resulting passive film will be discussed in the following.

4.4.1 Mechanism for Chemical Passivation in $CeCl_3$

Hinton et al.[6-8,57] have studied the passive film using X-ray photoelectron spectroscopy (XPS) and Auger electron spectroscopy (AES). They have suggested that the passive film formed in $CeCl_3$ contains a mixture of Al_2O_3, $Ce(OH)_3$, $Ce(OH)_4$, and CeO_2. The passive film of Al, which was immersed in 1000 ppm $CeCl_3$ for 5 days, was found to contain Ce mostly in the +3 valence state by Davenport et al. using X-ray absorption [58]. The mechanism of the formation of the passive film is considered to contain the following elements.

(i) Principal chemical reactions

The system Al/$CeCl_3$ solution contains Cl^-, Ce^{+3}, O_2, H_2O, H^+, OH^-, Al metal, and Al_2O_3 before any chemical reactions take place.

(a) The chemical reactions for passivation are as follows: [59-61]

$$Ce^{+3} + 3OH^- \text{ ----> } Ce(OH)_3 \qquad (4.13) \quad \Delta G_{298}<0$$
$$4Ce(OH)_3 + O_2 \text{ ----> } 4CeO_2 + 6H_2O \qquad (4.14) \quad \Delta G_{298}<0$$
$$4Ce(OH)_3 + O_2 + 2H_2O \text{ -----> } 4Ce(OH)_4 \qquad (4.15) \quad \Delta G_{298}<0$$

(b) There are two electrochemical reactions involved in the corrosion process. One is the anodic reaction, the other is the cathodic reaction.

Anodic reaction (metal dissolution)

$$Al \text{ ----> } Al^{+3} + 3e^- \qquad (4.16)$$

Cathodic reaction (oxygen reduction)

$$O_2 + 2H_2O + 4e^- \text{ -----> } 4OH^- \qquad (4.17)$$

(ii) Initiation of passivation process

As the Al alloy is immersed in the $CeCl_3$ solution, Al dissolution occurs at surface defects due to Cl^- attack and oxygen reduction occurs at cathodic sites. At the cathodic sites where high pH develops due to reaction (4.17), Al_2O_3 dissolves and Ce^{+3} reacts with OH^- to form $Ce(OH)_3$ which precipitates on the surface. This process involves reactions (4.13),(4.14), and (4.15).

(iii) Propagation of passivation process

$Ce(OH)_3$ continues to be formed at the cathodic sites of high pH and reacts very slowly with O_2 and/or H_2O to form $Ce(OH)_4$ or CeO_2, respectively, according to reaction (4.14) or (4.15). Ce^{+4} can be formed on the Al surface only, rather than in the aqueous solution, because of the absence of a stronger oxidizer than Ce^{+4} in the solution. This step involves reactions (4.13) to (4.17).

(iv) Termination of passivation process

Corroded sites on the surface can be repassivated by the formation of $Ce(OH)_3$ around the pits and accumulation in the pits. Cerium oxides and hydroxides are formed and mixed with aluminum oxides on the whole surface. After the pits are closed by $Ce(OH)_3$-rich particles, the precipitation of $Ce(OH)_3$ ceases due to the disappearance of high pH conditions. At this termination stage, the polarization resistance generally reaches about 10^6 ohm-cm2 according to EIS data (see Fig.20.b). If the sample remained immersed in the passivation solution, Ce(OH)3 would continue to be oxidized to form $Ce(OH)_4$ or CeO_2.

4.4.2 Stability of Passivating Film

The passivating film is assumed to be a mixture of Al_2O_3, $Ce(OH)_3$, $Ce(OH)_4$ and CeO_2. The solubility products, Ksp, for $Ce(OH)_3$, $Ce(OH)_4$, and CeO_2 in aqueous solution are $1.6 * 10^{-20}$, $7.4 * 10^{-48}$, and $1 * 10^{-63}$, respectively [59,60,62]. For a neutral solution, pH =7.

(i) $Ce(OH)_3(s) \text{ ---> } Ce^{+3}(aq) + 3OH^-$
$Ksp=[Ce^{+3}]\ [OH^-]^3 = [Ce^{+3}]\ [10^{-7}]^3 = 1.6 * 10^{-20}$,
i.e. $[Ce^{+3}]$ =16 mole/liter.

(ii) $Ce(OH)_4(s) \text{ --->} Ce^{+4}(aq) + 4\ OH^-$
$Ksp = [Ce^{+4}]\ [OH^-]^4 = [Ce^{+3}]\ [10^{-7}]^4 = 7.4 * 10^{-48}$,
i.e. $[Ce^{+4}] = 7.4 * 10^{-20}$ mole/liter

(iii) $CeO_2(s) + 2H_2O(l) \text{ ---> } Ce^{+4} + 4OH^-$
$Ksp = [Ce^{+4}]\ [OH^-]^4 = [Ce^{+4}]\ [10^{-7}]^4 = 10^{-63}$,
i.e. $[Ce^{+4}] = 1 * 10^{-35}$ mole/liter.

It is obvious that CeO_2 and $Ce(OH)_4$ are much more stable in neutral aqueous solutions than $Ce(OH)_3$. Therefore, $Ce(OH)_4$ and CeO_2 possess high stability and provide high corrosion resistance in neutral solutions, while $Ce(OH)_3$ will easily dissolve. When $Ce(OH)_3$ dissolves, the Al surface may be attacked by Cl^- which causes nucleation of pitting. According to the suggested mechanism, the passivated samples should be further exposed in air so that all $Ce(OH)_3$ can be oxidized to $Ce(OH)_4$ or CeO_2. The rate of oxidation for $Ce(OH)_3$ in an aqueous solution is very slow [61] due to the limited concentration of oxygen. If the samples are exposed in air for a period of time after being passivated, $Ce(OH)_3(s)$ will be oxidized to yellow $Ce(OH)_4(s)$ or $CeO_2(s)$. The oxidation reaction that takes place in air is still relatively slow at room temperature, yet it is faster than that in the aqueous solution. The formation of Ce^{+4} on the passive film will be accelerated if the reaction takes place at elevated temperature. If oxygen or air are supplied into the $CeCl_3$ solution during passivation, the oxidation reaction will also be accelerated.

The reduction reaction for Ce^{+4} is:

$$Ce^{+4} + e^- \text{ ---> } Ce^{+3}, \qquad E^\circ = 1.61 \text{ volts.}$$

It is impossible for Ce^{+3} to become Ce^{+4} in the $CeCl_3$ solution due to the absence of a stronger oxidizer than Ce^{+4}. According to Hinton et al. [6], cerium oxide and hydroxide in the valance states III and IV are formed in the solution and precipitate under the high pH condition. Their statement is incorrect, because Ce^{+4} can not be in the solution without the presence of a stronger oxidizer than Ce^{+4}. However, Ce^{+4} can be formed by oxidation of the white $Ce(OH)_3$ precipitate. The reduction reaction for H_2O_2 which is a stronger oxidizer than Ce^{+4} is:

$$H_2O_2 + 2H^+ + 2e^- \text{ ----> } 2H_2O, \qquad E^\circ = 1.77 \text{ volts}$$

The rate of the formation of CeO_2 and $Ce(OH)_4$ will be much accelerated by adding H_2O_2 to the $CeCl_3$ aqueous solution. Then the reaction:

$$Ce^{+4} + 4\ OH^- \text{ -----> } Ce(OH)_4$$

occurs at the cathodic sites at a rate which is much faster than that of reaction (4.10):

$$4Ce(OH)_3 + O_2 + 2H_2O \text{ --> } Ce(OH)_4.$$

Hence the passive film should be rich in $Ce(OH)_4$ which is much more stable than $Ce(OH)_3$.

4.5 Polymer Coatings

An accelerated corrosion test to evaluate the quality and the lifetime of polymer coatings, and models for delamination and filiform corrosion of polymer coatings will be discussed in the following.

4.5.1 An Accelerated Corrosion Test to Evaluate Polymer Coatings

In order to evaluate the effects of damage, such as a scratch or a pinhole, to the coating and the resistance to coating delamination, a hole of 0.5-0.75 mm diameter was drilled into the surfaces of epoxy coated Al/SiC, $CeCl_3$ passivated Al/SiC, $CeCl_3$ passivated Al 6061, Al-Li 2091-T6 and Cr-Mn conversion coated MgAZ31B. The results for these samples exposed to 0.5 N NaCl are shown in Table IV. The delamination of polymer coatings is a consequence of the cathodic reaction, $2H_2O + O_2 + 4e\text{----> } 4OH^-$, occuring at the Al surface under the coating or in a defect in the coating. The hydroxyl concentration dissolves the aluminum oxide and the Al metal, and possibly also attacks the polymer at the interface between the polymer and the substrate. Diffusion of Cl^- into the defect may accelerate the rate of delamination and cause pitting under the coating. For the samples with a hole, the cathodic reaction occurs at the interface between the coating and the substrate around the hole and produces high pH and loss of adhesion of the coating. The damage times for epoxy coated samples with a hole were much shorter than for those without a hole. For example, epoxy coated Al-Li did not show pits and/or delamination after 90 days of exposure to 0.5 N NaCl, but the surface with an artificial pit of 0.75 mm diameter showed delamination around the pit after only 5 days. Delamination can occur only when water and oxygen have penetrated through the coating layer and have reached the interface at the epoxy coating/substrate. This suggests that the occurrence of the delamination after 5 days for coatings with a hole should correspond to the same situation occurring after more than 90 days for coatings without a hole. Hence, an artificial defect can be used as an accelerated corrosion test to evaluate the quality of coatings and the lifetime of coatings.

For Mg in 0.5 N NaCl, the cathodic reaction is $2H_2O + 2e^- \text{ ---> } 2OH^- + H_2$. The alkali is generated under the coating without oxygen penetrating through the coating. Hence the water uptake dominates the delamination of epoxy coatings on Mg. Also, diffusion of Cl^- may accelerate the rate of delamination and cause damage in the coating due to the high pressure of hydrogen which is produced by the cathodic reaction and accumulates under the coating. Therefore, Cr-Mn conversion coated Mg with an epoxy coating pitted during exposure to 0.5 N NaCl [11]. The epoxy coated MgAZ31B for which water uptake was only 0.8 % showed filiform corrosion. Hence epoxy coated Mg is sensitive to filiform corrosion. For Cr-Mn pretreated Mg with an epoxy coating containing an artificial pit, delamination was observed visually after 49 days of exposure to 0.5 N NaCl. Further experiments including various polymer coatings on Mg with a hole and without a hole need to be performed. From these results, the relation between

damage times for coatings with a hole and without a hole can be determined. The lifetime of coatings can be evaluated in a short time using coated samples with an artificial defect.

4.5.2 Model for Epoxy Coated Samples with an Artificial Defect

For the purpose of the analysis of impedance data a suitable model must first be developed. Fig.62.a presents a general model and simulated impedance spectra for epoxy coated samples with an artificial defect. This model is valid for exposure times before delamination or filiform corrosion occurs around the damaged area. The parameters in this model are defined as follows: R_s is the solution resistance, C_c is the capacitance and R_c is the resistance of the coating, Rh is the solution resistance in the defect, C_{pit} is the capacitance and R_{pit} is the polarization resistance of the artificial pit. W, which describes the transmission line behavior in the low frequency range due to pitting, is expressed as $W = (K/F)(jw)^n$, where n is the slope of the Log/Z/ - Log f curve in the transmission line range, K is an experimental parameter and F is the area fraction of the pitted surface. Simulated spectra for different values of K (Fig.62.b) show capacitive behavior of the coating in the high frequency range, capacitive behavior of artificial pit in the frequency range of 10 to 10^3 Hz, the resistive component Rh in the frequency range of about $5 * 10^4$ Hz, and transmission line type behavior between 10^{-4} Hz and 10^{-1} Hz for curves 2 and 3 and below 10^{-3} Hz for curve 1. It is interesting to note that for small values of K a transmission line-type behavior occurs only in the lowest frequency range. The impedance spectra of the epoxy coated Al/SiC (Fig.43, curve 2-5), $CeCl_3$ passivated Al/SiC with an epoxy coating (Fig.54, curve 2-3), and epoxy coated Al-Li 2091-T6 (Fig.50, curve 2) are similar to the simulated spectra in Fig.68.b, curves 2 or 3. However a transmission line behavior could not be observed clearly in the impedance spectra for $CeCl_3$ passivated Al 6061 with an epoxy coating (Fig.52, curve 2). This result is probably due to a very small value of K for this system.

A new model has been developed for the delamination of the epoxy coating with an artificial defect (Fig.63.a). The parameters in this model are defined as follows: R_s is the solution resistance, Rd is the polarization resistance and Cd is the capacitance of the delaminated area, C_c is the capacitance and Rc is the resistance of the coating, Rh is the solution resistance in the hole, C_{pit} is the capacitance and R_{pit} is the polarization resistance of the artificial pit. W describes the transmission line behavior in the low frequency range due to pitting and is expressed as $W=(K/F)(jw)^n$. Simulated Bode-plots for the model in Fig.63.a are shown in Fig.63.b. The resistance of the coating R_c was not observed in Fig.63.b because Rc is much larger than R_d. The simulated spectra in Fig.63.b are very similar to the experimental spectrum for curve 3 of Fig.50 for Al-Li 2091-T6 which was coated with a epoxy layer containing an artificial defect.

5. CONCLUSIONS

The conclusions reached in the present evaluation of methods of corrosion protection for Al alloys, Al-based MMCs, Al-Li 2091-T6 and MgAZ31B are discussed in the following.

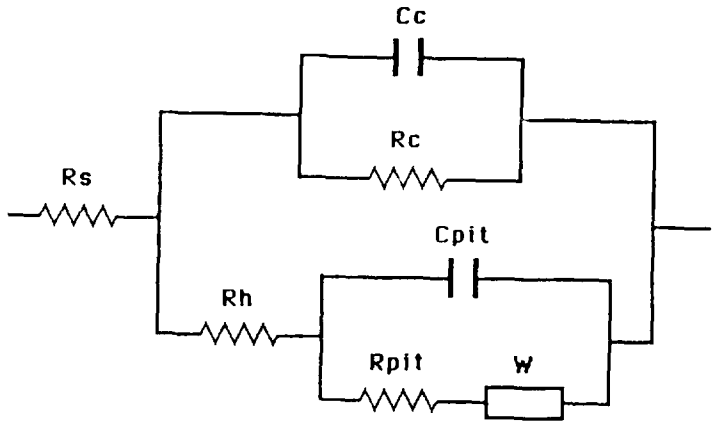

$$W = \frac{K}{F}(J\omega)^n, \quad n < 0$$

Fig.62.a Equivalent circuit (EC) for epoxy coated samples with an artificial defect.

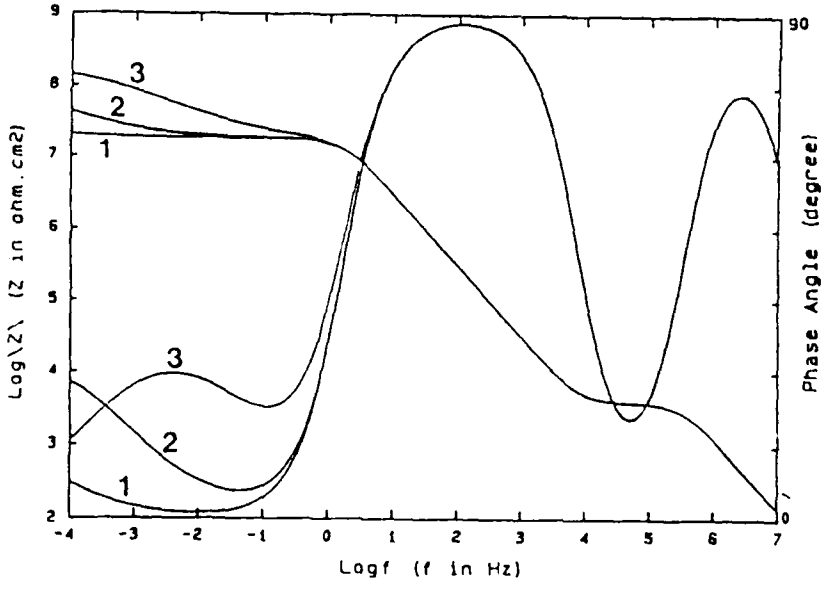

Fig.62.b Simulated spectra for epoxy coated samples with an artificial defect. R_S = 4.16 ohm, $R_C = 10^7$ ohm $R_{pit} = 10^6$ ohm, R_h = 200 ohm, $C_C = 2.5 \cdot 10^{-9}$ F, $C_{pit} = 10^{-7}$ F, n = -0.5, $F = 10^{-4}$
$K = 5 \cdot 10^{-1}$ ohm $(rad/s)^{-n}$ (curve 1),
K = 5 ohm $(rad/s)^{-n}$ (curve 2),
$K = 5 \cdot 10$ ohm $(rad/s)^{-n}$ (curve 3).

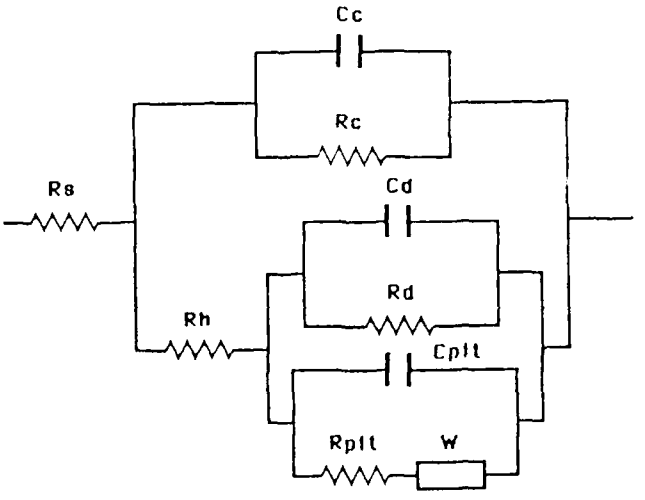

$$W = \frac{K}{F}(j\omega)^n, \quad n < 0$$

Fig.63.a Equivalent circuit (EC) for the delamination of epoxy coated Al-Li 2091-T6 with an artificial defect.

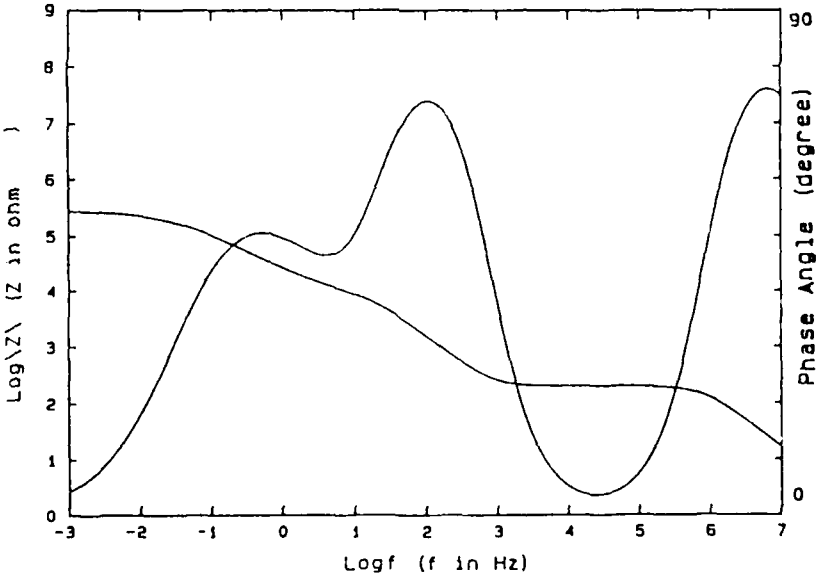

Fig.63.b Simulated spectra for the delamination of epoxy coated Al-Li 2091-T6 with an artificial defect.
R_s = 3 ohm, R_c = 10 7 ohm, R_d = 3 * 10 5 ohm
R_{pit} = 10 4 ohm, R_h = 200 ohm, C_c= 1 * 10 -9 F,
$C_t = C_{pit} + C_d$ = 1 -6 F, n = -0.7,
K/F= 1 * 10 5 ohm $(rad/s)^{-n}$

5.1 Al Alloys

For Al 6061, a chromate conversion coating (Alodine 600), conventional and hard anodized coatings (SAA + HWS), surface layers produced by chemical passivation in $CeCl_3$, an epoxy coating, and chemical passivation combined with the polymer coating provide excellent corrosion resistance to 0.5 N NaCl. Chemical passivation in $CeCl_3$ also provides excellent corrosion resistance for Al 7075-T6, but not for Al 7075-T73 due to Cu precipitates on the surface which cause galvanic corrosion problems.

5.2 Al/SiC MMCs

The corrosion resistance of bare Al/SiC is less than that of the corresponding Al alloy, and pitting and crevice corrosion occur due to SiC particulates in the surface. A chromate conversion coating (Alodine 600) and anodized layers (SAA + HWS) on Al/SiC provide satisfactory corrosion protection, but not as effectively as for Al 6061. Chemical passivation in $CeCl_3$ of Al/SiC provides better corrosion resistance than the chromate conversion coating or anodizing. The epoxy coating, and chemical passivation combined with the polymer coating provide excellent corrosion resistance to 0.5 N NaCl.

5.3 Al/Gr MMCs

For bare Al/Gr the corrosion resistance is very poor when pits have penetrated the Al face sheet and reached the graphite fibers. The chromate conversion coating (Alodine 600) on Al/Gr provide significant corrosion protection. Chemical passivation in $CeCl_3$ significantly increases the corrosion resistance of the Al 6061 face sheet and provides better corrosion resistance than the chromate conversion coating. The epoxy coatings and chemical passivation combined with the epoxy coating produce the best corrosion resistance. Anodizing did not produce a perfect coating because the face sheet of 50 μm thickness is too thin. As long as bare graphite is exposed in pinholes of the face sheet, the pinholes become larger during anodizing rather than forming the anodized film.

5.4 Al-Li 2091-T6

The corrosion resistance in a marine environment is much less for bare Al-Li 2091-T6 than for bare Al 6061 due to the presence of the reactive element Li which produces LiOH as corrosion product. The epoxy coatings on Al-Li 2091-T6 provided excellent corrosion resistance in NaCl. However, when the coating became damaged, rapid corrosion and coating delamination occurred at the damaged areas.

5.5 MgAZ31B

For bare MgAZ31B the corrosion resistance is very poor and pitting occurs in 0.5 N NaCl within a very short time. Conversion coatings (Dow #1, Dow #7, Dow #23, chrome-manganese) and an anodized process (Dow #17) did not provide significant corrosion protection. However, the epoxy coating and Cr-Mn conversion coating combined with the epoxy coating provided excellent corrosion resistance in NaCl. The same sucessful schemes of corrosion protection for MgAZ31B should also be applicable for Mg/Gr MMCs, although the combimation of the very poor corrosion resistance of Mg and the very active graphite cathode could pose additional

problems.

5.6 The corrosion behavior of degreased Al 6061 which was passivated in $CeCl_3$ for one week is similar to that of chromate conversion coated Al 6061(Alodine 600). This result suggests that passivation in $CeCl_3$ is a promising alternative to the use of chromate conversion coatings on Al alloys.

5.7 New mechanisms for the formation of the passive film in $CeCl_3$ on Al alloys and Al-based MMCs and for the formation of anodized layers on Al/SiC have been proposed. Also new models for the anodized layers on Al/SiC, polymer coatings with an artificial defect, and delamination or filiform corrosion of the polymer coatings with an artificial defect have been developed.

5.8 Electrochemical impedance spectroscopy (EIS) is a powerful tool to monitor the passivation process in $CeCl_3$ and the corrosion process during exposure to NaCl. The onset of localized corrosion can be detected and monitored. The pitting model can be used to analyze impedance spectra of as-received and $CeCl_3$-treated Al alloys and Al-based MMCs, and estimate the rate of the pit growth at the corrosion potential E_{corr}. This is a significant new finding of great practical importance. All other methods of pit growth rates apply a potential above the pitting potential in order to carry out the measurement. EIS can also detect the onset of coating delamination and can be used to estimate the growth rate of artificial defect in the coatings.

6. RECOMMENDATIONS FOR FUTURE RESEARCH

The following recommendations for future improvements of methods of the corrosion protection of Al and Mg-based MMCs have been reached in this project:

6.1 Improvement of the Corrosion Resistance of Al/SiC

The corrosion resistance of chromate conversion coated Al/SiC is much less than that of Al 6061 due to the presence of the SiC particulates in the coating. In order to improve the corrosion resistance of chromate conversion coated Al/SiC to the level of chromate coated Al 6061, an Al 6061 face sheet of at least 75 μm thickness is suggested.

Two methods for producing improved anodized coatings are suggested:
(i) After sealing in hot water, the anodized Al/SiC should be treated in $CeCl_3$ at R.T. or higher temperature. This process may enhance the corrosion resistance because the passive film produced in $CeCl_3$ will cover the SiC particulates which are exposed at the surface. However, crevice corrosion might still be a big problem.

(ii) Al 6061 face sheets of at least 75 μm thickness for conventional anodizing and 100 μm thickness for hard anodizing are suggested. There should be no problem with crevice corrosion and pitting for this treatment.

6.2 Enhancement of the Corrosion Resistance of Al/Gr

Although coatings can be formed on the Al 6061 face sheet of 50 μm thickness on Al/Gr, the corrosion resistance of the chromate coating and of the anodized layer on Al/Gr was much less than that of coated Al 6061. A sufficient

thickness of the Al 6061 face sheet is needed to perform the anodizing treatment and to produce chromate conversion coatings on Al/Gr successfully. An Al 6061 face sheet of at least 75 μm thickness for chromate and conventional anodized coatings and of at least 100 μm thickness for hard anodizing are suggested to be used with Al/Gr.

6.3 Accelerated Chemical Passivation in $CeCl_3$

It is impossible for Ce^{+3} to be oxidized to Ce^{+4} in the $CeCl_3$ solution due to the absence of a stronger oxidizer than Ce^{+4}. Since H_2O_2 is a stronger oxidizer than Ce+4, the rate of the formation of CeO_2 and $Ce(OH)_4$ will be much accelerated by adding H_2O_2 to $CeCl_3$ aqueous solution such that the solution contains Ce^{+4}.

6.4 An Accelerated Corrosion Test for Polymer Coatings

Epoxy coated samples without a hole should be exposed to NaCl until the occurrence of delamination of the coatings and corrosion of the Al surface are observed. The damage times of coated samples without an artificial defect could then be correlated with the damage times for coated samples with an artificial defect. The life time of coatings could be then determined by an accelerated corrosion test in a short time.

6.5 TEM Pictures for Anodized Al/SiC

TEM pictures for anodized Al/SiC need to be taken to study the structure of these films and clarify the role of the Al/SiC particulates.

7. REFERENCES

1. D. M. Aylor and P. J. Moran, J. Electrochem Soc., 132, 1277 (1985)
2. P. P. Trzaskoma, Corrosion, 42, 609 (1986).
3. W. F. Czyrklis, Corrosion/85, paper No. 196, NACE, Houston, Texas.
4. D. M. Aylor, R. J. Ferrara, and R. M. Kain, Mater. Perform., 23, 32 (1984).
5. S. Wernick and R. Pinner, "The Surface Treatment and Finishing of Aluminium and Its Alloys", 4th edition (1972)
6. D. R. Arnott, B. R. W. Hinton, and N. E. Ryan, Corrosion, 45, 12 (1989)
7. D. R. Arnott, B. R. W. Hinton and N. E. Ryan, Metals Forum, 9, 162 (1986).
8. B. R. W. Hinton, D. R. Arnott, and N. E. Ryan, Metals Forum, 7, 211,(1984)
9. Ullmann, Fritz, "Ullmann's Encyclopedia of Industrial Chemistry", (1985).
10. F. Keller, M. S. Hunter, and O. L. Robinson, J. Electrochem Soc., 100, 411 (1953)
11. F. Mansfeld, S. Lin, S. Kim, and H. Shih, Journal of Coatings Technology, 61, 33 (1989)

12. F. Mansfeld, and S.L. Jeanjaquet, Corr. Sci. 26, 727 (1986).

13. M. G. Fontana and N.D. Greene, "Corrosion Engineering", (1978)

14. J. E.. Hatch, "Alumium: Properties and Physical Metallurgy", (1984)

15. R. S. Busk, "Magnesium Products Design", (1987)

16. Amchem Products Inc., "Technical Service Data Sheet", No. AL-600-D, (1987): No. RL-53-D (1973); No. DE-17-D/S (1984)

17. Dow Chemical Company," Operations in Magnesium Finishing" (1982)

18. R. M. Burns and W. W. Bradley, "Protective Coatings for Metals", third edition, (1967).

19. Magnesium Elektron Ltd., "Chromate Treatments for Magnesium Alloys.", Worksheet No. 203, (1980)

20. H. Ackerman et al., "Metals Handbook", 9th edition, vol. 13, p.396 (1987).

21. Hysol Division, The Dexter Corporation, Technical information, Bulletin AC2-701A.

22. F. Mansfeld, S. Lin, S. Kim, and H. Shih, J. Electrochem. Soc. 135, 906 (1988)

23. F. Mansfeld and M. W. Kendig, Werkst. Korros., 36, 473, (1985)

24. M. W. Kendig, A. Allen, S. Jeanjaquet, and F. Mansfeld, Corrosion/85, paper no. 74, NACE, Houston, Texas.

25. F. Mansfeld, S. Kim, W. Won, and H. Shih, "A Quality Control Test for Chromate Conversion Coated Al Alloys Based on EIS.", to be published.

26. M. Kendig and F. Mansfeld, Mat. Res. Soc. Symp. Proc. 125, 293, (1988)

27. F. Mansfeld, S. Lin, S. Kim, and H. Shih, J. Electrochem Soc. 137, 78 (1990).

28. F. Mansfeld, S. Lin, S. Kim, and H. Shih, Corrosion/88, paper No. 380 ; Corrosion 45, 615, (1989).

29. F. Mansfeld, S. Lin, S. Kim, and H. Shih, Electrochim Acta 34,1123, (1989).

30. F. Mansfeld, S. Lin, S. Kim, and H. Shih, Corr. Sci. 27, 997 (1987).

31. F. Mansfeld, Corrosion/83, paper No. 255, NACE, Houston, Texas.

32. F. Mansfeld, S. Lin, S. Kim, and H. Shih, Werkstoffe and Korrosion 39, 487-492 (1988)

33. F. Mansfeld, Corrosion, 44, 558, (1988).

34. M. Kendig and F. Mansfeld, Corrosion, 39, 466 (1983)

35. H. Shih and F. Mansfeld, Corr. Sci. 29, 1235 (1989).

36. K. Cole and R. H. Cole, J. Chem. Phys., 9, 341 (1941)

37. F. Mansfeld and H. Shih, J. Electrochem. Soc. 135, 1171 (1988)

38. H. Shih and F. Mansfeld, Corrosion, 45, no. 8, 610 (1989).

39. J. P. Hoar and G. C. Wood, Electrochim. Acta., 7, 333 (1962)

40. H. H Uhlig and R.W. Revie, "Corrosion and Corrosion Control", (1985)

41. M. G. Fontana and R.W. Staehle, Advances in Corrosion Science and Technology, vol.1, (1970).

42. J. Hitzig, K. Juttner, and W. J. Lorenz, J. Electrochem. Soc., 133, 5 (1986)

43. F. Mansfeld and M. Kendig, Werkstoffe und Korrosion, 36, 473, (1985)

44. F. Mansfeld and M. W. Kendig, J. Electrochem. Soc., 135, 828, (1988)

45 J. Hitzig, K. Juttner, W. J. Lorenz, and W. Paatsch, Corrosion Sci., 24, 945 (1984)

46. G. V. Samsonov, "The Oxide Handbook",(1973)

47. H. Kaiser, K.D. Beccu and M.A. Gutjahr, Electrochim Acta, 21, 539 (1976)

48. D. M. Brasher and A. H. Kingsbury, J. Appl. Chem.,4, 62 (1954)

49. P. P Trzaskoma, E. McCafferty, C. R. Crowe, J. Electrochem. Soc., 130, 1804 (1983).

50. D. M. Aylor, R. J. Ferrara, and R. M. Kain, Mater. Perform., 23, 32 (1984).

51. D. M. Aylor, P. J. Moran, Corrosion/86, paper no. 202, NACE, Houston, Texas.

52. Z. Yu, H. Ni, G. Chang, The Electrochem. Soc., Proc. Vol 86-11 p.229 (1986)

53. V. S. Agarwala, ACS Symp. Ser., Vol. 322 (Polym. Mater. Corros. Control), p.211 (1986).

54. K. Asami, M. Oki, G. E. Thompson, G. C. Wood and V. Ashworth, Electrochim. Acta., 32, 337 (1987).

55. OCCAA,"Surface Coatings", vol. 2 (1984).

56. H. A. Francis, J. Electrochem. Soc.,112,1234 (1965).

57. D. R. Arnott, N. E. Ryan, and B. R. Hinton, Appl. Surf. Sci., 22-23(1), 236-51, (1985)

58. A. J. Davenport, H. S. Isaacs, and M. W. Kendig, J. Electrochem. Soc., 136, 6, 1837 (1989).

59. A. J. Bard, R. Parsons and J. Jordan, "Standard Potential in Aqueous Solution",(1985)

60. W.M. Latimer, "Oxidation Potentials", (1952)

61. "Thorpe's Dictionary of Applied Chemistry", vol.2, 4th edition(1938)

62. P. N. Kovaleuko and K. N. Bagdasarov, Peredavye Metody Khim. Tekhnol. ikontrdya Prcisv Sb. 154-62 (1964) (Russ)

63. W. J. Lorenz and F. Mansfeld, Corr. Sci., 21, 647, (1981).